UNIVERSITY OF BELGRADE

FACULTY OF PHYSICAL CHEMISTRY

Goitom K. Gebremariam

Investigation of the influence of electrolytes and the role of reduced graphene oxide as a support for metal catalysts on the catalytic activity toward the hydrogen evolution reaction

Doctoral Dissertation

Belgrade 2023

UNIVERZITET U BEOGRADU
FAKULTET ZA FIZIČKU HEMIJU

Goitom K. Gebremariam

Ispitivanje uticaja elektrolita i uloge redukovanog grafen-oksida kao nosača metalnih katalizatora na katalitičku aktivnost za reakciju izdvajanja vodonika

Doktorska disertacija

Beograd, 2023.

Mentor:

Prof. Igor Pašti, full professor
Faculty of Physical chemistry, University of Belgrade

Committee members:

Prof. Nemanja Gavrilov, associate professor
Faculty of Physical Chemistry, University of Belgrade

_____

Dr. Ana Dobrota, assistant professor
Faculty of Physical Chemistry, University of Belgrade

_____

Dr. Mila Krstajić Pajić, assistant professor
Faculty of Technology and Metallurgy, University of Belgrade

_____

Date of defense

_____

Acknowledgment

In the Name of the Father, the Son, and the Holy Spirit One God, Amen.

The doctoral dissertation was completed at the Faculty of Physical Chemistry University of Belgrade with computational simulations and data management facilitated by resources provided by the Swedish National Infrastructure for Computing (SNIC) at the National Supercomputer Centre (NSC) at Linköping University.

First, I would like to express my heartfelt gratitude to my advisor, Prof. Igor Pašti, a full professor and Vice-Dean for research and PhD studies at the Faculty of Physical Chemistry. His invaluable support has shaped my research trajectory, and I am genuinely grateful for his unwavering commitment, patience, and guidance throughout my PhD journey.

Additionally, I would like to acknowledge the valuable support and advice from Mr. Aleksandar Jovanović, a research assistant at the Faculty of Physical Chemistry. He has consistently offered assistance and advice, providing practical support during experimental work, solving problems and software issues.

I am deeply grateful to Prof. Nemanja Gavrilov, an associate professor at the Faculty of Physical Chemistry, and Dr. Ana Dobrota, an assistant professor at the same institution, and Dr. Mila Krstajić Pajić, an assistant professor at Faculty of Technology and Metallurgy, who served as committee members and made invaluable contributions to the quality of this dissertation through their suggestions and advice. I am truly honoured that you have agreed to join the thesis committee.

I extend my heartfelt gratitude to the Serbian government, particularly to the Ministry of Education, Science, and Technological Development of the Republic of Serbia, for awarding me a PhD scholarship through the World in Serbia project (Contract No. 451-03-68/2020-14/200146). I am deeply thankful for this opportunity.

I want to express my gratitude to Dr. Jadranka and Ms Christina, with whom I had the opportunity to spend some free time during my PhD in the laboratory. Your presence and the warm and friendly atmosphere you created in the lab are appreciated. I would also like to use this opportunity to express my gratitude to all the individuals and organizations who have played a crucial role in making this PhD work possible.

My most enormous gratitude extends to my family: My wife, Mrs Simret Gebreab and my son Sirak Goitom for their enthusiasm, encouragement and patience. I would also like to thank my parents, who gave me unconditional support and motivation in this journey and throughout my life.

Investigation of the influence of electrolytes and the role of reduced graphene oxide as a support for metal catalysts on the catalytic activity toward the hydrogen evolution reaction

Abstract

Efficient hydrogen production is crucial due to the global energy crisis and environmental concerns, which necessitates identifying catalytic trends for informed choices in hydrogen generation technologies and materials. Hydrogen evolution reaction (HER) volcano plots, initially established for acidic solutions and later adapted for alkaline media, play a crucial role in identifying catalytic trends related to HER. The first part of the thesis focuses on conducting a comprehensive analysis of the HER catalytic trends on nine polycrystalline monometallic surfaces in seven solutions, encompassing a wide pH range from highly acidic to highly alkaline.

Using theoretically calculated hydrogen binding energies (HBEs) on clean metallic surfaces and experimentally measured HER overpotentials it is shown, for the first time, that the volcano-like relationships are predominantly preserved across a broad spectrum of pH values, spanning from acidic to neutral and alkaline solutions. This signifies that HBE can be used as a descriptor for the identification of active electrocatalysts in a wide pH range, including pH neutral solutions. Accordingly, Cr was found to have high HER activity in pH-neutral solutions surpassing that of W, Fe, and Co. Furthermore, exposing metallic surfaces to high anodic potentials can lead to either enhanced or suppressed HER, depending on the metal and the electrolyte used. In view of the nontrivial impacts of surface oxidation, its effects might be seen either as a promotion in HER activity or as HER blocking (as in the case of Cr and W). The former case is specifically applicable to Ni and Co in alkaline and pH-neutral solutions, which can be attributed to the enhanced dissociation of water at the metal-oxide interface. This effect is more significant for Ni in NaCl solutions to the extent that, after undergoing oxidation, it becomes more active than Pt. Therefore, this section of the research work reveals that the shape of the volcano curve is largely preserved in the entire pH range, indicating that HBE can be employed to identify powerful catalysts for the HER regardless of pH.

Supporting metal catalysts on various supports is another possible design strategy to boost the catalytic activity and stability and improve their utilization. Kinetic Monte Carlo (KMC) simulations were employed in the second part of the thesis work to illustrate that the HER can be enhanced through hydrogen spillover to the support material. This effect happens when the catalysts have a high surface coverage of adsorbed hydrogen atoms under the reaction conditions. Drawing from the insights obtained through KMC, a range of catalysts supported on reduced graphene oxide were synthesized, and their performance in promoting the HER was then compared to their respective pure metal counterparts in alkaline environments. While the support effect is negative for Ag, Au, and Zn, it boosts the HER activity for Pt, Pd, Fe, Co, and Ni. The HER volcano plot, a plot of calculated HBEs vs measured HER activities, is preserved and demonstrates a positive shift in the strong binding region. Thus, this part of the thesis work highlights the potential of metal-support interface engineering in making effective catalysts for HER and provides general guidelines for selecting suitable combinations of catalysts and supports for enhanced electrocatalytic hydrogen production.

Key words: Hydrogen evolution reaction, electrocatalysis, volcano plots, reduced graphene oxide, catalyst support

Scientific field: Physical chemistry

Scientific subfield: Electrochemistry

UDK number: 541.138

Istraživanje uticaja elektrolita i uloge redukovanog grafen-oksida kao nosača metalnih katalizatora na katalitičku aktivnost za reakciju izdvajanja vodonika

Izvod

Efikasna proizvodnja vodonika je ključna zbog globalne energetske krize i zabrinutosti za životnu sredinu, što zahteva identifikaciju katalitičkih trendova za informisane izbore u tehnologijama i materijalima za proizvodnju vodonika. Vulkanske krive reakcije izdvajanja vodonika (HER), prvobitno uspostavljene za kisele rastvore, a kasnije prilagođene za alkalne medije, igraju ključnu ulogu u identifikaciji katalitičkih trendova povezanih sa HER. Prvi deo ove doktorske disertacije fokusira se na sprovođenje sveobuhvatne analize HER katalitičkih trendova na devet polikristalnih monometalnih površina u sedam rastvora, obuhvatajući širok pH opseg od visoko kiselih do visoko alkalnih.

Koristeći teorijskiizračunate energije vezivanja vodonika (HBE) na čistim metalnim površinama i eksperimentalno izmerene HER nadnapone, po prvi put je pokazanoda su relacije vulkanskog tipa pretežno očuvane u širokom spektru pH vrednosti, od kiselih do neutralnih i alkalnih rastvora. Ovo znači da se HBE može koristiti kao deskriptor za identifikaciju aktivnih elektrokatalizatora u širokom pH opsegu, uključujući pH neutralne rastvore. Shodno tome, otkriveno je da Cr ima visoku HER aktivnost u pH-neutralnim rastvorima, koja nadmašuje aktivnostV, Fe i Co. Štaviše, izlaganje metalnih površina visokim anodnim potencijalima može dovesti do pojačane ili potisnute HER, u zavisnosti od metala i korišćenog elektrolita. S obzirom na netrivijalne uticaje oksidacije površine, njeni efekti se mogu posmatrati ili kao promocija HER aktivnosti ili kao HER blokiranje (kao u slučaju Cr i V). Prvi slučaj je posebno primenljiv na Ni i Co u alkalnim i pH-neutralnim rastvorima, što se može pripisati pojačanoj disocijaciji vode na granici fazametal-oksid. Ovaj efekat je značajniji za Ni u rastvorima NaCl, do te mere da posle oksidacije postaje aktivniji od Pt. Stoga, ovaj deo istraživačkog rada otkriva da je oblik vulkanske krive u velikoj meri očuvan u čitavom pH opsegu, što ukazuje da se HBE može koristiti za identifikaciju pogodnih katalizatora za HER bez obzira na pH.

Postavljanje metalnih katalizatora na različite nosače je još jedna moguća strategija dizajna za povećanje katalitičke aktivnosti i stabilnosti i poboljšanje njihovog korišćenja. Kinetičke Monte Karlo (KMC) simulacije su korišćene u drugom delu teze da bi se ilustrovalo da se HER može pospešitiprelivanjem vodonika na potporni materijal. Ovaj efekat se dešava kada katalizatori imaju visoku površinsku pokrivenost adsorbovanih atoma vodonika u uslovima reakcije. Na osnovu uvida dobijenih putem KMC-a, sintetisanje niz katalizatora podržanih na redukovanom grafen–oksidu, a njihov učinak u promovisanju HER je zatim upoređen sa odgovarajućim čistim metalima u alkalnim sredinama. Dok je efekat nosačanegativan za Ag, Au i Zn, on povećava HER aktivnost za Pt, Pd, Fe, Co i Ni. HER vulkanska kriva, dijagram izračunatih HBE u odnosu na izmerene HER aktivnosti, je očuvana i pokazuje pozitivan pomak u regionu jakog vezivanja. Stoga, ovaj deo teze naglašava potencijal inženjeringa granica fazametal-podloga u pripremiefikasnih katalizatora za HER i pruža opšte smernice za odabir odgovarajućih kombinacija katalizatora i nosača za poboljšanu elektrokatalitičku proizvodnju vodonika.

Ključne reči: Reakcija izdvajanjavodonika, elektrokataliza, vulkanske krive, redukovani grafen-oksid, nosačkatalizatora

Oblast nauke: Fizička hemija

Naučna podoblast: Elektrohemija

UDK broj: 541.138

Table of contents

List of symbols

Symbol	Meaning	Dimension
C_{dl}	Double layer capacity	µF cm^{-2}
E	Potential	V
η	Overpotential ($E - E_{eq}$)	V
$\eta_{0.1}$	Overpotential needed for a current density of 0.1 mA cm^{-2} normalized with respect to the real surface area of the electrode	V
H_{UPD}	hydrogen intermediate adsorbed at underpotential	
H_{OPD}	hydrogen intermediate adsorbed at overpotential	
H_{ads}	Adsorbed (index '$_{ads}$') hydrogen atom	
OH_{ads}	Adsorbed (index '$_{ads}$') hydroxyl atoms	
$E_{M\text{-}H}$	Energy of metal hydride formation	eV
$E_{ads}(H)$	Energy of adsorbed hydrogen intermediate	eV
$\Delta_{ads}G_H$	Gibbs energy of adsorbed hydrogen intermediate	eV
$D_{Pt\text{-}H}$	Metal-H_{UPD} bond strength	KJ mol^{-1}
$\Delta H^{0\#}$	Reaction activation energy	KJ mol^{-1}
m	Mass	g
M	Molar concentration	mol dm^{-3}
α	Charge transfer coefficient	
I	Current	A
j	Current density normalized to the surface of the electrode	mA cm^{-2}
j_{geo}	Current density normalized to the geometrical surface area	mA cm^{-2}
j_{real}	Current density normalized to the electrochemically active surface area	mA cm^{-2}
j_0	Exchange current density	
T	Temperature	K, ^{o}C
F	Faraday constant	96485 kJ mol^{-1}
R	Gas constant	8.314 J mol^{-1} K^{-1}
K_i	*Reaction rate constant*	

Chapter one - Introduction

Subjects and research objectives

The most pressing challenges confronting this century are the depletion of non-renewable energy sources, the negative environmental impacts resulting from utilizing these resources, and increasing energy demand. The world relies heavily on fossil fuels to meet its energy demands; in 2019, fossil fuels supplied 84% of global energy consumption, and this pattern is projected to persist in the future. Besides their quick depletion and desiccation, fossil fuel resources also contribute to significant environmental contamination, leading to various outcomes such as the greenhouse effect causing climate change, acid rain, the degradation of sources of potable water, soil pollution, and other undesirable occurrences. Thus, there is a global push to limit the use of fossil fuels and reduce CO_2 emissions, with renewable energy sources being explored as a solution. One important example of a renewable energy source is nuclear energy. Despite its low emission of harmful gases, it has various disadvantages, such as managing nuclear waste, costly maintenance, and safety concerns. As a result, many people are reluctant to adopt it as a renewable energy source. Therefore, it is crucial to find sustainable, clean, and eco-friendly methods for producing energy [1], [2].

To tackle the environmental problem and fulfill the growing energy requirements, numerous renewable energy sources such as solar, wind, thermal, biomass, and wave power are being extensively explored as viable alternatives. Nevertheless, because of their seasonal and regional fluctuations, these renewable energy sources are intermittent, making it essential to develop efficient energy transformation and storage technologies, and a method of temporarily storing energy is required to meet demand [1], [3]–[5]. Developing both primary and secondary renewable energy sources is crucial for successfully transitioning to sustainable energy. While primary sources such as solar, wind, hydropower, and hydrothermal energy are important, secondary sources such as batteries and fuel cells are likewise necessary for energy storage and powering mobile gadgets such as cars. Using batteries for extensive energy storage and transportation is impractical due to the expensive metals and the relatively low energy density per unit weight [2].

In fuel cells, chemical energy created by the reaction of fuel and oxygen from the air is transformed into electrical energy. Although fuel cells utilize various fuels, hydrogen is the most extensively researched and utilized because of its high energy density and ability to generate only pure water as a byproduct of combustion. Despite its abundance, hydrogen is mostly found with other elements in nature. It is necessary to separate hydrogen from its components to use it as fuel. Currently, common hydrogen separation techniques rely on fossil fuels, which are not environmentally sustainable. The alternative is to use an environmentally benign, non-polluting method of extracting hydrogen.

Numerous ecological approaches for acquiring hydrogen rely on electrochemical reactions on hydrogen and oxygen electrodes. The reactions on these electrodes have been under scrutiny for many years since they are critical for several fields of science and industry, ranging from industrial electrocatalytic processes and biological processes to issues regarding corrosion and sustainable energy sources such as fuel cells. Electrocatalysis plays a significant role in improving efficiency, cost-effectiveness and mitigating harmful environmental impacts in all these areas. A viable method for producing hydrogen from water splitting powered by electricity has emerged to transform the significant excess electrical energy from renewable energy sources into clean fuel, i.e., hydrogen (H_2) [3]. Water splitting is thus one of the most straightforward and environmentally friendly solutions to store significantly intermittent

renewable energies on a large scale [4]. By temporarily storing this energy as hydrogen, fuel cells or direct combustion might be used to generate electricity as needed, or the stored hydrogen can be used as a fuel gas [5]–[7].

There are numerous ways to produce H_2, but almost all of them leave behind carbon footprints and are not long-term sustainable. A promising method for producing H_2 that is sustainable and pollution-free is electrochemical water splitting. Electrolysis of water can be carried out with little to no external power by harvesting, storing, and converting renewable energy from the environment [8]. Hydrogen, produced through renewable-powered water electrolysis, is hailed as the ideal fuel for the future. It boasts exceptional energy conversion efficiency, emits zero carbon, yields only water as a byproduct, and possesses high purity. Its gravimetric energy density surpasses gasoline, making it a promising energy source [8]–[10]. To decarbonize our energy systems, hydrogen is once again in vogue, and the hydrogen market is anticipated to increase globally by 47%, from 142 billion USD in 2019 to 209 billion USD in 2027 [10]. It is essential to switch to hydrogen-based fuels instead of conventional ones since hydrogen-fueled vehicles can deliver performance comparable to gasoline-fueled vehicles without releasing CO_2 or other pollutants [11].

During water electrolysis or the water splitting reaction, the cathodic and anodic electrochemical reactions known as the hydrogen evolution reaction (HER) and oxygen evolution reaction (OER) take place concurrently at two distinct electrodes [9], [12]. The theoretical minimum energy needed to split water is described by OER and HER, each of which has its theoretical reduction voltages. This voltage is 1.23 V at ambient temperature compared to the reversible hydrogen electrode [12]. The amount of energy needed for water splitting is substantially larger than the theoretical amount of 1.23 V due to various cell resistances and inefficiencies. This additional energy intake is named the cell overpotential [1]. An appropriate electrocatalyst must be identified to make hydrogen production through the HER reaction economically feasible and competitive with non-renewable methods. Incorporating an electrocatalyst enhances the kinetics of the electrochemical reaction, reduces energy usage, and improves efficiency, leading to more economical and efficient hydrogen production. Therefore, it is crucial to use a catalyst to lower the overpotential required to drive the HER and achieve high energy efficiency for water splitting.

To be viable for practical applications, electrocatalysts employed in water splitting must exhibit improved activity, stability, and cost-effectiveness [3]. Up until now, the most successful electrocatalysts for water electrolysis have been those made from precious metals, for example, Pt for HER and RuO_2 and IrO_2 oxides for OER. However, their scarcity and high cost make it challenging to scale up their use in industrial applications. Due to the current worldwide energy crisis, the cathodic half-reaction, HER, has drawn greater interest in electrochemistry. Researchers are looking for cost-effective methods to produce high-purity hydrogen, specifically through water electrolysis, to create "green" hydrogen using renewable energy sources. Finding new, effective catalysts is required as green hydrogen production is still rather expensive. The HER volcano curves serve as a prime example of how comprehending the trends in HER activity can assist us in this undertaking. The volcano curve is a graphical representation that plots the reaction rate against the free energy of adsorption for an intermediate. It is designed based on Sabatier's principle, which states that an ideal electrocatalyst should have adsorption energy that is balanced, neither too high nor too low compared to the intermediate involved in an electrocatalytic reaction [9].

Trasatti's original work demonstrated a volcano-type relationship between the HER exchange current densities (j_0) of various metals and their respective energies associated with the formation of metal

hydrides [13]. Nørskov *et al*. [15] proposed another form of the HER volcano curve, in which they correlated literature data of the j_0 for the HER in acidic environments with the theoretically calculated hydrogen binding energy (HBE). Nevertheless, this methodology has faced criticism [14], which contends that it is overly simplistic. However, the HER volcano plot continues to be a captivating showcase of HER activity patterns and is extensively utilized by researchers to identify materials with optimal binding energies for the advancement of new HER catalysts. Following a span of around ten years, Sheng *et al*. [15] have constructed HER volcano plots specifically tailored for alkaline environments, employing computed HBE. This volcano plot has generated significant interest among scientists. Nevertheless, it is crucial to consider whether the volcano curve remains consistent across various electrolytes, particularly in pH-neutral solutions, as the investigation of pH-neutral solutions in this context has been lacking in a comprehensive manner. The issue is particularly notable when it comes to seawater electrolysis techniques, which encounter several problems [16]. Additionally, while the impact of surface oxidation on acidic solutions has been taken into account and studied [17], an in-depth examination of the situation of alkaline solutions is missing. In contrast, it is widely known that in an alkaline solution, surface oxidation boosts the dissociation of H_2O at the metal|oxide phase boundary, hence promoting the HER [18], [19]. Hence, the inquiry is whether phase boundary engineering can offer a way to avoid the HER volcano or move its apex from platinum to more readily available and less expensive catalysts.

In the first segment of this thesis work, the trends of the HER activity of nine metals (Au, Ag, Cr, Co, Fe, Pt, Ni, W, and Zn) across seven different electrolytes (0.1 mol dm^{-3} HCl, 0.1 mol dm^{-3} $HClO_4$, 1 mol dm^{-3} KH_2PO_4, 0.5 mol dm^{-3} NaCl, 0.1 mol dm^{-3} LiOH, 0.1 mol dm^{-3} KOH solution, and 1 mol dm^{-3} KOH) will be analyzed. This section of the thesis aims to examine whether volcano plots are preserved across various electrolytes and over a broad pH range. In addition, the influence of metal oxidation on their electrocatalytic HER activity will be investigated. Moreover, an investigation will be conducted to determine whether HBE can serve as a descriptor for identifying electrocatalysts in solutions with a neutral pH. More importantly, the study will help us identify better HER electrocatalyst/s for neutral solutions.

Enhancing the efficiency of metal surface electrocatalytic activity, which is influenced by interactions with various species and intermediates, can also be achieved by combining metal catalysts with carefully chosen supporting materials. Researchers are focused on developing carbonaceous and carbon-free support materials to enhance metal catalyst performance, aiming to improve catalytic activity, stability, and utilization. These materials should exhibit high electrical conductivity, corrosion resistance, favorable interaction with nanocatalysts, stability in electrochemical conditions, and cost-effectiveness. Moreover, they should possess a large surface area to promote effective nanoparticle dispersion while also ensuring secure anchoring to prevent detachment in the course of the electrochemical reaction [20]. It is widely acknowledged that HER activity can be influenced by interfacial processes, such as interfacial water dissociation on metal surfaces decorated with transition metal oxy-hydroxides [18]. While carbon-based materials with high surface area and good electrical conductivity are widely utilized as catalyst support materials, recent advancements have led to the development of various complex carbonaceous materials. Among all carbon-based support materials and carbonic morphologies, graphene stands out as the most promising owing to its exceptional properties, such as exceptionally high surface area, remarkable stability, and outstanding electrical conductivity [20], [21]. Additionally, several investigations show that graphene actively participates in the electrocatalytic reaction while promoting the proper dispersion of catalytic particles. This was notably examined in relation to electrochemical

HER, where increased catalytic activity was achieved by using graphene-based materials as catalyst supports [21]–[23].

The phenomenon of hydrogen spillover has been recognized and studied extensively for a significant period of time [26], [27] and has been deemed highly significant in electrocatalytic processes [24], [25]. Researchers have effectively harnessed the phase boundary and the phenomenon of hydrogen spillover to create highly efficient electrocatalysts for HER. These catalysts have demonstrated their effectiveness in both acidic [26] and alkaline environments [27], [28]. As an illustration, Tan and colleagues [26] conducted an extensive theoretical screening of binary catalysts, focusing on the spillover effect. Through this screening, the researchers identified 11 prospective candidates for novel electrocatalysts. Among them, Pt_1Ir_1-MoS_2 was successfully synthesized and subjected to experimental testing. As anticipated, this catalyst demonstrated remarkable HER activity in acidic conditions.

Gutić *et al*. [21] devised a straightforward procedure for the synthesis of rGO-supported Ni electrodes for HER. The prepared composites (Ni@rGO) exhibited improved electrocatalytic activity toward HER in alkaline media in comparison to pure electrodeposited Ni. This improvement was explained to be caused by the spillover of H_{ads} atoms at the Ni|rGO phase boundary. Moreover, according to Chanda *et al*., the rGO-modified Ni foam electrode has novel HER catalytic activity in an alkaline environment that outperforms Pt/C catalyst under similar conditions. The authors combined empirical measurements and theoretical DFT calculations to arrive at a conclusion that when H_2O is discharged on the Ni surface, H atoms are produced and spilled over onto the rGO support. The rGO support acts as a recipient for the H adatoms, facilitating the continuous cleansing of active sites on the surface of Ni and acting as an alternative route for H_2 generation [23]. Hence, a fundamental inquiry arises regarding the possibility of employing interfacial phenomena, particularly hydrogen spillover, to alter the form of the volcano curve. This alteration would involve shifting its apex towards more-economical HER electrocatalysts or towards greater HER activity.

The second part of the thesis work will focus on examining the impacts of hydrogen spillover on the HER in an alkaline environment. To investigate this, Kinetic Monte Carlo (KMC) simulations will be used to explore the potential for enhancing HER rates by facilitating hydrogen spillover onto the substrate. Building upon the findings obtained from the Kinetic Monte Carlo (KMC) simulations, a set of catalysts will be synthesized utilizing r(GO) as a support material. The HER activities of these catalysts in alkaline conditions will then be evaluated and compared to the activities of the respective pure metal catalysts. Moreover, the effect of hydrogen spillover on the electrocatalytic activity of the supported metals will be examined by constructing volcano plots.

It is anticipated that the results will aid in improving knowledge of how metal oxidation affects the electrocatalytic activities of the considered metals in acidic, alkaline, and neutral solutions. In addition, the results will provide basic information for further research on HER electrocatalysts in neutral solutions. Drawing upon the findings derived from the KMC simulations, along with the utilization of readily available hydrogen adsorption energy data and previous experience with rGO as catalyst support, it is anticipated that the HER activity of M@rGO catalysts will be improved in cases where there is a strong binding between the catalyst and hydrogen.

Chapter two - General background

2.1. Hydrogen production processes

Hydrogen is primarily used in the production of ammonia (specifically, the manufacture of fertilizers), the refinement of petroleum, and, to a lesser extent, the refining of metals [6]. Since hydrogen is not naturally occurring on the globe, around 44.5 million tons of H2 are generated each year utilizing various methods, including steam methane reforming (SMR), coal gasification, and water electrolysis. The first two processes account for 96% of the total hydrogen production, whereas water electrolysis contributes only 4% [29]. The predominant approach for obtaining hydrogen is through fossil fuels, which offers an efficiency rate of approximately 80% and proves to be cost-efficient. The most popular fossil fuel for producing hydrogen is natural gas, where methane and water vapor react at 1000 K to produce hydrogen and CO, which can then react with water at 400 K to produce hydrogen again. SMR inevitably involves the depletion of limited fossil fuels and the release of carbon dioxide [1]. In addition, SMR and coal gasification produce H_2 and other byproduct gases, including CO and CO_2, necessitating a complex purification process [20]. The increase in global temperature due to CO_2 emissions from fossil fuel combustion has led to concerns over rising sea levels and the potential submergence of coastal cities. Furthermore, burning fossil fuels containing sulfur contributes to environmental pollution by forming sulfurous fogs and acid rain in industrialized areas [2].

Thermolysis is another method for obtaining hydrogen through the thermal dissociation of water. It requires a high temperature of 2800 K, an expensive catalyst, and a significant energy expenditure, making it impractical for industrial use. Photocatalytic splitting of water is another method to obtain hydrogen. The electrolyte contains photocatalytic nanoparticles in a colloid suspension, and UV radiation is applied to split the water. This method is environmentally friendly, but its efficiency is low, ranging from 5% to 25%. Massive quantities of H_2 are also produced by hydrolyzing reactive metals and metal hydrides. Yet, this process cannot be favored as a more environmentally friendly way to produce hydrogen because the metal hydride precursors are typically toxic metals made through fine chemical industries that harm the environment [30].

Electrolysis plays a crucial part in the production of H_2, wherein water is separated into its components using an electric voltage and a catalyst. Currently, this method contributes around 5% to the overall industrial hydrogen production, with efficiency for production ranging from 30% to 40%. Future technological developments and the identification of improved catalysts are anticipated to boost this method's effectiveness. The fact that water is readily available as a hydrogen source makes electrocatalytic and photocatalytic water electrolysis the most environmentally friendly methods for producing hydrogen [20].

Various water electrolysis methods have been investigated, and they can be classified based on the electrolytes employed. These include proton exchange membrane electrolysis (PEMEL), alkaline electrolysis (traditional alkaline water electrolysis (AEL) and anion exchange membrane electrolysis (AEMEL)), high-temperature electrolysis (HTE) utilizing solid oxide electrolysis cells (SOEL), and microbial electrolyzers cells (MEC) [7], [9], [12], [31], [32]. Despite being categorized as a slightly different type of electrolysis, MEC is suitable for the mass synthesis of hydrogen using renewable energy sources [32]. Due to its high operating temperature, SOEL technology necessitates significant energy consumption. However, the lower-temperature operating systems AEL and PEMEL have attained high degrees of technological maturity [31]. Currently, it is challenging to produce hydrogen on a large-scale

using water electrolysis by virtue of the high cost of noble and PGM catalysts in acidic conditions and the low energy conversion efficiency of non-noble and non-PGM catalysts in basic conditions. While numerous water electrolyzers have been made experimentally through the development of durable electrocatalysts, most still necessitate cell voltages well above 1.8 V to attain a current density of 200 mA cm^{-2}. Unfortunately, this level of performance falls short of meeting commercial requirements [4].

2.2. Proton exchange membrane water electrolysis

Proton-exchange membrane water electrolyzers (PEMELs) function in acidic environments and consist of an anode and a cathode, with a polymer electrolyte membrane (PEM) separating them. This membrane is usually less than 50 μm thick and serves to separate gases and minimize ionic resistance. PEMEs operate at a temperature of about 100 °C, the same as an AEL. The PEM is frequently made up of Nafion, a prevalent electrolyte used in polymer electrolyte fuel cells (PEFC). Nafion has a satisfactory level of proton conductivity, allowing it to reach a current density of more than 2 A cm^{-2} [32]. Furthermore, PEM has the ability to separate product gases, which boosts the Faraday efficiency of PEMEs to about 100%. Additionally, PEM facilitates operation at high pressure, making it ideal for upscaling and compressing hydrogen gas for transportation purposes. It is possible to increase the operating pressure to approximately 100 bar, but the PEM must be thicker in such instances, resulting in increased proton conductivity resistance. Operating at high pressure reduces the relative size of product gas bubbles and their corresponding Ohmic resistance [32]. Industries are increasingly adopting the PEMEL system owing to its compact design, high system competence (around 52-69%) at high current density, dynamic operation, quick response, operation at low temperatures, and the capability to produce highly pure H_2 at high pressure (30-80 bar) [10]. While PEMEL devices have stricter requirements for water quality, they have the advantage of operating with pure water as the electrolyte solution. In contrast, alkaline electrolyzers necessitate the recovery and recycling of KOH electrolytes [10].

However, the local acidic environment in PEMELs severely restricts the selection of electrocatalysts to a small subset of PGMs like Pt, Pd, IrO_2, and RuO_2. The PGMs such as Pt and Pd are typically used to catalyze the cathodic HER, while electrocatalysts based on Ir or Ru are used for the anodic OER [33]. Moreover, the highly acidic conditions and the use of the PEM systems increases their cost and stability concerns [29]. High catalyst loadings, approximately three mg_{PGM} cm^{-2}, are needed for significant current densities in PEMEL, but this leads to high costs and hampers large-scale implementation. Additionally, recycling PGM catalysts becomes challenging with the use of fluorinated membranes like Nafion in PEM-based electrolysis due to environmental regulations [33]. Acid-based PEMEL cells also face issues with electrolyte vaporization, leading to corrosion of the electrolytic cell and contamination of the produced H_2 gas [29].

2.3. Alkaline water electrolysis

For several decades, starting from the 1920s, the chlorine and fertilizer industries have extensively utilized AEL as a well-established and widely adopted method for H_2 production [10]. AEL consists of an anode and a cathode submerged in an alkaline solution, typically 20-30% KOH. A diaphragm is placed between the two electrodes to enable the flow of hydroxide ions (OH^-) through the KOH solution. This diaphragm also keeps oxygen and hydrogen separated to avoid their recombination [32], [33]. AEL is the most established technology for producing hydrogen commercially up to a megawatt scale. Nevertheless, it has disadvantages arising from the use of a diaphragm. Immersing a diaphragm in an alkaline solution results in high Ohmic loss, which restricts the maximum current density. Furthermore,

the diaphragm cannot entirely prevent the mixing of oxygen and hydrogen. Consequently, it is not possible to attain high pressure, which would have been advantageous for a large stack design [32]. AEL systems have high efficiency (~ 55–70%) but are limited by low heating value, low current density, and low operating pressures, which increase system size and H_2 production costs [10]. In addition, the HER activity in alkaline environments is much lower compared to acidic environments [3], posing a significant challenge for alkaline-HER technology [31]. AEL systems face limitations in using thin diaphragms in order to reduce ionic resistance without compromising gas crossover and overall effectiveness. As a result, the maximum current densities achievable in AEL are around 0.2-0.4 A cm^{-2}, despite the use of concentrated KOH electrolytes (25-30 wt% KOH) [33].

Despite the aforementioned limitations, this kind of electrolyzer is prevalent since it doesn't require costly materials. When compared to PEMEL cells, water splitting in alkaline media allows us to use other affordable metals, such as nickel, avoiding those of the PGMs [3]. Additionally, the KOH solution employed as the electrolyte is inexpensive and provides non-noble metals with greater stability, reducing corrosion and dissolution. This leads to longer-lasting catalytic activity, making it a more attractive option compared to acidic catalysis. Furthermore, the use of alkaline electrolytes has the benefit of generating fewer vapors when operating at high temperatures. This is because alkaline electrolytes have a lower vapor pressure, which helps produce pure H_2 gas [29]. Due to these factors, AEL is widely considered to be the most dependable approach for producing H_2 on a large scale [9], [31]. Both AEL and PEMEL technologies function within a temperature range of 50 to 80 ^oC and at up to 30 bar pressures. These technologies achieve a token stack efficiency of approximately 70% [31] while AEL systems have lower capital costs than PEMEL due to the absence of precious catalysts [7]. As of 2020, the investment costs for AEL systems were in the range of 800 to 1500 € kW^{-1}, whereas PEMEL systems ranged from 1400 to 2100 € kW^{-1}. Additionally, when compared to the PEMEL system, AEL systems have a longer lifetime and lower annual maintenance costs [31].

Chapter three - Trends in electrocatalysts for hydrogen evolution reaction

3.1. Literature review

3.1.1. Hydrogen electrode reactions

The creation of the Voltaic pile, also known as Volta's column, by Alessandro Volta in 1800 is widely acknowledged as the beginning of electrochemistry. Volta's invention of the voltaic pile transformed the study of electricity. Unlike static electricity studied by scientists like Benjamin Franklin, it produced a continuous current. This breakthrough opened up new research avenues, focusing on the chemical production of electricity and the effects of electricity on chemicals. The invention of the pile attracted the attention of Napoleon Bonaparte, and in 1801 he even served as Volta's lab assistant. In 1800, William Nicholson constructed a battery similar to Volta's electric battery and performed several experiments with it. During these experiments, Nicholson and Anthony Carlisle discovered that when they placed the battery poles in the water, they produced bubbles of gas identified as oxygen and hydrogen, which is now considered the first practical demonstration of water electrolysis. In 1801, Humphrey Davy conducted experiments on Volta's column, and he discovered that the generation of electricity through the voltaic pile was not solely dependent on the contact between different metals but involved chemical reactions as well. He used the pile's current to break compounds into their components, and in 1807, Davy successfully separated Na and K through electrolysis. The foundational experiments conducted by Michael Faraday in 1833 paved the way for the subsequent advancements in electrochemistry. These experiments introduced the concept of ions as agents of electrical conduction and established the relationship between atoms and electricity. Faraday published the two vital laws of electrochemistry in 1834, which accurately predict the quantity of product obtained through electrolysis, a process of passing an electric current through a chemical compound or its solution. In 1853, Hermann Helmholtz proposed the first model of the double electric layer, while Gaston Plante created the first lead-acid battery in 1859, which marked an important milestone in the evolution of electrochemistry. During the late 1800s and early 1900s, many researchers contributed to the establishment of modern electrochemistry principles. Following World War II, substantial advancements were made in the domain of electrochemical kinetics. The rapid growth of the electronics industry facilitated the emergence of modern electrochemical techniques, including cyclic voltammetry, chronoamperometry, pulse polarography, electrode impedance, and various others.

Electrochemical reactions involve the transformation of chemical energy into electrical energy or vice versa, requiring an electrolyte and electroactive species. These reactions differ from purely chemical reactions as they transfer electrical energy between the system and an external source, leading to the accumulation or release of chemical energy within the system. Electrochemical reactions are defined as heterogeneous chemical reactions where electron exchange occurs solely at the interface between an electrode's surface and an ion or molecule in the electrolyte. In an electrochemical setup, oxidation and reduction reactions happen in spatially separated regions of the system. These reactions occur specifically at the interface between an electronic and ionic conductor, which is the electrode. Such reactions are referred to as redox reactions, where reduction occurs when a particle in the electrolyte gains an electron, and oxidation occurs when a particle in the electrolyte loses an electron. The process of oxidation is referred to as an anode reaction, and it occurs at the anode. On the other hand, the reduction is known as

a cathode reaction and takes place at the cathode. Electrochemical reactions involve the flow of electric current due to the directed movement of electrons. Moreover, unlike chemical reactions, the course of electrochemical reactions can be changed by adjusting the voltage applied to the electrodes. This allows the reaction to proceed in either the direction of spontaneous (galvanic cell) or the opposite direction (electrolytic cell). The applied voltage determines the direction of the reaction if the voltage is greater than the electromotive force of the cell, an electrolytic cell will occur [34], [35].

Electrochemical reactions typically occur in three stages: the transportation of reactants to the surface of the electrode, the electrochemical reaction itself, where electrons are exchanged between the electrode and the reactant, and the transportation of the resulting products away from the electrode. If multiple electrons are exchanged, the reaction mechanism has multiple electrochemical stages. Apart from the previously mentioned stages of an electrochemical reaction, additional processes can occur. These processes involve the physical or chemical adsorption of reactants, intermediates, or products, including dissociative adsorption and chemical reactions involving reactants, intermediates, or products. Other processes that may occur include surface diffusion of electrochemical reaction products and crystallization, which is typical of metal deposition reactions.

The various stages of an electrochemical reaction occur sequentially, and each stage has its own rate of occurrence. The overall speed of the reaction is determined by the rate of the slowest stage, which is known as the "slow stage." The speed control of an electrochemical reaction can be categorized based on the slowest stage involved. These categories include activation control, where the slow stage is the transfer of electrons; diffusion control, where the slow stage is the mass transport from the electrolyte to the surface of the electrode; reaction control, where a chemical reaction is involved, and the slow stage is the performance of that reaction resulting in the formation of the reactant; and mixed control, which occurs when two different stages have equal slowness. Activation-diffusion control is the most common type of electrochemical reaction control, but it can also be reaction-diffusion and activation-reaction control [34]–[36].

Water electrolysis involves two simultaneous electrochemical reactions at separate electrodes: the cathodic HER and the anodic OER. A typical water electrolysis cell comprises an anode, a cathode, a power source, and an electrolyte. When an electric current is applied, electrons flow to the cathode, producing H_2, while ions migrate across the electrolyte to the anode, where they release electrons to produce O_2. Efficient H_2 production relies on understanding the water electrolysis mechanism. However, the OER efficiency at the anode poses a significant challenge to its widespread industrial implementation. The OER mechanism is more challenging than the HER mechanism in terms of both thermodynamics and kinetics. This is due to the fact that it necessitates the sequential transfer of four electrons as well as the dissolution of O-H bonds to create O-O bonds. Depending on the type of electrolyte employed, water electrolysis can take place in acidic, pH-neutral, or alkaline conditions. Equations (3.1) and (3.2) outline the mechanism of HER and OER in acidic electrolytes, while equations (3.3) and (3.4) describe how these reactions occur in alkaline electrolytes.

$$4H^+ + 4e^- \rightarrow 2H_2 \quad (3.1)$$

$$2H_2O \rightarrow 4H^+ + O_2 + 4e^- \quad (3.2)$$

$$4H_2O + 4e^- \rightarrow 2H_2 + 4OH^- \quad (3.3)$$

$$4OH^- \rightarrow O_2 + 2H_2O + 4e^- \quad (3.4)$$

The HER and OER involve multi-step mechanisms with multiple potential pathways. The mechanism of HER, which is influenced by the pH of the solution [37] can be summarized in acidic environments as follows:

$$H^+ + e^- + * \rightarrow H_{ads} \quad (3.5)$$

$$H_{ads} + H_{ads} \rightarrow H_2 + 2* \quad (3.6)$$

$$H^+ + H_{ads} + e^- \rightarrow H_2 + * \quad (3.7)$$

In an alkaline media, the HER mechanism can be presented in a similar way:

$$H_2O + e^- + * \rightarrow H_{ads} + OH^- \quad (3.8)$$

$$H_{ads} + H_{ads} \rightarrow H_2 + 2* \quad (3.9)$$

$$H_2O + H_{ads} + e^- \rightarrow H_2 + OH^- + * \quad (3.10)$$

Within this particular mechanism, * signifies an unoccupied active site on the catalyst's surface. The reaction initiates with a Volmer step (Equations 3.5 and 3.8), and the intermediate species (H_{ads}) is subsequently eliminated from the surface via either the Tafel reaction (Equation 3.6 and 3.9) or the Heyrovsky reaction (Equation 3.7 and 3.10). Even on Pt catalysts, the HER proceeds significantly slower in alkaline environments compared to acidic environments. This is due to the sluggish H_2O dissociation involved in the Volmer step (3.8). The preferred mechanism depends on various factors, including the surface coverage of H_{ads}. In situations where the surface coverage is high, there is a higher likelihood of the Volmer-Tafel mechanism occurring due to the increased probability of the surface recombination step. Conversely, when the surface coverage is low, the Volmer-Heyrovsky mechanism is favored [9].

3.1.2. Kinetics of the HER/HOR

The overall processes of anodic hydrogen oxidation reaction (forward step) and cathodic HER (reverse step) in acidic and basic conditions can be described as follows.

$$H_2 \rightleftharpoons 2H^+ + 2e^- \quad \text{(in acidic media)} \quad (3.11)$$

$$H_2 + 2OH^- \rightleftharpoons 2H_2O + 2e^- \quad \text{(in alkaline media)} \quad (3.12)$$

Although the HER/HOR reactions may appear simple, they are actually more complicated than outer-sphere electrode reactions because they involve adsorption and the formation of H_{ads} atoms as an intermediate on the surface of the electrodes. The two common mechanisms through which HER/HOR reactions proceed are the Heyrovsky-Volmer or the Tafel-Volmer mechanism. The corresponding reaction steps in acidic and alkaline media are described in eq. 3.5 to 3.7 and eq. 3.8 to 3.10, respectively.

Electrocatalysis is distinct from catalysis in that the electrodes' potential impacts the rate of the reaction. To make things simpler, let's look at how potential influences the speed of a single electron, adsorption-free outer-sphere electrode reaction [38].

$$R \rightleftharpoons O + e^- \quad (3.13)$$

In this case, both oxidized (O) and reduced (R) species coexist in the solution and the rate of the reaction can be expressed as follows:

$$\upsilon = \vec{K} C_R^S - \overleftarrow{K} C_O^S \quad (3.14)$$

In the above equation, $\vec{K}$ and $\overleftarrow{K}$ represent the heterogeneous rate constants (measured in cm s^{-1}) of the anodic and cathodic reactions, respectively. Meanwhile, C_O and C_R indicate the concentrations (in mol cm^{-3}) of the reacting species that are located in close proximity to the interface between the metal and solution (denoted by the superscript 'S').

The resultant overall currents (measured in amperes (A)) can be expressed as:

$$I = \vec{I} - \overleftarrow{I} = \upsilon FA = \vec{K}FAC_R^S - \overleftarrow{K}FAC_O^S \tag{3.15}$$

where A corresponds to the electrode's surface area (measured in cm^2), while F denotes the Faraday constant (measured in C mol^{-1})

Based on the theory of activated complex, the rate constant K is exponentially related to the standard free energy of activation ($\Delta G^{\#}$) as follows:

$$k = k'\exp\left(\frac{-\Delta G^{\#}}{RT}\right) \tag{3.16}$$

The $\Delta G^{\#}$ for cathodic ($\Delta\overleftarrow{G}^{\#}$) and anodic ($\Delta\vec{G}^{\#}$) reactions in electrochemical processes depend on the electrode potential (E) in the following ways:

$$\Delta\vec{G}^{\#} = \Delta\vec{G}^{\#,0} - (1-\alpha)F(E-E^{o'}) \tag{3.17a}$$

$$\Delta\overleftarrow{G}^{\#} = \Delta\overleftarrow{G}^{\#,0} + \alpha F(E-E^{o'}) \tag{3.17b}$$

where $E^{o'}$ is the formal electrode potential and α is the charge-transfer coefficient

Equation 3.15 will be modified, by inserting equations 3.16 and 3.17 and incorporating the standard rate constant k^0, which denotes the situation where the bulk concentrations of oxidized and reduced species are equal ($C_O^b = C_R^b$), to yield the following expression for the total current density:

$$j = \frac{I}{A} = C_R^S Fk^o \exp\left(\frac{(1-\alpha)F(E-E^{o'})}{RT}\right) - C_O^S Fk^o \exp\left(\frac{-\alpha F(E-E^{o'})}{RT}\right) \tag{3.18}$$

At equilibrium (j = 0), the partial current densities for both anodic and cathodic reactions have the same absolute value, which is known as the exchange current density (j_0). Assuming that the surface and bulk concentrations are also equal under equilibrium conditions ($C^s = C^b$), then we can express j_0 as:

$$j_o = Fk^o C_O^{b\,(1-\alpha)} C_R^{b^\alpha} \tag{3.19}$$

Finally, if we assume that mass transport is quick and that the bulk concentrations of oxidized and reduced species are identical and introduce the overpotential ($\eta = E - E_{eq}$, where E_{eq} is the electrode potential at equilibrium conditions), we get the famous Butler Volmer equation:

$$j = j_o\left\{\exp\left(\frac{(1-\alpha)F\eta}{RT}\right) - \exp\left(\frac{-\alpha F\eta}{RT}\right)\right\} \tag{3.20}$$

The eq. 3.14 can be simplified at "low" ($\eta < \frac{RT}{\alpha F}$) or "high" ($\eta >> \frac{RT}{\alpha F}$) values of overpotential. In the first scenario, known as micro polarization region ($|\eta| < 10$ mV at T = 298 K), the exponents in the eq. 3.20 can be expanded using the Taylor series. This expansion results in a linear relationship between *j* and η:

$$j = \frac{j_o F}{RT}\eta \tag{3.21}$$

When the overpotential η reaches sufficiently large values ($|\eta| \geq 50$ mV at T = 298 K), one of the exponents in equation 3.20 becomes significantly smaller in comparison to the other. Consequently, it can be disregarded, leading to the formulation of equations 3.22a and 3.22b for large negative and large positive η, respectively:

$$|j| = j_o \exp\left(\frac{-\alpha F \eta}{RT}\right) \tag{3.22a}$$

$$|j| = j_o \exp\left(\frac{(1-\alpha) F \eta}{RT}\right) \tag{3.22b}$$

If we graphically represent these equations on a semi-logarithmic scale, commonly referred to as Tafel plots [3], they result in straight lines.

$$\eta = a + b \log|j| \tag{3.23}$$

The parameters *a* and *b* are known as Tafel constants. By determining the slope b, we can estimate *a*, and by extrapolating the linear portion of the log|j|/η curve η = 0, we can calculate j_0. Tafel plots are an effective tool for analyzing the kinetics of electrode processes.

Based on the elementary processes (eq. 3.5 to 3.7), it is conceivable to imagine two potential mechanisms in acidic conditions: Volmer-Tafel and Volmer-Heyrovsky [39].

(a) Volmer-Tafel: Initially, protons are discharged (known as the Volmer step), which causes an increase in the amount of H_{ads} on the catalyst's surface. As the amount of H_{ads} coverage increases, there is a greater likelihood that two hydrogen atoms will combine to form a molecule. The rate of discharge eventually reaches equilibrium with the rate of H_{ads} recombination and H_2 production.

(b) Volmer-Heyrovsky: Both methods share the same initial proton discharge. In this particular path, as the H_{ads} coverage on the surface increases (assuming the Volmer-Tafel is negligible), the likelihood of proton collisions with the adsorbed hydrogen also increases. Eventually, a steady state is reached when there is a balance between the proton discharge and electrochemical desorption.

The process of HER seems to exhibit characteristics of both the Volmer-Tafel and Volmer-Heyrovsky mechanisms. The Volmer-Tafel pathway is more common at low overpotentials, while the Volmer-Heyrovsky becomes more prevalent as the overpotential increases [40]. The mechanisms described above can result in three different RDSs: Volmer, Heyrovsky, and Tafel. Both mechanisms exhibit an exponential increase in catalytic current with overpotential, but the rate of increase differs for different RDSs, allowing for the identification of the RDS and the surface mechanism of a catalyst. The Tafel

slope, which remains constant regardless of the catalytic current magnitude, corresponds to a specific RDS among the three mentioned [39].

As already mentioned earlier, the Tafel slope provides information about the RDS and the plausible HER mechanism, specifically related to the electron-transfer kinetics in the catalytic reaction. A smaller Tafel slope indicates a significant increase in current density (*j*) with changes in overpotential, suggesting faster electrocatalytic reaction kinetics. A lower Tafel slope is desirable as it enables higher catalytic current at a relatively lower overpotential. The j_0 refers to the charge transfer that occurs under equilibrium conditions. A greater j_0 signifies an accelerated charge transfer rate and a diminished reaction barrier [39]. Thus, a better electrocatalyst is typically characterized by a lower Tafel slope and a higher j_0 [2] [3]. In the HER potential region at 25°C, different Tafel slopes are theoretically predicted based on the RDS, i.e., 120 mV dec^{-1}, 30 mV dec^{-1}, 40 mV dec^{-1} for the Volmer, Tafel, and Heyrovsky limiting reactions, respectively. Typically, a Tafel slope of 120 mV dec^{-1} is observed in most materials at practical current densities. This is attributed to the slow discharge of protons or the sluggish electrochemical desorption of H_{ads} atoms. However, in acidic environments where the Volmer step is exceptionally rapid, PGMs tend to exhibit a lower Tafel slope of 30 mV dec^{-1}. While the literature commonly associates a Tafel slope of 120 mV dec^{-1} with the Volmer step for HER, Shinagawa *et al*. discovered that this slope can also be obtained when the Heyrovsky step is the RDS at high H_{ads} coverage (>0.6) [41].

Moreover, there is a scenario where different steps proceed at a similar rate, making the Tafel slope analysis uncertain [38]. Watzele *et al*. discussed the challenges and uncertainties in understanding the HER. The authors used electrochemical impedance spectroscopy to study the relative contributions of two pathways (Volmer-Heyrovsky and Volmer-Tafel) to the HER at different electrode potentials and pH values. Their results showed that both pathways contribute similarly to the reaction, and neither dominates [42]. In comparison to reactions involving outer-sphere electrodes, it is essential to remember that the kinetics of electrocatalytic processes are complex due to the formation of adsorbed intermediates. Thus, the Butler-Volmer equation should consider the surface coverage of these species, which often varies with the electrode potential. This makes it challenging to interpret the Tafel slopes in electrocatalytic reactions such as the HER.

3.1.3. Electrocatalysts for the HER/HOR

Due to increasing environmental concerns regarding fossil fuels, renewable energy sources have gained significant popularity. Hydrogen has emerged as a promising energy carrier since the 1970s due to its high energy density and absence of carbon dioxide emissions [43]. Extensive research has been devoted to electrochemical energy conversion devices, such as electrolyzers, fuel cells, and solar hydrogen devices, which offer the potential to establish a secure, environmentally friendly, and sustainable H-based energy system. Electrolyzing water with renewable energy sources is a viable approach to storing renewable electricity as hydrogen gas. However, the thermodynamics and kinetics of water splitting pose challenges, leading to the need for high voltage inputs (1.8-2.5 V) in traditional water electrolysis. The kinetics of electrolytic water-splitting is significantly reduced by the large overpotential resulting from the two-electron transfer pathway for cathodic HER and the four-electron coupled anodic OER pathway [15]. Therefore, to enhance energy conversion efficiency and minimize overpotential and activation energy for both the HER and OER, the utilization of highly efficient electrocatalysts becomes essential. Platinum-based catalysts are effective and stable for both HOR and HER under acidic conditions [44]. Currently, fuel cells and electrolyzers rely on PEMs that operate at low pH (pH = 0). While these systems offer high power densities, they necessitate significant quantities of Pt for the oxygen reduction reaction (ORR) in fuel cells and Ir for OER in electrolyzers. The HER/HOR requires only minute quantities of Pt

due to its exceptional activity [51]. However, for reasons that are not yet fully understood, the kinetics of HER/HOR on Pt are significantly slower in alkaline electrolytes compared to acid electrolytes. This necessitates larger quantities of Pt to catalyze HER/HOR in an alkaline media [15], [45]. In recent years, there has been extensive exploration of HER catalysts based on cost-effective transition metals [43], [46], [47]. Despite extensive research, an inexpensive and readily available electrocatalyst for HER has yet to be discovered. To better comprehend the process, it is necessary to examine the mechanism of HER, which is influenced by the pH of the solution [37].

In acidic conditions, the HER follows the mechanism described in Equations 3.5 to 3.7. However, in alkaline conditions, the HER mechanism occurs according to Equations 3.8 to 3.10. As previously stated in Section 3.1.1, the HER begins with a Volmer step (Eq. 3.5 and 3.8), and the intermediate species H_{ads} is then eliminated from the surface through either the Tafel reaction (Eq. 3.6 and 3.9) or the Heyrovsky reaction (Eq. 3.7 and 3.10). In both mechanisms, the HER can be described as a two-step process, with either the Volmer step involving adsorption or the Heyrovsky/Tafel step involving desorption determining the rate of the reaction. The electrolytes' pH, in particular, has a significant impact on the mechanism [47].

In highly acidic environments, H^+ transfer is fast, but proton diffusion limitations are already evident at pH around 3, and to achieve non-limited H_2 production at the desirable rate, the HER should be conducted at a very low pH. At such low pH, the HER is fast and reversible on Pt and PGMs. Nevertheless, Pt-based catalysts are costly and unsuitable for large-scale H_2 production. Cheaper metals like Ni show promise as alternatives, but they have lower performance compared to Pt and can experience stability problems due to their tendency to dissolve in acids as they are less noble. The HER in alkaline media is considerably slower (even on Pt) compared to acidic media due to the sluggishness of the Volmer step (3.8) that involves the dissociation of H_2O. However, the HER in alkaline media offers the opportunity to use cheaper non-PGMs such as Ni, and alkaline solutions have no diffusion concerns. In practical applications, large-scale water electrolysis to produce H_2 is carried out in concentrated alkalis utilizing stable and inexpensive Ni-based catalysts, whose decreased activity relative to Pt is offset by their lower price [37].

Based on the mechanism of the HER, the HER process involves consecutive and competing steps of hydrogen adsorption and desorption on/from the surface of the electrode. A catalyst surface that exhibits weak binding strength is unable to effectively adsorb the reactant, while a surface with strong binding strength faces challenges in liberating the product to complete the HER process. As a result, an ideal HER electrocatalyst should have well-balanced H bonding and releasing properties in accordance with the Sabatier principle [43]. According to the Sabatier principle, the most active catalyst must adsorb reactive intermediates in a manner that is neither too strong nor too weak.

Several researchers have attempted to make a link between the activities and the physicochemical properties of the electrodes in the HER/HOR. The relationship between the HER/HOR j_o and the Gibbs free energy of adsorption ($\Delta_{ads}G_H$) of the H_{ads}-intermediate on the catalyst surface is one of the most commonly used correlations. The primary reason for this is that the H_{ads} atoms are the key intermediate in the HER/HOR in accordance with equations 3.5–3.10. In the late 1950s, Parsons proposed a relationship between the HER activity in terms of j_o and the $\Delta_{ads}G_H$, resembling a Volcano curve where the maximum HER activity occurs when $\Delta_{ads}G_H$ is equal to 0 eV [48]. However, he couldn't include experimental data due to the unavailability of tools to estimate $\Delta_{ads}G_H$. Krishtalik's gas-phase measurements of M-H bond strength improved this limitation, and Trasatti was able to draw a Volcano curve (Figure 3.1a) for over 30 different metals [13]. The volcano plot was subsequently modernized by

Nørskov *et al*. [49] (Figure 3.1b) by incorporating HER activities in acidic media and considering DFT-calculated hydrogen adsorption energies, and it was reviewed by Quaino *et al*. [17]. The volcano plot based on DFT energies was also shown to be applicable to HER in alkaline media [15] (Figure 3.1C). The HER in Pt is thermoneutral; Pt is located at the apex of the Volcano plot. Nevertheless, even with optimal $\Delta_{ads}G_H$ value does not ensure that metal will be an effective catalyst for HER, as evidenced by the example of Cu in [17]. There are some differences in the dependences of j_o on the $\Delta_{ads}G_H$ plotted by different authors as a result of the use of different methods for calculating the $\Delta_{ads}G_H$ value. The $\Delta_{ads}G_H$ in the old volcano plot (Figure 3.1a) [13] is based on the M-H binding energy of the corresponding metal hydrides, and in the modern volcano plots (Figure 3.1b, c) it is based on DFT calculations [15], [49].

According to the volcano curves, noble metals or the PGMs with $\Delta_{ads}G_H$ close to zero have the highest catalytic performance for HER [3] in line with the prediction by Parson [48]. Being located at the apex of the volcano plot, the HER activity of Pt outperforms other metals due to its unique characteristic of having a thermo-neutral reaction at the equilibrium potential. In contrast, metals located on either side of the "volcano plot" do not exhibit this favorable property [13], [49]. On the left side of the volcano maxima, the rate of the reaction declines as the hydrogen chemisorption energy (ΔE_{Had}) decreases because there are insufficient surface sites available for H + H recombination. On the right side of the maxima, the reaction rate decreases as ΔE_{Had} increases because as the hydrogen becomes more unstable on the surface, proton transfer becomes increasingly challenging. The volcano plot encompasses *sp* metals, coinage metals, and d-metals and represents their HER catalytic activities. These activities, measured j_0, vary over six orders of magnitude, mainly due to the differences in their affinity towards hydrogen adsorption. The key requirements for an effective HER catalyst are: (i) having a ΔG value near zero at the equilibrium potential (in line with the Sabatier principle), (ii) the metal's d-band should include the Fermi level, and (iii) a strong and long-range interaction must exist between the metal's d-band and the hydrogen 1s orbital [17]. For *sp* metals, the rate-determining step in the HER process is the Volmer reaction [17]. The Pt and PGMs (such as Rh, Ir, Ru, and Pd) are by far the best catalysts for HER at very low pH [7], [37], Pt being widely used to compare the performance of other HER electrocatalysts [43]. Pt successfully catalyzes the HER with a Tafel slope of 30 mV dec^{-1} and at low overpotential near zero [50]. In the past few decades, scientists have studied the HER on a variety of transition metals, including Cu, Au, Mo, Pd, Rh, Fe [15], [51], [52], Ag, Pt, Pd, Co W [15], Ni [15], [53], [54], and Ti [55].

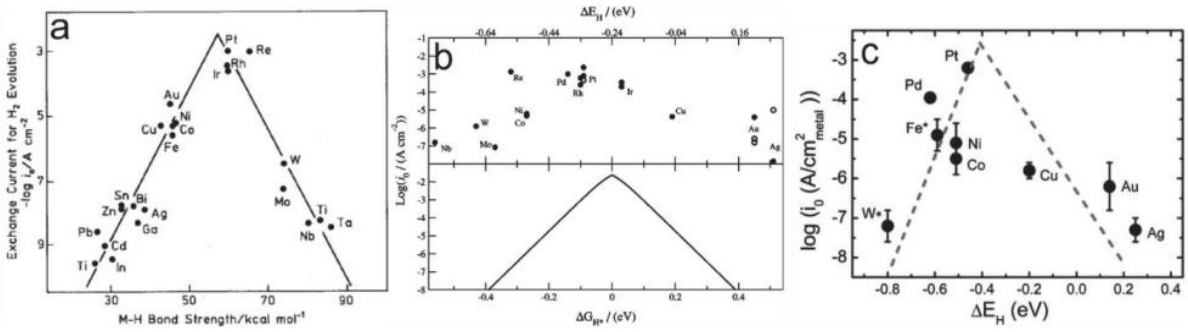

Figure 3.1 The volcano plots: in a) acidic media (j_0 *vs* $E_{M\text{-}H}$) [13], in b) acidic media [49] and c) alkaline media [15]. For b and c, j_0 is plotted against DFT calculated energy of hydrogen absorption on the catalyst.

Noble metals and PGMs are the most efficient electrocatalysts for HER. However, their high cost and limited availability have spurred investigations into methods to either substitute them or improve their performance by combining them with more economical transition metals [50]. Research is actively focusing on three types of non-PGM electrocatalysts: transition metal complexes, alloys (binary, tertiary

and etc.), and carbonaceous nanomaterials. Among the various binary systems studied thus far, excluding the PGMs, the electrocatalytic performance of nickel-molybdenum (Ni-Mo) alloys has been found to be the most efficient for HER [22]. Among the non-PGM electrocatalysts, transition metal complexes MX (where M is Ni, Mo, Co, W, and X is Se, S, C, P, N, etc.) are also one of the most practical options due to their high electrocatalytic activity and electrochemical stability. Metal selenides [56], phosphides [57] [58], nitrides [59], and carbides [60] have been investigated for catalyzing HER. Transition metal sulfides are highly promising options for the HER because they offer a combination of affordability and ease of preparation [50]. Molybdenum sulfide materials are among the best catalysts for HER because of their high activity and superb stability [61]. Transition metal carbides (TMCs) (Mo_2C and WC) have been shown to have potent catalytic activity against HER because of their high electrical conductivity, H-adsorption capabilities, and d-band electronic density state (which is close to that of Pt) [3]. Yet, compared to Pt surfaces, the HER j_0 for TMCs' is 2-3 orders of magnitude lower [62]. Several strategies have been employed to improve the performance of materials for the HER. These include modifying the structure to increase surface active sites, introducing dopants (both cation and anion), and regulating crystallinity [50]. Additionally, an interesting approach is the utilization of core-shell, over-, and sublayer, doped, and supported structures, aiming to replace pure Pt as an electrocatalyst for HER [63].

An important approach to enhance the catalytic activity, stability, and utilization of metal catalysts (nanoparticles) is to employ different supports, and the current scientific research is primarily focused on the development of different types of catalyst support materials, both carbon-based and carbon-free [20]. Furthermore, modifying the chemical and physical properties of the support material for carbon-based catalysts is crucial as carbon commonly plays a vital role in numerous catalysts, including Pt electrocatalysts [50]. Another crucial area of research is the development of meticulously controlled nanocomposite and nanostructured catalysts with proper design for promoting HER [64]. Furthermore, the utilization of single-atom catalysts enables the reduction of precious metal loading [63].

While bulk/polycrystalline and single-crystal surfaces provide valuable insights into the HER mechanism, they are not practical for commercial H_2 production. In effect, the usage of catalysts is greatly improved by the high dispersion of catalysts on a support material [31]. Alkaline HER activities can also be improved by pairing Pt with water dissociation promoters, which is pertinent for utilization in real-world industrial applications. However, because of their inexpensive cost and availability, non-noble metal based HER electrocatalysts have attracted a lot of attention [65]. Furthermore, research has indicated that the kinetics of HER is significantly influenced not only by the nature of the electrode (crystallinity and orientation) but also by the pH and composition of the electrolyte [65], [66].

3.1.4. Electrochemical behavior of single-crystal and polycrystalline metal electrocatalysts in an acidic medium

As discussed in Section 2.4, the HER is quick on Pt and PGMs (such as Pt, Ir, or Ru) under lower pH (acidic) settings because of their resistance to corrosive and aggressive acidic environments and their insolubility in acids. As a result, Pt and PGMs have been recognized the most effective electrocatalysts in acidic media, with Pt being one of the quickest electrocatalysts known. It is important to note that various elements, such as the electrolyte's composition and the electrode's crystal shape and orientation (single-crystal, polycrystalline, amorphous, etc.), might have an impact on the kinetics of the HER. Due to its remarkable electrocatalytic performance, a majority of research efforts are currently dedicated to investigating the HER mechanism occurring on the Pt surface in acidic environments [65]. However, the high cost and limited availability of PGMs render them impractical options, leading to ongoing research efforts to discover affordable electrocatalysts. HER volcano plot shows that very few metals, mostly noble metals, have the ability to effectively catalyze the HER on their own. Thus, developing alloys that

combine different metals, including those with strong and weak hydrogen bonds, is a practical approach to using affordable metals for electrocatalysis in HER [56].

Not many published reports specifically address the sensitivity of the structure of (single crystal) metals to the HER/HOR. The HER/HOR on platinum single crystals in an acidic solution was studied by Marković *et al*. [67]. The results revealed that, at constant temperature (274 K), the HER/HOR activity of the crystal facets in terms of j_0 increased in the order Pt(111) << Pt(100) < Pt(110). Moreover, the j_0 on Pt(110) surface was found to be three times that of the Pt(111) surface. The same order of HER/HOR catalytic activity of Pt(*hkl*) in both acidic and alkaline electrolytes was reported by [67], but there are significant differences in the actual rates of these reactions, as depicted in Figure 3.2. Using the Tafel slope measurements, the Tafel step with a slope of ~30 mV dec^{-1} and the Heyrovsky step with a slope of ~40 mV dec^{-1} are believed to be the RDSs for Pt(110) and Pt(100), respectively. However, none of the projected values from the microkinetic analysis match the Tafel slope value of 74 mV dec^{-1} for Pt(111). Tafel slope values of about 30 mV dec^{-1} are typically measured for polycrystalline platinum, which closely matches the anticipated values for the Tafel step being the RDS [65], [68]. Moreover, the Volmer-Tafel mechanism with the Tafel step as the RDS has been identified for HER on Pt(111) by using complex and intricate DFT calculations [69]. The HER on the low-index planes of single-crystal Au electrodes was studied by [70] in order to determine the degree of sensitivity of the reaction rate on the surface crystallographic structure. The catalytic activity in acidic media was found to proceed in the order Au(111) > Au(100) > Au(110), with the most and least active planes differing by an order of magnitude. The authors suggested that the reaction follows a similar mechanism on the three investigated Au facets and that the catalytic activity rises with surface atomic density. The investigation of the adsorption step (the discharge of the first proton) of the HER on Ag(111) and Ag(110) revealed that Ag(111) had linear Tafel slopes in acidic environments, whereas Ag(110) had a distinct shift in slope. Moreover, the HER current density on Ag(110) was found to be considerably lower than on Ag(111) [71]. Brisard *et al*. conducted a study on Cu(111) and Cu(100) surfaces to investigate the ORR as well as the HER/HOR reactions in acidic conditions. They found that at low overpotentials, the HER reaction was more prominent on Cu(111) compared to Cu(100). Nevertheless, the HER becomes more significant on Cu(100) surfaces at higher overpotentials. This is attributed to the influence of the surface structure on the adsorption of spectator species (such as (bi)sulfate anions) that impede the HER process on the investigated surfaces [72].

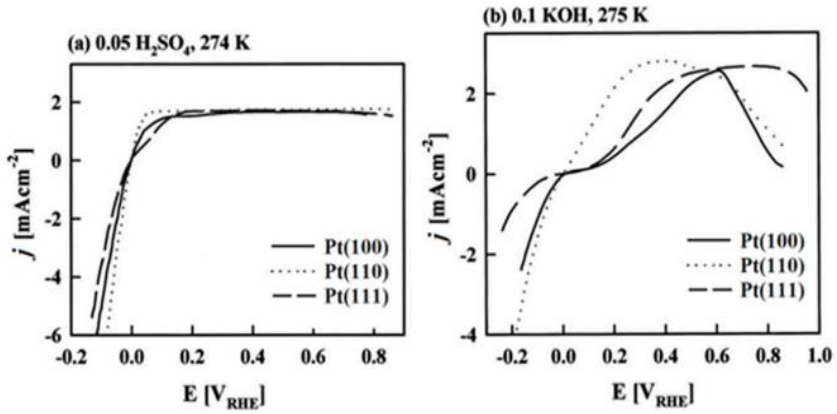

Figure 3.2 The HER/HOR current potential polarization curves on single crystal platinum electrodes, at a potential scan rate of 20 mV s^{-1}, in (a) acid and (b) alkaline media [37].

The majority of the old articles from which the experimental data on the HER at single crystal surfaces originate do not give a more in-depth, atomic-level explanation of why one metal single crystal facet demonstrates superior HER performance compared to others. Nevertheless, the variation in activity between the Pt facets was explained in terms of structure-dependent adsorption energies of the active intermediate. In particular, hydrogen can either be adsorbed relatively strongly (underpotential-deposited hydrogen, H_{UPD}) or relatively weakly (overpotential deposited hydrogen, H_{OPD}) on a Pt surface. The more-weakly bound H_{ads} intermediate (H_{OPD}), which serves as the reactive intermediate, is formed on potentials close to or negative to the Nernst potential of the hydrogen electrode [37]. Although the precise function of H_{UPD} remains unclear, it has been suggested that H_{UPD} competes with H_{OPD} for identical adsorption sites and that it changes its adsorption energy [73]. It has already been reported that the H_{UPD} rates are much faster (smaller charge transfer resistance R_{ct}) in acid compared to alkaline electrolytes [74]. There is no doubt that the energy of H adsorption (E_{ads}(H)) varies with H_{ads} coverage, mostly due to the repulsion between two nearby H_{ads} atoms [37]. The experimental findings and theoretical models were harmonized by a model which suggests the existence of an unspecified quantity of H_{UPD} in deeper potential wells, specifically in a subsurface state. This arrangement allows for the availability of top sites for the adsorption of H_{OPD}. Studies on polycrystalline metals are substantially more prevalent, primarily due to the abundance of available sites for H adsorption. As a result, there are numerous options for the reactive intermediate state in these systems [73].

3.1.5. Electrochemical behavior of single-crystal and polycrystalline metal electrocatalysts in neutral and alkaline medium

PGMs still have excellent HER performance in alkaline environments, but the HER/HOR activity of PGMs declines by ~ 2 orders of magnitude, being in the range from 0.55 to 0.69 mA cm^{-2} for polycrystalline Pt and Pt/C catalysts in lower concentration alkaline solutions [38]. But then again, the practical applications of PGMs are limited because of their high price and limited availability. The utilization of alkaline electrolytes like KOH and NaOH offers an economically viable solution for industrial applications, as it enables the utilization of non-PGMs as electrocatalysts. Additionally, alkaline electrolytes provide enhanced stability for non-PGMs, eliminating the risks of corrosion or dissolution [75]. Non-noble metals have been employed as cathode catalysts for the HER in alkaline water electrolysis for many years. Initially, iron was utilized, but it was eventually substituted with steel. In recent times, there has been a growing interest in developing HER catalysts using abundant and cost-effective transition metals like Ni, Co, Fe, W, and Mo in alkaline environments as a substitute for noble metal catalysts [29], [75]. In particular, there has been a transition toward the use of Ni-based catalysts due to their superior corrosion stability in alkaline environments compared to steel, despite slightly lower activity levels [38]. Until recently, the dependence of the rate of HER on the electrolyte pH has been largely ignored due to the lack of suitable experimental setups for accurately assessing the rapid HER kinetics in acidic media.

However, it has been observed over time that the pH effect has a greater impact on the most active metals. For instance, when moving from pH = 0 to pH = 13, the HER activities of Pt, Ir, and Pd drop by factors of 210, 120, and 90, respectively [76], [77]. On the other hand, non-PGM electrodes, such as Au, Ni, or Cu, experience a lesser impact, with a 10-fold reduction in HER activity [13], [15], [77]. Additional studies conducted in neutral solutions have shown that the decrease in activity is in direct correlation with the pH level [78]. For a variety of electrocatalysts, including carbon-supported nanoparticles, and single and polycrystalline electrodes, various experimental results show that their HER activity relies on pH. A consistent trend is observed across these surfaces, where the activity progressively declines with the rise in pH [79]. Accordingly, distinct kinetic parameters (j_0, Tafel slope, and reaction activation

energy, $\Delta H^{0\#}$) for Pt(111) electrodes in acidic and alkaline solutions are reported by [80] as shown in Table 3.1.

Table 3.1 Kinetic and thermodynamic parameters for Pt(111) surfaces in acid (0.1 M $HClO_4$) and alkaline (0.1 M NaOH) conditions; $\Delta H^{0\#}$ $D_{Pt\text{-}H,}$ and ΔH_{HUPD} represent reaction activation energy, metal-H_{UPD} bond strength and enthalpy of adsorption for H_{UPD} respectively [80].

Pt(111)	***jo* (mA cm^{-2})**	**Tafel slope (mV/dec)**	**$\Delta H^{o\#}$ (KJ/mol)**	**ΔH_{Hupd} (KJ/mol)**	**$D_{Pt\text{-}H}$ (KJ/mol)**
Acid	0.21	- 74	18	- 42	~240
Alkaline	0.01	- 150	46	- 41	~240

A sharp decline in activity in the HER studies on Pt(111), Au(111), and polycrystalline Ir (Ir_{pc}) with the increase in pH from pH = 1 to 13 (Figure 3.3 (a-c)) is reported by [81]. The current potential (*I-E*) curves for Au(111) in acidic pH exhibit a shift towards greater overpotentials compared to Pt(111) and Ir_{pc}, despite having the same current density. This behavior, also observed by other groups [66], indicates that the mass transport of reactive H_3O^+ species is responsible for regulating the HER under these experimental conditions.

However, above pH=5 and potentials negative of -1.5 V for Au(111), -0.9 V for Pt(111), and -0.7 V for Ir_{pc}, the polarization curves for each metal become pH-independent, showing that under these circumstances, the HER currents are primarily regulated by the pH-independent transformation of H_2O to H_2, and thus the primary distinction between the HER in alkaline and acidic media is that in alkaline solutions the kinetics of the HER is constrained by a slow water dissociation step [79]. The idea of reducing water molecules is reinforced by the results obtained from polycrystalline Ni and Pt modified with Ni [82]. Examining the impact of surface geometry on the kinetic rates is another way to investigate how pH affects the HER. In particular, while the activity of Pt low-index single crystal surfaces varies only slightly in acidic media, it varies significantly in alkaline solutions [67], [73], [83]. Scanning tunneling microscopy (STM) images of the as-prepared Pt(100), Pt(110), and Pt(111) electrode surfaces have different surface morphology [81] and the degree of activity Pt(110) > Pt(100) > Pt(111), was directly related to the density of defects present on the surface [73]. According to Danilović *et al*. [84], the highly defected Pt(110) exhibits higher activity compared to the relatively "perfect" Pt(111). Moreover, the variation in activity is explained by the fact that the adsorption of hydroxyl and H_{UPD} species is influenced by the structure of the crystal surface, which ultimately impacts the formation of the electroactive intermediate, H_{OPD} [85]. For a more thorough understanding of the HER's structure-activity relationship, Marković *et al*. [81] have conducted a comparative study between the HER activity of Pt(111) and Pt(111) decorated by electrochemically deposited Pt islands (Pt-islands/Pt(111)). The activity of the Pt-islands/Pt(111) surface for the HER in alkaline media was found to be approximately 5 to 6 times higher compared to the pristine Pt(111) surface. However, in acidic media, the HER activity enhancement on the Pt-islands/Pt(111) surface was only around 1.5 times. This pronounced pH effect demonstrates that the low-coordinated single-crystal Pt atoms significantly affect the rate of the HER RDS in an alkaline solution, and it has been proposed that the dissociative adsorption of water is promoted by the low-coordinated Pt atoms in alkaline solutions [81]. Hence, in the case of materials possessing ideal M-H_{ads} energetics, such as Pt, it is possible to enhance the surface reactivity for the HER by strategically designing active sites that facilitate highly effective dissociative adsorption of H_2O.

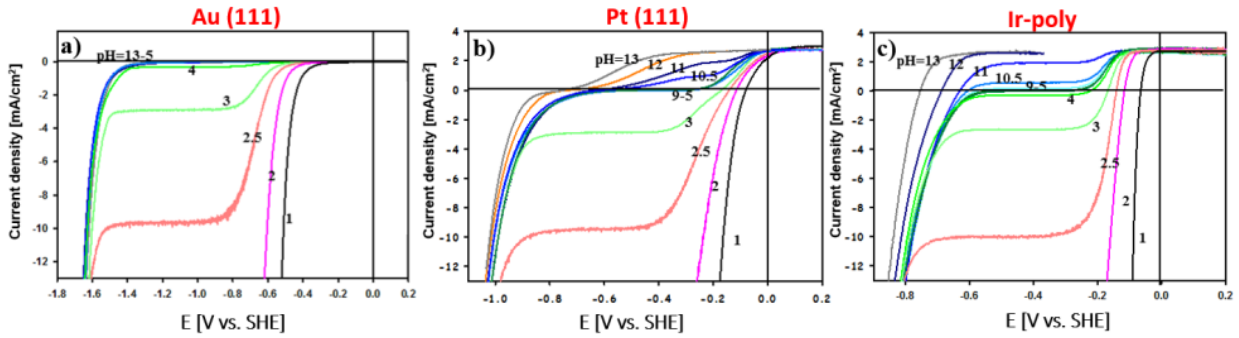

Figure 3.3 pH-dependent polarization curves for (a) Au(111), (b) Pt(111), and (c) Ir-poly. The experiments were conducted using 0.1 M $NaClO_4$, which was purged with H_2 gas and pH adjusted with the addition of $HClO_4$ or NaOH [79].

In the current literature, there are several prevailing hypotheses explaining why HER kinetics are slower in alkaline solutions than in acidic ones: (i) The HBE is pH-dependent [15], [78], [86]. This concept has helped to explain numerous experimental findings, even though some inconsistencies still exist [78], [86], [87]. For illustration, if the HBE were to increase, it would account for the positive potential shift of H_{UPD} on PGM-electrodes when they change from an acidic to an alkaline electrolyte. Nevertheless, despite demonstrating considerably lower HER activity in alkaline electrolytes than in acidic ones, the Pt(111) surface remains largely unaffected by this shift caused by the H_{UPD} [77], [88], [89]. Furthermore, if there were a universal increase in the HBE with pH, it would result in an enhancement of the HER electrocatalytic activity of metals that weakly bind hydrogen (such as Au). However, this contradicts the experimental observations [77]. (ii) The proton donor (H_3O^+ or H_2O) is pH dependent [79]. In other words, the proton donor can switch from H_3O^+ in an acidic environment to H_2O in an alkaline environment. (iii) At the electrode|electrolyte interface, there is a pH-dependent water reorganization energy: According to Koper *et al.* [90], the water-reorganization energy related to proton-electron transfer would be higher because interfacial fields are stronger in an alkaline environment. Recent studies by Rossmeisl *et al*. have associated the reduction in HER activity at high pH with changes in the configurational entropy of the proton as it crosses the outer Helmholtz plane [91]. Furthermore, buffer molecules could ease H_3O^+ transport limitations to the interface or serve as proton donors [92]. To gain a comprehensive understanding of the effect of pH on HER, a deeper comprehension of the structure of the H_{ads} intermediates, and H_2O adlayers on the surfaces of the catalyst is required. Improved computational methods that account for pH effects and go beyond HER activation energies are necessary.

Strong acidic/alkaline electrolytes have been largely used in electrocatalytic HER research. Nevertheless, neutral or near-neutral electrolytes offer several advantages, such as reduced corrosion, an increased range of electrocatalysts, and avoid the need for costly anion/cation exchange membranes and acidic/alkali resistant catalysts. It is worth mentioning that the use of cost-effective earth-abundant catalysts under neutral pH conditions is a desirable goal for feasible solar-to-hydrogen fuel systems [46], [93]. Moreover, pH-neutral electrolytes enable the utilization of bifunctional catalysts, simplifying electrochemical systems and potentially resulting in notable cost reductions. Furthermore, neutral environments facilitate the utilization of seawater as an electrolyte and the desegregation of metal-based electrocatalysts with biocatalysts to produce biofuels [9].

The mechanism of HER in neutral solutions is proposed to be similar to that of the alkaline media proceeding through the adsorption step (Eq. 3.8) followed by the desorption steps (either Eq. 3.9 or 3.10). The effectiveness of the reaction steps is largely determined by the bonding of H_2O, OH, and H to the

catalyst's surface [81]. In pH-neutral electrolytes, the HER process involves a two-step reduction process, whereas, in strongly acidic or alkaline electrolytes, the reduction occurs in a single step with H_3O^+ ions or H_2O molecules, respectively [94]. Figure 3.4 illustrates that H_3O^+ ions are the main reactants involved in the initial reduction phase of the HER process. This occurs at low cathodic overpotentials, and as the overpotential increases, the HER process becomes diffusion-controlled [95] exhibiting constant current. Only at higher overpotentials does the second reduction phase take place, during which the principal reactants in HER change from H_3O^+ ions to H_2O molecules, leading to a steady rise in reduction current [93]. For instance, the HER electrocatalytic performance of Pt in the pH range of 5 to 9 does not align with the predicted shift in thermodynamic potential (i.e., -59 mV/pH) [96]. Initially, Conway *et al*. [97] found that the reactant changes from hydronium ion to water at a pH nearly > 5. Subsequently, the Mayrhofer group [98] studied how mass transport affects pH changes at the electrode-electrolyte interface and found that even at reasonable reaction rates, the pH of unbuffered or inadequately buffered electrolytes at the vicinity of the electrode surfaces differs substantially from bulk electrolytes, especially when the bulk electrolyte pH is between 4 and 10.

Furthermore, Takanabe's research team uncovered that the HER processes in near pH-neutral solutions are influenced by the nature of the reactants, the state of the electrolytes (buffered or unbuffered), and their concentrations [82], [95], [96]. They investigated the relationship between HER and pH using various unbuffered 0.5 M Na_2SO_4 solutions and found that HER activity is based on the activity of H_3O^+ ions rather than the kind of supporting electrolyte. Depending on theoretical diffusion-limited current density, the authors categorized HER activity into three pH regions: acidic (1-5), neutral (5-9), and alkaline (9-13) [96]. The neutral region was found to have insufficient H_3O^+ ions, limiting HER activity. The supply of H_3O^+ ions can be made consistent by buffered electrolytes, which helps overcome the limited H_3O^+ ion availability near electrode surfaces [95]. Moreover, research on electrocatalysts using buffers to maintain neutral pH and ionic salts for high solution conductivity has shown that buffers can enhance HER activity, possibly by serving as a proton donor [99]. The HER activity in pH-neutral and alkaline conditions is significantly different, even though they are both thought to be influenced by the RDS of water-dissociation. Some studies suggest that the HER activity is better in neutral electrolytes, while others claim the opposite. The mechanisms for HER in pH-neutral solutions remain highly debated, as described in several representative studies [93]. Conway *et al*. proposed that the weakly bonded H_{OPD} species, rather than strongly bonded H_{UPD} ones, are reaction intermediate in HER, and higher H_{OPD} on the surface of Pt leads to better HER activity [97], [100]. They found that in alkaline solutions, as opposed to acidic ones, the surface coverage of H_{OPD} is significantly lower, making the Volmer step the RDS and slowing the reaction rate in the alkaline media.

Yan and colleagues proposed that HBE can serve as the sole factor to account for the gradual reduction in HER activity observed across PGM catalysts in different buffer electrolytes with a pH ranging from 0 to 13 [78], [86]. According to them, HBE is larger in higher pH electrolytes, resulting in intermediate HER kinetics in neutral electrolytes. Additionally, they recommended OH^- can tune the HBE and affect HER activity. Shao *et al*. [101] conducted a study using surface-enhanced infrared absorption spectroscopy and found that the HBE of Pt catalysts is influenced by the modified electric field, H_{ads} coverage, Pt-H_2O, as well as H_{ads}-H_2O interactions, leading to a weakened HBE with increased pH levels; this can cause slower reaction kinetics and lower HER activity in high pH environments. However, the HBE descriptor is not sufficient to explain the HER catalytic behaviors on well-defined Pt(111) surfaces [90]. According to Marković and Koper, the HER catalytic behavior on such surfaces is also determined by the presence of adsorbed hydroxyl molecules [19], [79], [90]. They suggest that the activity of HER

in alkaline solutions can be enhanced by carefully balancing the rate of H adsorption and OH desorption. Despite debates over the precise mechanisms involved, the combination of $Ni(OH)_2$ (for the strongest OH_{ads} bond strength) with Pt (for optimal H_{ads} adsorption free energy, $\Delta_{ads}G_H$) has been found to significantly enhance the activity of the HER in alkaline electrolytes. This bi-functional tuning approach has also been favorably applied to pH-neutral solutions, suggesting that it is a viable method for speeding the kinetics of HER in pH-neutral solutions [93], [102]. Recent studies have concentrated on the development of composite catalysts to reduce the use of expensive PGMs in acidic or alkaline electrolytes for efficient HER. However, only a few studies have explored their use in neutral electrolytes, which goes against the goal of developing cost-effective large-scale H_2 production [93].

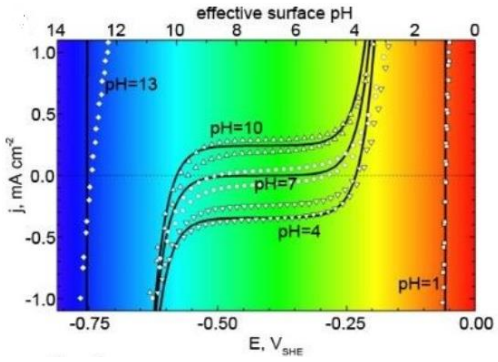

Figure 3.4 The pH-dependent polarization curves obtained by cyclic voltammetry (rotation speed: 1600 rpm; potential scan rate: 10 mV s^{-1}) in H_2-saturated, unbuffered electrolytes of bulk pH = 1 (□), 4 (▽), 7 (O), 10 (Δ) and 13 (◊) [98].

3.1.6. Supported HER catalysts (in acidic and alkaline media)

3.1.6.1. The effect of interfacial processes on the HER

As stated earlier, the HER/HOR catalytic activity of Pt in acidic media is exceptionally high, and a minimal quantity of the catalyst is needed for the reactions to take place [76], [85], [103]. Conversely, it has long been known that the HER/HOR kinetics on Pt is considerably slower in alkaline media than in acidic media [104], [105]. Moreover, unlike in acidic media, the Tafel slope obtained for Pt electrodes in alkaline solutions is around 120 mV dec^{-1}, signifying that the Volmer or the Heyrovsky step is the RDS [41]. In accordance with the Sabatier principle [69], [106], mechanistic investigation on the HER [18], [78], [103], [107], [108] have historically linked reaction rates to thermodynamic descriptors, predominantly the H binding strength of the metal electrodes. Using carbon-supported Pd, Pt, and Ir electrodes, Durst *et al*. demonstrated that the HER/HOR j_0 of the electrodes decreased by a similar factor while going from low (pH = 0) to high (pH = 13). Similar research on the pH dependence of HBE and HER/HOR activities on Ir/C, Pt/C, Rh/C, and Pd/C in various buffer solutions (pH from 0 to 13) [63] revealed a universal correlation between log (j_o) and HBE demonstrating that HBE is the primary descriptor for HER/HOR activities and that the catalysts may share the same fundamental steps and RDSs. While investigating polycrystalline Pt disk electrodes at various pH levels, Sheng *et al.* revealed that the HER/HOR activity of Pt is shown to decline with pH, while the HBE linearly increases with the pH [78]. The basis of the pH-dependent HER/HOR kinetics has been hypothesized to be a pH-dependent HBE [76], [78]. The evidence for such a pH-dependent HBE has particularly been gathered from the pH-dependent changes of the voltammetric peaks in the polycrystalline Pt hydrogen region (i.e., H_{UPD} region). Yet, the molecular-scale origin of the pH-dependent HBE has continued to be elusive, and Koper *et al*. claim that the characteristics of the "hydrogen" peaks on polycrystalline Pt are also more likely to

be influenced by the adsorption of oxygenated species than by the adsorption of hydrogen alone and thus their peak potentials cannot be explicitly used to represent HBE. Moreover, the H_{UPD} on a Pt(111) electrode does not change significantly with pH, yet the HER/HOR kinetics still exhibit a very strong pH dependence.

Marković *et al*. [81] proposed that in addition to the H adsorption energy, the type of proton source (H_3O^+ or H_2O) and the presence of spectator species are important in understanding the role of pH in the HER/HOR. They suggested that in alkaline environments, HER/HOR require different types of sites for H_{ads} and OH_{ads}, and the presence of OH_{ads} can affect the kinetics by rivaling for the same surface sites (blocking effect) or modifying adsorption energy (energetic effect) of the active intermediates [79], [81]. They also found that the isosteric heat of adsorption for OH_{ads} on Pt(111) surfaces is pH-independent, indicating that the pH-sensitive barrier to water dissociation limits the effectiveness of HER in alkaline conditions [89].

Alloying Pt with water dissociation promoters such as Ni and Ru is a popular technique to enhance the alkaline HER activities [3] [80]. Through the process of alloying, the HER activity of Pt is enhanced, a phenomenon that was previously explained by the higher oxophilicity of Ru and Ni toward stronger OH adsorption [86]. In such a case, a bi-functional mechanism was suggested to elucidate the enhancing effect of Ru on the activity of Pt, according to which the OH adsorption takes place on Ru and H adsorption on Pt [65]. However, it was later revealed that the weakening of the Pt-H_{ads} interaction in the presence of Ru is primarily responsible for the greater activity of PtRu systems [116]. Thus, an optimized HBE is believed to play a key role in HER/HOR activity, while the impact of OH_{ads} is less significant [109]. Selective positioning of Cu atomic layers on Pt(111) surfaces has been shown to accelerate HER in acidic media, resulting in a 2-fold increase in activity. This was explained by a structure-sensitive H adsorption on Pt- and Cu-modified Pt surfaces [110].

Moreover, the HER performance on Pt(111) in alkaline conditions is enhanced with the presence of oxophilic entities such as Pt-islands and transition metal oxy-hydroxides like $Ni(OH)_2$. This improvement is attributed to the dissociation of water molecules [111]. Likewise, Markovic *et al*. suggested that low-coordinated metal sites on the surface of PGMs accelerate the water dissociation step [19], [79], [81]. Decorating the Pt surface with $Ni(OH)_2$ creates additional active sites for strong OH_{ads} adsorption, facilitating the rearrangement of H_2O molecules and promoting OH^- transfer [19], [90]. Although the higher activation barrier for the Volmer step is thought to be the cause for the slower HER rate under alkaline conditions, the microscopic picture is still unclear. The slower HER rate in alkaline conditions is attributed to factors like slower OH^- transport, stronger O-H bond in water compared to H_3O^+, and the surface's ability to adsorb hydrogen. To explore this further, Markovic and Koper, among others, separately constructed a model of a Pt(111) surface using 3d metal hydroxide nanoclusters [18], [90] and observed a synergistic effect where $Ni(OH)_2$ clusters facilitated water dissociation, leading to the OH adsorption on $Ni(OH)_2$ and H adsorption on the adjacent Pt surfaces (Figure 3.5). In alkaline electrolytes, the Tafel slope of unmodified Pt(111) aligned with the estimated Volmer step, illustrating that the Volmer step is the RDS on Pt(111). However, on $Ni(OH)_2$/Pt(111), the Tafel slope reduced to 41 mV dec^{-1}, suggesting a transition to the Heyrovsky step as the RDS. By modeling water dissociation and H-adsorption processes at the interface of the $Ni(OH)_2$/Pt(111)/H_2O, the synergistic effect was verified theoretically. Furthermore, Koper *et al*. provided experimental evidence challenging the notion that the HBE alone serves as the sole descriptor for the HER kinetics on the Pt(111)-$Ni(OH)_2$ system [111].

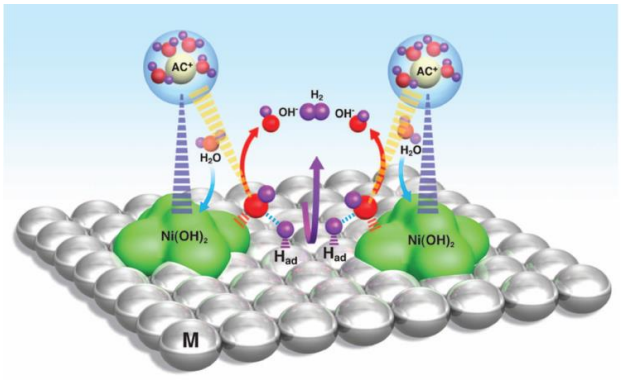

Figure 3.5 Schematic illustration of the synergistic effect of $Ni(OH)_2$ and Pt (represented by M) for improved HER in alkaline environments [111]

For additional clarification on the nature of such synergistic enhancements, Marković *et al*. [18], [79] conducted a study combining Pt(111) with different oxophilic 3d metal hydroxides. They found that each catalyst had similar H_{ads} capabilities but varying abilities for OH adsorption. The HER activity followed a volcano-like pattern, with the Pt(111)-$Ni(OH)_2$ catalyst having the weakest OH interaction, exhibiting the highest activity, around seven times greater than bare Pt(111) in alkaline KOH solution. This suggests that the kinetics of HER depend on both the rate of H adsorption and the rate of OH desorption, and a balance is needed between the transition state energies for water dissociation and the final state energetics of H_{ads}/OH_{ads}. Therefore, it is anticipated that the transport of OH^- ions from the catalyst surface into the electrolyte and the cleavage of the O−H bond in water are integral parts of the RDS in this bi-functional process occurring in alkaline electrolytes [19], [65].

The HER activity of Cu, Ag, Au, Ru, Ir, Pt, V, Ti, and Ni modified by $Ni(OH)_2$ was investigated by the Marković group [81], aiming to minimize the impact of water activation and splitting energetics. The findings revealed that all $Ni(OH)_2$/M surfaces exhibited significantly higher activity compared to their respective bare electrodes. Additionally, similar trends in HER activity were observed for the $Ni(OH)_2$/M catalysts in both alkaline and acidic solutions. Moreover, there was no noticeable variation in activity between $Ni(OH)_2$/Pt and $Ni(OH)_2$/Ir, showing that the HER is nearly entirely regulated by a comparable H adsorption energy on these two surfaces, just like in an acid solution. $Ni(OH)_2$ was therefore expected to promote the water dissociation step in both Pt-group and IB-group metals while the H_{ads} recombination step occurs on the nearby oxide/metal interfaces.

Moreover, the presence of Li^+ cations in the electrolyte was found to have a greater impact on the HER when surface oxophilic groups are present, surpassing the benefits of surface decoration with $M(OH)_2$ [111]. This highlighted the importance of "spectator" species in the electrolyte and stimulated further research [80]. The HER performance of Pt and PtNi was studied in relation to alkali metal (AM) concentration and pH, revealing that the nature of the cation affects the HER kinetics, with Li^+ having the most significant effect [112]. This can be attributed to the reduced destabilization of OH_{ads}, promoting interfacial oxophilicity and facilitating water dissociation. The presence of cations can be explained by the formation of an OH_{ads}-(H_2O)-AM^+ adduct, where the cation facilitates the removal of OH_{ads} from the adduct and its transport out of the double-layer. This effect is expected to be more pronounced with more acidic cations, which explains the greater HER activity observed with smaller alkali cations [65].

Trasatti's research, conducted around 50 years ago, suggested that the orientation of H_2O molecules at the interface could potentially account for variations in activity observed across various metallic surfaces. Although experimentally assessing these effects is challenging, investigating the water structure and

dynamics at the electrode-electrolyte interface is crucial to comprehend the underlying mechanisms of interfacial interactions and their impact on HER activity. Ultrahigh vacuum (UHV) and DFT calculations have shown that interfacial water does not significantly affect H_{UPD} energetics, but it is expected to significantly influence alkali cations and OH adsorption [113].

Hydrogen spillover, a well-established phenomenon [114], [115] is another important interfacial process for the electrocatalytic process [24], [25] and hydrogen storage [116]. Its impact on the HER has been extensively investigated. Recent studies have demonstrated that hydrogen spillover can significantly enhance the HER performance of Pt and Pt-alloy catalysts, particularly in alkaline environments [24], [25].

3.1.6.2. The effect of support/substrate on the HER activity

Developing affordable and efficient electrocatalysts is crucial for facilitating HER/HOR under fundamental conditions. However, the main challenges lie in the high cost and slower catalytic kinetics of PGM catalysts in alkaline electrolytes compared to acid electrolytes [117]. One strategy to enhance catalytic activity and stability is to support metal catalyst NPs on various materials. Carbon-based and carbon-free catalyst support materials are actively researched, aiming for corrosion resistance, high electrical conductivity, and favorable interactions with catalysts. The ideal support material should also exhibit stability in different electrochemical conditions, have a large surface area for effective NP dispersion, and be cost-effective due to the already high cost of noble metals [20], [118].

The most well-known non-carbon support materials are transition metal oxides (TMO) which stand out for their propensity to maintain stability in electrochemical conditions [20], [118], [119]. Oxide-supported metal catalysts (M/TMO) are found to have increased electrocatalytic performance for HER/HOR, which is explained by several factors, such as the support effect, the bicomponent active site effect, and the chimney effect. In the case of the support effect, effective sites for the adsorption and desorption of H are provided by the TMO support, which boosts the stability and electronic structure of the catalyst. When it comes to the bicomponent effect, the bicomponent system can speed up the H_{ads} recombination after the catalyst (active site), which has a moderate HBE, is connected to the TMO component, which can promote H_2O dissociation or OH adsorption. In the case of the chimney effect, smooth adsorption of H_{ads} and facile desorption of H_2 from the catalyst surface is made possible by the favorable chemical environment of the M/TMO interface, which is resistant to the adsorption of OH and H_2O. These positive outcomes highlight the critical idea that the M-TMO interaction can modify the interfacial catalyst electronic structure, which in turn affects the H adsorption/desorption [117]. Moreover, supported metal nanostructures may reorganize to offer new active sites under specific reaction conditions, e.g., promoting the HER/HOR [117], [120].

Popular oxide materials used in fuel cells and water-splitting technology include titanium dioxide (TiO_2), which is known for its availability and high electrochemical stability [20]. Transition metal carbides, such as tungsten carbide (WC), are also promising catalyst support materials due to their stability in acidic conditions, higher conductivity, resistance to poisoning, and strong interactions with noble metal catalysts [121]. For instance, using WC hollow spheres as a support for Pt NPs demonstrated significant improvements in kinetic parameters and HER activity compared to commercially available Pt/C catalysts. These enhancements are attributed to the higher number of active sites, high specific surface area, and strong attachment of Pt NPs facilitated by the hollow and cracked microstructure of the catalyst [122]. Electrocatalyst supports are essential for stabilizing catalytic metal atoms and regulating their reactivity via electron transfer. Particularly, there are strong interactions between late transition metal (oxide) catalysts and layered supports of early transition metals. The performance of these catalysts is

influenced by various factors such as NP size and shape, the composition of the oxide support, and the degree of support reduction [63].

Among the various carbon-based supports, carbon black is one of the earliest and most popular carbon-based supports used in fuel cells due to its affordability, wide availability, and good mesoporous distribution. Nevertheless, carbon black does have certain limitations, including inadequate electrochemical stability and the requirement for activation. Therefore, researchers have focused on modifying and functionalizing carbon-based supports and exploring alternative support materials for water splitting [32]. Several complex carbonaceous materials have been developed recently to improve stability, electrical conductivity, and surface area [119]. Hallow graphite spheres have excellent catalyst support properties because they can confine the catalysts inside them, increasing their stability. Moreover, carbon nanofibers significantly increase the catalysts' stability while promoting catalysis [20]. Similarly, because of their graphitic structure, which makes them more corrosion-resistant, carbon nanotubes are significantly more stable catalyst supports than standard carbon. Furthermore, their high surface area and electrical conductivity make them better catalytic supports [119]. Ordered and disordered mesoporous carbons are additional examples of carbonaceous supports with enhanced characteristics [20], [119], [123]. Graphitic materials, particularly those based on graphene, are known to have inferior HER catalytic properties [24]. Nevertheless, graphene holds great potential as a catalyst support material owing to its remarkable attributes, such as its large surface area, stability, and higher conductivity [20], [21]. Several studies show that graphene can promote the proper dispersion of catalytic particles and actively participate in the HER electrocatalytic reaction, resulting in increased catalytic activity [21]–[23].

Qiu *et al*. [124] used single-atom Ni dopants fastened to 3D nanoporous graphene to examine the HER in acidic solutions. The HER catalytic activity of this composite was found to be superior to that of graphene and traditional Ni-based catalysts with a low overpotential (~ 50 mV), low Tafel slope (45 mV dec^{-1}) along with superior cycling stability in 0.5M H_2SO_4 solution. Deng *et al*. studied NiCo NPs enclosed in ultrathin graphene shells (only 1–3 layers) and observed exceptional HER electrocatalytic performance. Through DFT simulations, the authors proposed that the exceptional performance stems from electron transfer between the CoNi core and the graphene surface, affecting the electron density and electronic potential distribution. Additionally, when the graphene structure was doped with N atoms, the authors observed a significant increase in the electron density within graphene shells, which caused a shift in the energy of H_{ads} and further improved the HER electrocatalytic performance [125]. Zhang *et al*. [126] have studied the HER and methanol oxidation reaction on graphene-supported Pt NPs and observed enhanced activity with lower overpotential, lower Tafel slope, and greater stability. These enhancements were attributed to the synergistic effects between the Pt NPs and graphene support.

The performance of Pt-Pd alloys supported on r(GO) was investigated by Lin et al. [134]. These alloys displayed outstanding electrocatalytic activity and satisfactory stability for HER and ORR in both acidic and alkaline electrolytes. Compared to the commercially available Pd/C and Pt/C catalysts, the rGO-supported Pt-Pd alloys demonstrated superior performance. Chanda *et al*. have used a straightforward electrochemical procedure to prepare rGO from GO on a Ni foam electrode and discovered that the rGO-modified Ni has novel HER catalytic activity in alkaline environments that outperformed the Pt/C catalyst under similar conditions. The authors complemented the experimental measurements with theoretical DFT calculations. They concluded that H atoms generated by H_2O discharge on Ni spillover the rGO, serving as acceptors for H adatoms. This mechanism facilitates an ongoing cleaning of active sites on Ni and provides an alternative route for H_2 generation [23].

Moreover, Gutić *et al*. [21] developed a simple method to prepare Ni@rGO catalysts for the HER. They have prepared a series of Ni@rGO catalysts by electrochemically reducing a GO film while also depositing Ni on its surface. The composites exhibited improved electrocatalytic activity compared to pure Ni electrodes. The deposition time significantly influenced the HER activity, with the deposit obtained at 100 s deposition time ($Ni@rGO_{100}$) showing the best performance. The authors also synthesized Ni-Mo alloys supported on rGO (NiMo@rGO), which displayed higher HER activity than bare NiMo composites and the previously mentioned Ni@rGO electrodes. The contribution of rGO in enhancing catalytic performance depended on deposition time, with $NiMo@rGO_{200}$ being the most active [22]. The authors proposed that HER activity of the composite is provided by the formation of the Ni-Mo system and the formation of an interfacial region with rGO.

3.1.6.3. The effect of hydrogen spillover in electrocatalytic processes

In 1964, Khoobiar observed that when WO_3 was exposed to a Pt catalyst (supported on Al_2O_3), WO_3 underwent reduction by H_2 gas to form blue WO_{3-x}. The change in color was attributed to the chemisorptive dissociation of H_2 molecules on the surface of Pt, which then migrated to the WO_3 particles, causing their reduction to blue WO_{3-x} particles. The term "spillover" was later conceived by Boudart *et al*. [127] to describe the migration of H atoms from the metal particles to the substrate. This phenomenon involves the spillover of H atoms from surfaces with a high concentration to surfaces with a low concentration of hydrogen. In 1971, Pajonk and Teichner discovered that after being exposed to hydrogen for a long time at a high temperature, pure supports (such as Al_2O_3 or SiO_2) could hydrogenate ethene and benzene. This process occurred through indirect contact with metal particles on the supported catalyst, and it was attributed to the spillover of hydrogen species [25], [128]. The discovery of H spillover on a Pt/WO_3 catalyst in 1964 has sparked ongoing interest and extensive research. It has resulted in notable advancements in hydrogen storage and catalysis applications [129], [130]. As shown in Figure 3.6, there has been a significant advancement in understanding, characterizing, and utilizing the phenomenon of hydrogen spillover [128].

Spillover refers to the migration of active species from one surface to another surface that does not adsorb or form active species. In the context of hydrogen, it involves the production of H atoms on a catalyst surface, which then migrate to the support surface. The process consists of three steps: dissociation of gaseous hydrogen molecules on the catalyst, migration of H atoms to the support, and diffusion of H atoms onto substrate surfaces [25]. Hydrogen adsorption typically starts on metals with strong M-H bonds and can travel via surface diffusion to a substrate with weaker M-H binding. Eventually, the weak M-H bond is broken, forming H_2 molecules that escape the electrode surface [50]. Tsao *et al*. [131] used the inelastic neutron scattering (INS) technique to verify a spillover mechanism involving hydrogen dissociation, diffusion, and adsorption in a Pt-activated carbon structure.

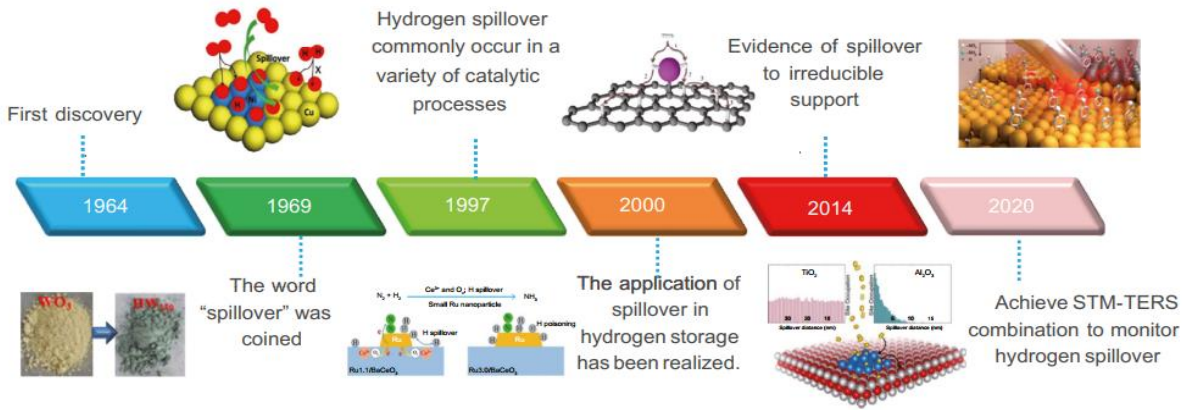

Figure 3.6 Historical development of hydrogen spillover [128]

Karim *et al*. [24] examined the hydrogen spillover from Pt NPs to metal oxide surfaces. They arranged multiple pairs of iron oxide and Pt NPs on reducible (TiO_2) and non-reducible (Al_2O_3) supports, varying the distance between the pairs. Using in-situ X-ray absorption spectro-microscopy, they quantified the reduction of Fe_2O_3 particles through hydrogen atoms produced on Pt. Experimental and DFT calculation results revealed that hydrogen spillover onto non-reducible Al_2O_3 is significantly slower compared to reducible TiO_2, with a difference of 10 orders of magnitude. Furthermore, the spillover on Al_2O_3 is limited to short distances from the Pt metal particles. Additionally, Prins *et al*. verified that H spillover is energetically implausible on non-reducible support, as indicated by the lack of hydrogen-deuterium (H-D) exchange on the OH groups of such supports [25]. While the transfer of hydrogen from metal catalyst sites to defect-free carbon supports is energetically unfavorable, it has been theoretically and experimentally confirmed that this process can occur in carbon supports with defects [132].

Shen *et al*. [128] published findings indicating that H_2 molecules undergo dissociation into individual H atoms on transition metal (TM) NPs. Subsequently, these H atoms migrate to the surface of graphene by forming bonds with carbon atoms (C-H bonds). Tsao *et al*. [131] used INS to directly observe the behavior of molecular H_2 in a Pt-doped activated carbon system, providing evidence that H atoms can diffuse to the carbon surface during the spillover process. In addition, investigations utilizing INS have shown that H atoms generated on Pt or Pd surfaces have the potential to diffuse to unsaturated reaction sites on carbon supports, particularly at irregular boundaries or edges, where they form C-H bonds [25], [128]. Konda *et al*. [130] observed H spillover from a Pd catalyst to activated carbon fibers, resulting in the formation of new C-H bonds. Yoo *et al*. [133] also confirmed the presence of C-H bonds in defective carbon nanotubes doped with Pd NPs, validating the spillover of atomic hydrogen species onto the carbon support. DFT studies indicate that H spillover can potentially take place via the transfer of protons and electron pairs at the surface [128].

As discussed in the previous Section, according to Chanda *et al*. [23], the rGO-modified Ni foam electrode has novel HER catalytic activity in an alkaline medium that outperforms the Pt/C catalyst under similar conditions. Experimental measurements complemented with theoretical DFT calculations lead the authors to conclude that H atoms, generated by H_2O discharge on Ni, spill over the rGO, which acts as an H adatom acceptor allowing for continuous cleaning of Ni-active sites and acting as an alternative route for H_2 generation. Similarly, the significant catalytic activity improvement of Ni electrodeposited on rGO [21] and Ni-Mo alloys supported on rGO [22] was explained to be caused by the spillover of adsorbed H atoms onto the r(GO) substrate.

Zhou *et al*. [134] conducted a study investigating binary HER electrocatalysts' hydrogen spillover behavior. They focused on the difference in work function ($\Delta\Phi$) between the catalyst and support, which is an essential criterion for designing such catalysts [135]. The researchers prepared multiple samples loaded with Pt and observed their H spillover behavior in detail. Using theoretical simulations and experimental data, the authors found that the extent of H spillover, and thus the HER activity, increased in the order selenides < sulfides < oxides < phosphides, which is opposed to the trend in $\Delta\Phi$ between Pt and supports. The highest H spillover occurred on Pt-CoP, with the lowest $\Delta\Phi$ between the catalyst and the supports. The authors proposed that the interfacial charge density can be diluted by the smaller $\Delta\Phi$, weakening H adsorption at the interface and promoting H adsorption on Pt metal. After Pt loading, as the result of efficient H migration from Pt to CoP, the Tafel slope for CoP, with the least $\Delta\Phi$, reduced drastically by 3.6 times. At the same time, the overpotential at 10 mA cm^{-2} decreased to 53 mV from 242 mV. Fu *et al*. [136] have discovered a way to enhance hydrogen production efficiency using a hybridized electrocatalyst made of Ni_3S_2 and Cr_2S_3. They found that the spillover of adsorbed H atoms at the interface of Ni_3S_2/Cr_2S_3 helps promote essential chemical processes and mitigate the inhibitory effect caused by high H_{ads} coverage resulting from high current density. The authors used experimental and theoretical approaches to identify the key mechanisms responsible for the improved performance of

the electrocatalyst. As a result, the hybrid electrocatalyst achieved a high current density of 3.5 A cm^{-2} at an overpotential of 251±3 mV in a KOH electrolyte solution.

Hydrogen spillover is significantly influenced by metal and support; metal affects hydrogen dissociation and diffusion, while support impacts spillover distance. Various spillover mechanisms can be enabled by adjusting metal-support interactions based on elements such as metal and support type, cluster size and shape, and support polymorphism. This helps in constructing catalytic reactions and improving their effectiveness. Yet several characterization techniques are required to comprehend the dynamic behavior of the hydrogen spillover effect [128].

3.1.7. Trends in HER and the Volcano plots

Electrocatalysis involves analyzing the impact of different material properties on reaction rates to establish trends and link material properties to reaction rates through catalytic descriptors. The adsorption energies of intermediates are commonly used as catalytic descriptors due to their relation to the exchange current density (j_0) [137]. As mentioned in Section 3.1, in the late 1950s, Parsons predicted a qualitative relationship between HER j_0 and the free energy of hydrogen adsorption ($\Delta_{ad}G_H$), which resembles a Volcano curve where the maximum HER activity occurs when $\Delta_{ad}G_H \approx 0$ eV [48]. Later in 1972, Trasatti introduced a "volcano" curve that depicts the correlation between the $\log|j_0|$ and the energy of hydride formation (E_{M-H}). The curve utilized E_{M-H} instead of $E_{ads}(H)$ because the latter data was not accessible during that period. Trasatti's volcano plot (Figure 3.1a) suggests that PGMs are the most effective materials for HER, Pt being the most efficient, followed by Re, Rh, Pd, and Ir, which are located towards the top of the curve but not at its highest point. The plot also indicates that metals with stronger or weaker hydrogen binding strength are on either side of the curve. The weakly binding branch of the “volcano” contained *sp*-metals with considerably weaker binding compared to noble metals. In contrast, positioned between the noble metals and *sp*-metals are the triad of iron and coinage metals (Au, Cu, Ni, Co, and Fe). This group of metals has weak hydrogen adsorption strength, leading to slow coverage of the active surface. The other group of metals, including W, Mo, Nb, Ti, and Ta, are usually coated with a thick layer of oxides that strongly adsorb hydrogen, resulting in lower catalytic activity.

Surface rate modeling, similar to what Parsons used, and DFT calculations of atom-specific free energies have enabled the development of HER volcanoes that show the relationship between M-H bonding and HER activity for both metals and metal alloys [138]. In contrast to Trasatti’s volcano plot, contemporary volcano plots rely on DFT-derived adsorption energies, as E_{M-H} trends used by Trasatti do not consistently conform to $E_{ads}(H)$ trends [17]. Nørskov *et al*. have developed the modern HER volcano plot in acidic solutions [49], where theoretically computed HBEs were correlated with HER j_0 (data from literature). According to Nørskov’s volcano plot, shown in Figure 3.1b, it can be inferred that Pt is a superior electrocatalyst for HER compared to other metals. This is mainly because the HER is thermo-neutral on Pt at the equilibrium potential. The position of some metals such as Ag, Au, and W in the modern volcano plot (Figure. 3.b and c) are not the same as that of Trasatti’s volcano plot (Figure 3.1a) because the trends in E_{M-H} do not follow the same trend as that of the $E_{ads}(H)$. More recently, Sheng *et al*. have shown that the j_0 for the HER in alkaline solutions can be linked to the calculated HBE on various monometallic surfaces through a volcano-type relationship (Figure. 3.5c) [15]. The HER activity exhibits significant variations across the plot, with Pt being at the highest peak and W and Ag situated at the base of each side of the plot, consistent with the findings in acidic solutions (Figure 3.1a and b) [13], [49]. The volcano plot reveals that metals with strong HBEs, such as Ni, W, Fe, Co, and Pd, are located on the left side of the curve, while metals with weaker HBEs, such as Cu, Ag, and Au, are on the right side.

The effect of pH on the volcano plots in acidic and alkaline solutions can be explained by the lower HER activity of the metals in alkaline media than in acidic media [20]. Thus the peak of the plot is shifted to lower j_0 or to higher overpotential (for specific current) values. Moreover, the volcano plots of the HER,

which show the correlation between the activity of the HER and the experimentally determined HBE for Pt in pH-buffered electrolytes, offer compelling evidence that HBE is the only factor determining the HER activity on the surfaces of monometallic elements, particularly Pt, in alkaline conditions [78].

Moreover, Greeley *et al*. [139] demonstrated the applicability of HER volcano plots for bimetallic systems. Using theoretical approaches, they investigated the HER on pseudomorphic Pd overlayers on different single-crystal transition metal substrates. By correlating experimental j_0 values with theoretical $\Delta_{ads}G_H$, a volcano-type relationship was observed (Figure 3.7). The study revealed significant variations in HER activity among the systems attributed to differences in the electronic structure of the Pd overlayer. Being positioned at the peak of the volcano plot, Pd*/PtRu alloy is theoretically identified as the most active catalyst for the HER. However, it exhibits lower activity in experimental calculations. This discrepancy can be attributed to limitations in mass transfer, resulting in lower measured rates.

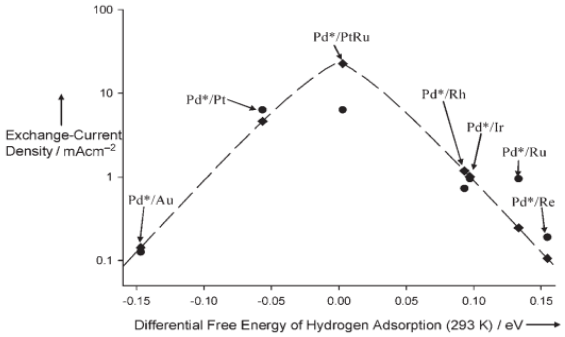

Figure 3.7 Hydrogen evolution j_0 as a function of the theoretical differential free energy of hydrogen adsorption, $\Delta_{ads}G_H$. The theoretical j_0, as predicted by the model, is represented by the dashed line, while the predictions for specific overlayers are shown as black diamonds. The experimental measurements are depicted as black circles. Pd*/X denotes a pure overlayer of Pd on a substrate of metal X [139].

Danilovic *et al.* [140] conducted a study comparing the HER activities of various metals in acidic and alkaline environments. They plotted the activities of coinage metals (Au, Cu, Ag), PGMs (Pt, Ir, Ru), and a valve metal (Ti) against HBE. In acidic media, Pt and Ir showed the highest activity, while metals that either bind hydrogen too weakly (Ag) or too strongly (Ti) are on each side of the volcano plot (Figure 3.8a). In alkaline media, the HER exhibited a volcano-like behavior (Figure 3.8b), with lower overpotentials required for 5 mA cm^{-2} compared to acidic solutions. Additionally, Ir showed greater activity than Pt in alkaline solutions, suggesting differences in the reaction mechanism at different pH levels. Moreover, the activity trend of coinage metals in an alkaline solution (Ag < Au < Cu) was found to differ from that in an acidic solution (Au < Cu < Ag) [84].

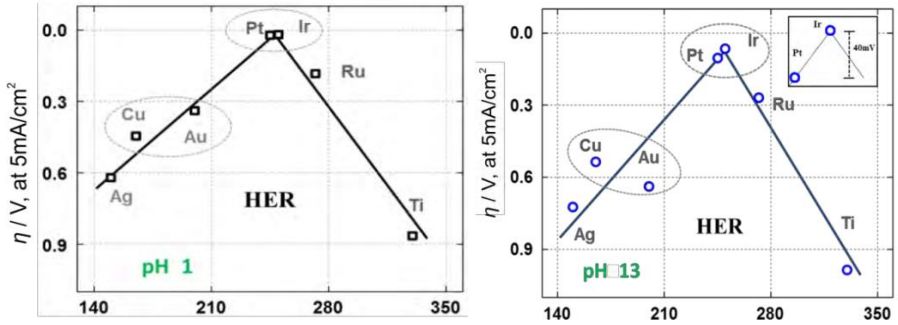

a) b)

Figure 3.8 Volcano plots, measured a) in 0.1 M $HClO_4$ (pH 1), b) in 0.1 M KOH (pH 13), of a variety of metals indicating their HER activity, overpotential (η) at 5 mA cm^{-2}, as a function of their calculated HBE [140].

Durst *et al*. [74] investigated the HER/HOR processes on PGM electrodes in acidic and alkaline environments. They found that the activity dropped by two orders of magnitude when moving from acidic to alkaline conditions on electrodes that can form a H_{UPD} layer, such as Pt, Ir, Pd, and Rh. The authors constructed HER/HOR volcano plot with the activities measured in acid electrolytes, using the H_2-pump proton exchange membrane fuel cell (PEMFC) method on carbon-supported Pt, Ir, Pd, and Rh NPs, and using the RDE method for Pt, Pd, Rh, Ir, Mo, Cu, Ni, Au and Ag extended surfaces (by taking data from ref. [13], [49]). The study's outcomes indicated that the activities of Pt, Ir, and Rh surfaces could be enhanced using the H_2-pump PEMFC method. By decreasing mass transport resistance, this method enabled the measurement of the true kinetics of the HER/HOR. The experimental activities obtained using this method perfectly matched the predicted Volcano trend (Figure 3.9a). The authors proposed that the HER/HOR Volcano plots for acid electrolytes be constructed utilizing the activities of Pt, Ir, and Rh surfaces that they had obtained using the H_2-pump arrangement, which allowed them to estimate the genuine HER/HOR kinetics with suitably low mass transport resistances.

Moreover, the authors have compared the activities of the metals measured in both acid and base (Figure 3.9b). The activities of Pt, Ir, and Pd were investigated by H_2-pump PEMFC in acidic media, and the activities of Ni, Cu, Au, and Ag in alkaline media (obtained by RDE measurements) were taken from Sheng *et al*. [15]. As compared to non-noble metal electrodes (Ni, Cu, Au, and Ag), or those that do not generate an H_{UPD} layer, the HER/HOR activity of noble metal electrodes (Pt, Ir, and Pd) appears to be more affected by electrolyte pH, and this was evident in their volcano plots (Figure 3.8b) [74].

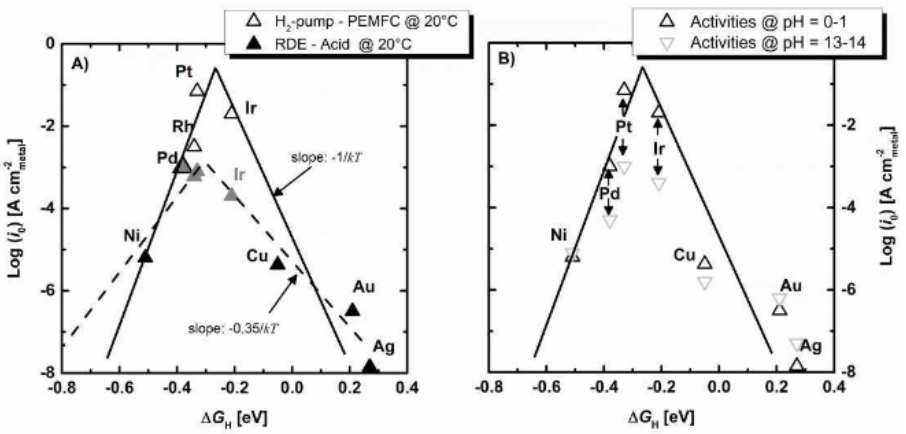

Figure 3.9 HER/HOR volcano plot computing the H adsorption energies as a function of the surface normalized HER/HOR j_0 measured in (A) acid and (B) in both acid (black triangles) and alkaline (grey triangles) electrolytes. Activities in acid were obtained from H_2-pump PEMFC measurements on carbon-supported Ir, Pt, Rh, and Pd nanoparticles (open triangles, recalculated for T = 293 K using the corresponding activation energy) and from RDE measurements for Pt, Ir, Pd, Rh, Ni, Cu, Au and Ag surfaces (data taken from Trasatti et al. and Nørskov *et al*. [13], [141], closed triangles). Activity data in the base were taken from Sheng *et al*. [15] and determined by RDE measurements for Cu, Ni, Au, and Ag.

3.1.8. Criticism of volcano plots

Several attempts were made to find correlations between electrode properties (such as work function, latent heat of melting, the presence of unoccupied d orbitals, etc.) and the reaction rate of the HER [142], but with limited success. The sole correlation that remains intact is the volcano plot, which relates the reaction rate to the E_{ads}(H) on the electrode. This concept is based on the Sabatier principle, a fundamental idea in gas-phase heterogeneous catalysis. The first volcano plot (Figure 3.10a) was compiled by Trassati in 1972, as described in Section 3.1 and Section 3.1.7. Since reliable adsorption energy values were unavailable at the time, Trassati used the energy for hydride formation ($E_{M\text{-}H}$) to construct the volcano plot. The Volmer reaction exhibits unfavorable energetics for high adsorption energies (low E_{M-H}). As the adsorption energy decreases (E_{M-H} increases), the reaction rate increases, reaching its optimum near $\Delta_{ads}G_H = 0$. As the adsorption energy becomes increasingly negative, the Volmer reaction rate continues to rise. However, in the subsequent step, the energy of the initial state progressively decreases. This means that a stronger adsorption bond must be broken in either the Heyrovsky or Tafel step to continue the reaction. As a result, the second step becomes slower and ultimately limits the overall rate of the reaction [143].

The experimental evidence suggests that the relationship between the energy of adsorption (E_{M-H}) and the rate of the HER is not straightforward. While the rate initially increases with increasing E_{M-H}, there is also a descending branch. However, Schmickler *et al*. [17] pointed out that under electrochemical conditions, all metals on this branch are coated by an oxide film, obstructing the reaction. If we exclude the metals coated by oxide film, there is no proof of a volcano plot, and only the ascending branch will exist. Different research groups have reported experimental values for reaction rates that differ significantly. To address this, the Nørskov group [141] developed contemporary volcano plots that use reliable adsorption energies calculated through DFT, with an estimated error of ±0.1 eV for hydrogen adsorption. Once again, incorporating metals covered with oxides (such as W, Nb, and Mo) in the strong binding region of Nørskov's volcano plot has presented a challenge to the descending part of the plot. Schmickler group [17] also calculated these adsorption energies for various densely-packed metal

surfaces, mainly fcc(111), and found the same values as the Nørskov group for the same metals. Schmickler group constructed plots (Figures 3.9a and b) that relate the j_0 of metals in both acidic and alkaline media as a function of their adsorption energies, but without including metals that form oxides. The plots look similar, but acid solutions show slightly faster rates than alkaline solutions for the fastest reactions.

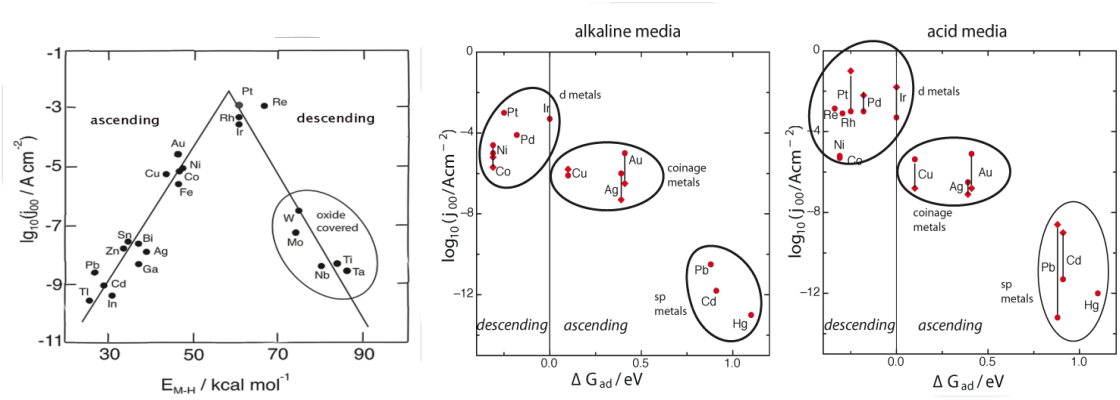

a) b) c)

Figure 3.10 a) Trasatti's volcano plot [13], 'Volcano' plots (excluding the oxide forming metals) for HER b) in alkaline and c) in acid aqueous solutions [17]. Note that ascending and descending branches are reversed with respect to Trasatti's volcano plot.

When comparing the volcano plot (Figure 3.10b and c) with Trasatti's plot (Figure 3.10a), a general similarity emerges when excluding metals covered by oxide films from Trasatti's plot. However, there are some significant deviations, some caused by new experimental data and others resulting from differences in trends between E_{ads}(H) and $E_{M\text{-}H}$ used in Trasatti's plot. For instance, the position of nickel on the plots is different due to this trend difference, and the higher rate at silver may be due to improved sample preparation. Neither of the plots (Figure 3.10b and c) bears any resemblance to a volcano, but similar to Trasatti's plot, there is a general trend of rising reaction rate with falling adsorption energy ($\Delta_{ads}G_H$). According to Schmickler *et al*., three categories of catalysts were identified: *sp* metals (Cd, Hg, Pb), which exhibit the poorest performance, coinage metals (Cu, Ag, Au), which fall in the middle; the d metals (Rh, Ro, Ir, Pd, Pt) are considered the best catalysts while Ni and Co are mediocre. The electrocatalytic properties of metals are related to the electronic structure of their *sp* and d bands.

Poor catalysts primarily have *sp* bands near the Fermi level, while catalysis is enhanced by narrower and more structured d bands. The reaction rate is mainly governed by Sabatier's principle, except for Ni and Co, which have compact and minimal overlap with hydrogen, making them effective catalysts. However, for other metals, the reaction rate decreases due to highly exothermic hydrogen adsorption and the complex pathway involving multiple intermediate states. Therefore, to be a good catalyst, a material must satisfy one of these three conditions: (i) adhere to Sabatier's principle, where ΔG is roughly equal to zero at the equilibrium potential, (ii) have a d-band that extends over the Fermi level, and (iii) have a certain distance (0.5 Å) between the active catalyst (adsorption site) and the proton, as electron transfer from the former to the latter requires this distance. The position of the d band and the strength of interaction between the metal d-band and 1s orbital of H are interconnected with the adsorption energy. However, there can be instances where these conditions conflict or contradict each other. Therefore, metals with a strong interaction between their d-band and the 1s orbital of H are more likely to perform better [30].

According to Schmickler *et al*., the *sp*-metals follow Sabatier's principle. Still, because these metals are less active, extrapolation from a distant point in the potential is necessary to obtain j_0 values, which leads to significant experimental errors. On Trasatti's plot, the behavior of *sp* metals aligns with Sabatier's

principle, as supported by Figure 3.10c in alkaline media. Nevertheless, the data in acid solutions neither contradict nor strongly support Sabatier's principle. The Volmer reaction being the RDS on these metals, supports Sabatier's principle [17], [37]. Coinage metals (Ag, Au, and Cu) exhibit moderate catalytic activity, and their j_0 values require extrapolation over a smaller potential range compared to *sp* metals. The rates of HER on the coinage metals are similar, which result from two compensating factors: the position of the d band and the energy of adsorption become more favorable in the order Au < Ag < Cu, while the coupling (interaction with hydrogen) increases in the opposite direction Cu < Ag < Au. As a result, the overall rates of these metals are influenced by factors beyond Sabatier's principle, resulting in a plateau rather than a volcano-shaped trend.

The d metals, including Pt, Ir, Pd, Rh, Re, Co, and Ni, possess favorable catalytic properties as their Fermi level falls within the d band. Schmickler *et al*. note that the rates of the d metals are generally rapid, except for Co and Ni. These rates exhibit a notable disparity between acid and alkaline solutions and do not follow a volcano-shaped trend, indicating that Sabatier's principle alone does not govern their catalytic behavior. While Sabatier's principle suggests that the d metals (excluding Co and Ni) should form the descending branch of the volcano plot, this is not observed due to the presence of two different adsorbed hydrogen species, H_{UPD} and H_{OPD}. The reaction selectively favors the intermediate with the more favorable energy (H_{OPD}), thus avoiding the predicted descending branch. Ni and Co are similar metals, and Schmickler *et al*. focused explicitly on Ni(111) to explain the catalytic properties of Ni and Co, as it is the most dense stable surface.

In contrast to other d metals (excluding Co), the HER on Ni must proceed through the strongly adsorbed hydrogen (H_{UPD}) state, which follows Sabatier's principle. Schmickler group has used their own theory to calculate the $\Delta_{ads}G_H$ on Ni(111) and found that the Ni(111) surface follows the Volmer-Heyrovsky mechanism. This agrees with the experimental observation that the Volmer-Heyrovsky mechanism operates on Ni and Co, with the Heyrovsky step being the RDS. Their findings indicate that the Volmer step is fast and is in line with Sabatier's principle [17]. Furthermore, the authors pointed out that when dealing with nanostructures, the situation becomes even more intricate since there are several potential adsorption sites with varying adsorption energies. Thus, determining which adsorption site to utilize in constructing volcano plots can be more challenging.

Several volcano-type plots have been published in the literature, apart from the original work by Trasatti. One notable contribution is the modern volcano plot by the Nørskov group [141], who utilized E_{ads}(H) calculated by DFT, resulting in a more reliable and extensive dataset. Another volcano plot was presented by the same group [142] in another publication, which employed kinetic modeling, assuming the Tafel reaction as the RDS and the Volmer reaction always in equilibrium. Sheng *et al*. [15] also assembled a modern volcano plot for alkaline solutions. According to Schmickler *et al*., all of these plots lose their volcano shapes when the oxide-covered metals are removed from consideration. Upon conducting a comprehensive literature review, it was discovered that there are considerable discrepancies and conflicting information, and some authors have pointed out that the "volcano" correlation for the HER could be misleading [137]. Although volcano trends for HER have been established both in acidic and alkaline media, they failed to account for why the majority of metal catalysts in alkaline medium exhibit ~2-3-fold lower activity than in acid solutions [76], [78]. Moreover, the volcano plots have received criticism for ignoring potential differences in the mechanisms of the HOR and HER occurring on the same catalyst [38] as well as the possible existence of various types of H adsorbates with different adsorption energies [142], [144]. The bond strengths utilized in "volcano" plots for the HER are based on strongly bound H_{UPD}. However, Conway's hypothesis suggests that the intermediate in the reaction could be a weakly bonded H_{OPD} [97]. The connection between H_{UPD} and H_{OPD} is still uncertain in electrochemistry, which raises questions about the relationship between H_{UPD} and the kinetics of the HER. The volcano plot assumes that the catalyst is in a steady state and that the reaction is diffusion-

limited, but this may not always be the case. Other factors such as pH, electrolyte, temperature, and the presence of other species can also affect the catalyst's activity for the HER [145]. Therefore, relying solely on the volcano plot may not offer a complete understanding of the catalyst's activity. Despite these limitations, HER volcano plots can still be useful for the initial screening and comparison of catalysts. Additionally, researchers have employed volcano plots to create bimetallic systems that exhibit improved electrocatalytic performance in the HER/HOR by combining metals situated on the opposite branches of the curve [38]. Greeley *et al*. utilized DFT to evaluate the stability and HER activity of over 700 binary surface metal alloys. They identified that the BiPt surface alloy exhibited significant potential as a promising candidate, showcasing HER activity comparable to or surpassing Pt [108].

Chapter four - Materials and methods

4.1. Electrochemical measurements

4.1.1. Materials

Polycrystalline metallic rotating disk electrodes (RDE) with a Teflon diameter of 10 mm were used for the electrochemical measurements as working electrodes. The RDEs used were Ag, Au, Co, Fe, Pt, and W with diameters of 3 mm, Ni with a diameter of 3.2 mm, and Cr and Zn with a diameter of 5 mm. The metals purchased from Goodfellow Cambridge Ltd. (UK) are at least 99.95% pure (except Cr, with 99.7%). Sigma Aldrich chemicals were utilized to prepare electrolytic solutions with different concentrations. The prepared electrolyte solutions were 0.1 mol dm^{-3} HCl, 0.1 mol dm^{-3} $HClO_4$, 1 mol dm^{-3} KH_2PO_4, 0.5 mol dm^{-3} NaCl, 0.1 mol dm^{-3} LiOH, 0.1 mol dm^{-3} KOH solution, and 1 mol dm^{-3} KOH. Ultrapure deionized water was used to prepare the electrolytic solutions and hydroxides were anhydrous with ≥ 99.9% trace metal basis. In all the electrochemical measurements, ultra-pure argon was used to de-aerate the electrolytes.

In this study, a commercial graphene-oxide material, ACS Graphene Oxide Powder, was employed as a catalyst support for the synthesis of metal-reduced graphene oxide (M@rGO) composites. Electrolytic-quality copper substrates served as the foundation for supporting both pure metals and reduced graphene oxide (rGO) in the composites.

To produce the M@rGO composites, an electrochemical process was employed. Electrochemical measurements were conducted using a standard three-electrode setup. The reference electrode utilized was Ag/AgCl (saturated with KCl), while a graphite rod served as the counter electrode. The potentiostat/galvanostat used was the PAR 263A from Princeton Applied Research, USA, and impedance measurements were facilitated by coupling it with a 5210 Dual Phase Analog Lock-in Amplifier, controlled through the POWERSuite software package.

For the experiments, practical-grade chemicals were employed without additional purification. The specific chemicals used in the electrodeposition bath can be found in Table A1 in the Appendix.

4.1.2. Setup for electrochemical measurements

For electrochemical measurements, an IVIUM Vetex.One software was utilized in a single-compartment, three-electrode glass cell. The cell contained a double-junction Saturated Calomel Electrode (SCE), which functioned as a reference electrode, while a graphite rod was used as a counter electrode for acidic solutions. On the other hand, a 3×3 cm Ni foam was utilized as a counter electrode for pH-neutral and alkaline solutions. The experimental duration for each electrode was short, lasting less than 10 minutes. Thus, any potential release of silicates from the glass in alkaline solutions can be disregarded for this study.

4.1.3. Electrode preparation

Prior to conducting the experiments, each disk electrode underwent a preparation process. First, they were polished to achieve a mirror-like finish using 0.05 μm alumina powder. Following this, the electrodes were sonicated for 15 seconds to ensure cleanliness and remove any residual particles. After the sonication step, the electrodes were rinsed with the working solution and swiftly transferred to the electrochemical cell.

The measurements were promptly initiated upon electrode transfer to minimize the formation of oxides on the metal disk surfaces. This swift initiation helped maintain the integrity of the experimental conditions and ensured accurate results by preventing unwanted oxidation on the electrode surfaces.

4.1.4. Methodology of electrochemical measurements

Cyclic voltammetry (CV) was utilized to perform HER measurements, with a potential sweep rate of 10 mV s^{-1}. Prior to the potential sweep, the electrode potential was held steady at values of -1 V, -0.6 V, and -0.24 V vs. SCE for alkaline, pH-neutral, and acidic solutions, respectively, until the current density fell below 1 μA cm^{-2}. Subsequently, three cycles were executed to reach deep negative potentials, following which the electrode underwent cycling between 0 and +1.4 V vs. reversible hydrogen electrode (RHE) at a sweep rate of 20 mV s^{-1}. Then, the HER measurement was repeated as described. The electrodes remained under constant potential control throughout the experiment and were not permitted to relax to the open circuit potential.

Although glass (from SCE) may release silicates into alkaline solutions during long-term experiments, this potential impact can be disregarded since the experiments conducted for each electrode were relatively short, lasting less than 10 minutes. All electrochemical measurements were carried out at room temperature. Potentials are referred to as SCE, and to calculate HER overpotentials, potentials are converted to the RHE scale using the equation: $E_{RHE} = E_{SCE} + 0.244\ V + 0.059\ V \times pH$. Hardware settings were employed to rectify electrolyte resistance, up to 75% of the resistance value, determined through single-point impedance measurement at 0 V vs. RHE (100 kHz).

4.1.5. Real surface area and roughness factor measurements

Roughness factor (RF) measurements were performed on freshly polished electrodes using CV in a narrow potential window, except for Fe and Pt. The measurements were carried out in 1 mol dm^{-3} KOH solution by cycling the electrodes between −0.1 and 0 V vs. RHE at various sweep rates of 10, 20, 50, 75, 100, 150, and 200 mV/s. Prior to the measurements, the electrodes were exposed to intense HER at deep negative potentials to minimize the presence of oxides. Next, a graph was generated by plotting the current, specifically at the midpoint of the potential window, against the sweep rate. This graph produced a linear relationship, and the slope of the line was used to determine the double-layer differential capacity based on the equation: $i = dQ/dt = (dQ/dE) \cdot (dE/dt) = C \cdot v$, where i represents the current, C represents the capacitance of the electrode, and v represents the sweep rate. The slope of the current vs. sweep rate line was used to calculate the electrode capacitance, which was then divided by 20 F cm^2 to give the electrochemically active surface area (ECSA) [146], [147]. Then, the measured HER currents were normalized by ECSA. The RF was then calculated by dividing the ECSA by the geometrical cross-section of the electrode disk. Applying this method to Fe resulted in a significant dispersion of the current vs. potential scan rate data, which determined the RF unreliable. As a result, we opted to determine the RF for the Fe disk through impedance spectroscopy instead. The RF values for the investigated metals are given in Appendix (Table A1). The impedance spectrum of the Fe disk was recorded in the frequency range of 0.1 Hz to 100 kHz after exposing it to HER at -0.3 V vs. RHE in 1 mol dm^{-3} KOH. The capacitance was determined by fitting the spectra and assuming an oxide-free surface, and the ECSA was obtained by dividing the capacitance by 20 μF cm^{-2}. To determine the RF and ECSA of Pt, cyclic voltammetry was used in 0.1 mol dm^{-3} $HClO_4$. ECSA was calculated by integrating the peaks of H_{UPD}/H desorption and dividing the charge under these peaks by 210 μC cm^{-2} [147]. It is important to mention that there are various techniques available for determining the ECSA, including the method based on adsorption capacitance, which may be appropriate for certain metals examined in this study [148]. Nevertheless, this approach was not validated for all the catalysts studied in this work. Consequently, we

relied on capacitance measurements to estimate ECSA whenever possible or, in the absence of a standard method, as in the case of Pt.

4.1.6. Metal deposition on drop-casted-GO films

n this study, metal-reduced graphene oxide (M@rGO) composites were synthesized through an electrochemical process. The electrochemical measurements were carried out using a typical three-electrode setup, as explained in Section 4.1.1. The electrode potentials were recalculated to the RHE (Reversible Hydrogen Electrode) scale using the formula: $E_{RHE} = E_{Ag/AgCl} + 0.197\ V + 0.059\ V \times pH$. For the deposition process, copper substrates with a precisely cut geometric surface area of 0.2826 cm^2 were utilized. These substrates served as the deposition surface for both the metals and the M@rGO composites. Before deposition, the copper substrates underwent a thorough cleaning procedure involving concentrated hydrochloric acid, acetone, and water to ensure their cleanliness.

Thin films of graphene oxide (GO) were prepared by drop-casting an aqueous-ethanol suspension onto the copper substrates and then dried under vacuum conditions. The deposition process was conducted on either bare copper substrates or graphene oxide-modified copper substrates. Table A2 in Appendix A provides details of the composition of the electrodeposition baths and the specific deposition conditions. The as-prepared electrodes were labeled as M-t or M@rGO-t, where "t" represents the deposition time in seconds. To record the polarization curves for HER, linear sweep voltammetry was employed at a scan rate of 10 mV s^{-1} in an Ar-purged 1 mol dm^{-3} aqueous KOH solution. All measurements were conducted using the above-described cell configuration.

4.1.7. Characterization of the polycrystalline electrocatalysts

The surface morphology of pure Ni and Ni@r(GO) deposits was examined by scanning electron microscopy (SEM) using a JEOL JSM 6460 LV electron microscope.

4.1.8. Co-deposition of Ni and rGO and the measurements of HER activity

In this experiment, Ni (nickel) and Ni@rGO (nickel-reduced graphene oxide) composites were electrodeposited on a polished Ti (titanium) rod with a cross-sectional diameter of 3 mm. The electrodeposition bath used for this process comprised 0.2 mol dm^{-3} H_3BO_3, 0.5 mol dm^{-3} NH_4Cl, and 0.125 mol dm^{-3} $NiSO_4$. Additionally, 0.1 g dm^{-3} of GO (Graphenea, Spain) was added to the bath to produce the Ni@rGO composite. The electrodeposition process was performed in a two-electrode electrochemical cell. The Ti rod was positioned upright in the cell, and a spiral-shaped Ni electrode was placed symmetrically around it. The deposition was carried out under constant current conditions, specifically at a current density of -50 mA cm^{-2}, for a total duration of 90 seconds.

Once the electrodeposition was completed, the electrodes were rinsed with deionized water to remove any residual traces from the process. Subsequently, they were transferred to a three-electrode electrochemical cell for conducting HER measurements. Electrochemical measurements were done in the same way as described in Sections 4.1.2 and 4.1.4 in one compartment three-electrode electrochemical cell where a 3×3 cm Ni foam served as a counter electrode, and KOH solution was used as an electrolyte in all experiments. To prevent the obstruction of the surface by bubbles, the Ti rod was oriented in an upward position.

4.2. DFT calculations

The first-principle DFT calculations were executed using the Vienna ab initio simulation code (VASP) [149]–[151]. The Generalized Gradient Approximation (GGA) in the parametrization by Perdew, Burk, and Ernzerhof [152] combined with the projector augmented wave (PAW) method was used [153]. For the first part of the thesis work, cut-off energy of 350 eV and Gaussian smearing with a width of σ =

0.025 eV for the occupation of the electronic levels were used. The (2 × 2) Zn (0001) and Cr (110) surfaces were investigated. In the second part of the research, a cut-off energy of 40 Ry was employed for the calculations. Additionally, a larger charge density cut-off, 16 times larger than the energy cut-off, was used. The investigation focused on the densely packed (111) surface of Face-Centered Cubic (FCC) metals, including Ag, Au, Ni, Pd, and Pt. Furthermore, the (0001) surface of Hexagonal Close-Packed (HCP) metals, Co, and Zn, as well as the Fe(110) surface of Body-Centered Cubic (BCC) metal, were also examined. For each of these surfaces, corresponding p(2×2) cells with specific characteristics and four-layer slabs were used in the calculations. To ensure accurate integration of the electronic states, a Monkhorst–Pack Γ-centered 4×4×1 k-point mesh was employed. This k-point mesh was used to integrate the first irreducible Brillouin zone, allowing for a comprehensive analysis of the electronic properties and structural characteristics of the selected metal surfaces [152]. For both cases, four-layer slabs were used. In this study, the adsorption of atomic hydrogen was investigated at a coverage of 0.25 monolayer (ML). The binding energy of the adsorbed hydrogen atom (HBE) was calculated relative to an isolated H_2 molecule using the following formula:

$$\mathrm{HBE} = E_{Surf+H} - E_{surf} - 1/2E_{H2} \quad (4.1)$$

Here, $E_{\mathrm{Surf+H}}$ represents the total energy of the surface with an adsorbed hydrogen atom, E_{Surf} is the total energy of the clean surface, and E_{H2} is the total energy of an isolated H_2 molecule. For metals other than the ones investigated in this work, literature data calculated at the same level of theory using periodic DFT calculations were used. The compiled data for these metals can be found in Table A1 in Appendix A.

4.3. KMC simulations

In this study, Kinetic Monte Carlo (KMC) simulations were conducted using the KMCLib v1.1 [154] code. KMC simulations are used to model the dynamics of rare events in a system based on the provided elementary processes and their reaction rates. The system's initial configuration was defined on a regular grid in space, and all the relevant elementary processes and their associated rates were input into the KMCLib code. During the simulations, the system was propagated from one state to another on the free energy landscape determined by the provided elementary processes and rates. Sufficient time was given to the simulations to allow the system to equilibrate. After equilibration, statistical data were collected to analyze various aspects of the system's behavior.

Some of the key statistics collected during the simulations included:

1. Integral H_2 production rates on the support: This refers to the rates at which hydrogen molecules were produced on the catalyst support.
2. Overall H_2 production rate: This indicates the total rate of hydrogen production in the system.
3. Hydrogen coverage of the catalyst and the support: This quantifies the fraction of available sites on the catalyst and the support that were occupied by hydrogen atoms.
4. Spatial maps of H_2 production (normalized from 0 to 1): This provides a visual representation of the spatial distribution of hydrogen production, with values normalized between 0 and 1 to facilitate comparisons.

By analyzing these statistics, the researchers gained valuable insights into the hydrogen production process and the behavior of the system under study.

Chapter five - Result and discussion

5.1. The polarization (I-E) curves for the monometallic polycrystalline electrocatalysts

To analyze the catalytic capabilities of the polycrystalline metals being studied, we computed the overpotentials for the HER at a current density of -0.1 mA cm^{-2}_{real}. Our selection of the current density was not arbitrary; instead, we based it on the established standard measure of HER activity -10 mA cm^{-2}_{geom}) set by McCrory *et al*. [155]. The cited study compares high surface area catalysts using the same value (-10 mA cm^{-2}_{geom}), and their RFs are around 10^2. This implies that if normalized to the ECSA, the comparison could be made using approximately 10^2 times lower current densities. To have a more genuine comparison of catalytic activities among the investigated metals, the current values were normalized with respect to the ECSA of each disk electrode to obtain real surface area normalized current density (j_{real}) values. ECSA of the electrodes were calculated as described in section 4.1.5. To explore the impact of the presence/formation of oxides, the HER activities of the metals were examined in two distinct states: when freshly polished and after being exposed to HER oxidation potentials.

It should be noted that the oxidation process was performed only on specific electrodes deemed significant for investigation. Polarization curves (j_{real} vs. E) are then plotted for all the metals in each solution. The corresponding overpotential values required to achieve a current density of -0.1 mA cm^{-2}_{real} ($\eta_{0.1}$) were then determined as presented in Tables 5.1 and 5.2. By measuring the overpotential at a constant current density, an insight into how the electrode material significantly influences the potential or energy needed to facilitate hydrogen production can be gained [106]. The superior electrocatalyst is always characterized by a lower overpotential at the desired current density [43].

Figures 5.1 represent the analyzed metals' polarisation curves in 0.1 mol dm^{-3} HCl and 0.1 mol dm^{-3} $HClO_4$. When examining the HER activity of metals in a 0.1 mol dm^{-3} HCl solution for freshly polished electrodes (as shown in Figure 5.1a), the metals follow the sequence of Pt > Ni > W > Co > Ag > Fe > Cr > Zn > Au. After oxidative treatment, the HER activity of Pt slightly increased, while that of W decreased, and Cr remained relatively unchanged. For the case of the freshly polished electrodes in 0.1 mol dm^{-3} $HClO_4$ (Figure 5.1b), the HER activities of the metals follow the order Pt > Ni > Co > W > Cr > Ag > Au > Fe > Zn. Surprisingly, the HER performance of Cr is high in 0.1 mol dm^{-3} $HClO_4$ after Pt, Ni, Co, and W. Following an oxidative treatment, the HER activity of Ag and Au has improved significantly, whereas the HER activity of Pt has slightly increased. However, the HER activity of Cr and W has decreased after oxidative treatment. The decrease in the activity of Cr in 0.1 mol dm^{-3} $HClO_4$ and that of W in both the acidic electrolytes following oxidative treatment can be attributed to the spontaneous passivation of the Cr and W electrode in acidic environments. Upon careful comparison between the two acidic solutions (Table 5.1), it can be observed that though Ag and Au display slightly enhanced catalytic performances in HCl solutions, the majority of the metals, such as Pt, Co, Cr, Fe, Ni, W, and Zn, demonstrate better catalytic activities in $HClO_4$ when compared to HCl. The reason for this difference in catalytic activities can be attributed to chlorine ion poisoning in 0.1 mol dm^{-3} M HCl and to the non-adsorbing property of ClO_4^- anion in 0.1 mol dm^{-3} $HClO_4$ [78].

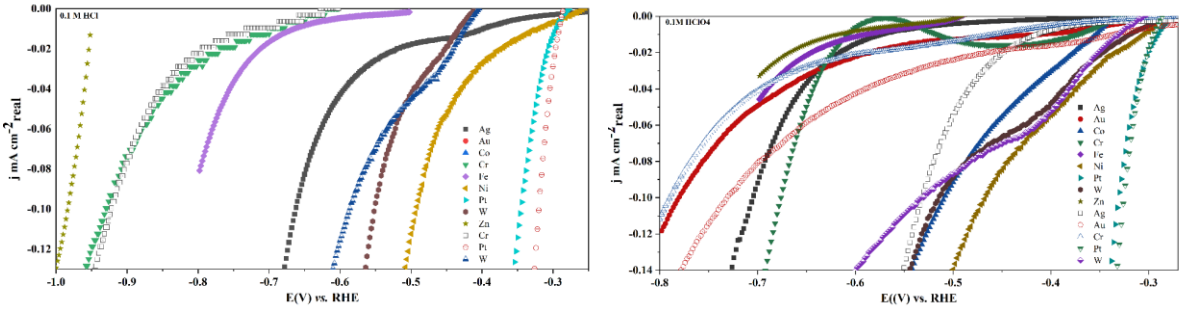

a) b)

Figure 5.1 HER polarization curves for freshly polished and oxidatively treated electrodes in a) 0.1 mol dm^{-3} HCl solution and b) 0.1 mol dm^{-3} $HClO_4$ solution. Solid symbols indicate freshly polished electrodes, while empty or half-empty symbols represent oxidatively treated electrodes.

Figure 5.2 represents the polarization curves of the analyzed metals in pH-neutral solutions, specifically 0.1 mol dm^{-3} NaCl and 1 mol dm^{-3} KH_2PO_4. In the case of freshly polished electrodes, as shown in Figures 5.2a and b, the HER activity in both pH-neutral solutions exhibits a similar trend, decreasing in the following order: Pt > Ni > Cr > W > Fe ~ Co > Au > Ag > Zn. Interestingly, similar to the observations in 0.1 mol dm^{-3} $HClO_4$, Cr exhibits remarkably high HER activity in the pH-neutral solutions, surpassing that of tungsten W, Fe, and Co. This suggests the potential utility of Cr as a catalyst for HER in seawater splitting applications. Following the oxidative treatment, the HER activity of Pt, W, Fe, and Cr in 0.1 mol dm^{-3} NaCl solution declined, while Ni, Co, Ag, and Au increased. Similarly, in 1 mol dm^{-3} KH_2PO_4 solution, the HER activity of Ni, Cr, Ag, Au, Co, and Fe improved, while that of W decreased after oxidative treatment. Following oxidative treatment, the decline in the HER activity of Cr in a 0.1 mol dm^{-3} NaCl solution could be ascribed to the formation of stable oxides that are not soluble in pH-neutral and alkaline solutions in the HER potential region. In contrast, the decrease in HER activity of Pt and Fe in the NaCl solution can be attributed to Cl^- ion poisoning. Additionally, the reduction in HER activity of W in both the pH-neutral solutions could be due to the limited concentration of OH^- ions (10^{-7} mol dm^{-3}), which may not be sufficient to dissolve the oxides present/formed on the surface of W. One intriguing discovery in our research is that following the oxidative treatment, the HER activity of Ni in 0.5 mol dm^{-3} NaCl exceeded that of Pt. The possible reasons behind this observation will be elucidated in subsequent sections. Upon careful comparison between the two neutral solutions (Table 5.1 and 5.2), it is evident that the HER performance of all the freshly polished and oxidatively treated metals is better in KH_2PO_4 compared to the NaCl solution. This difference can be attributed to chloride ion poisoning of the metal electrodes in NaCl (simulated seawater) solution.

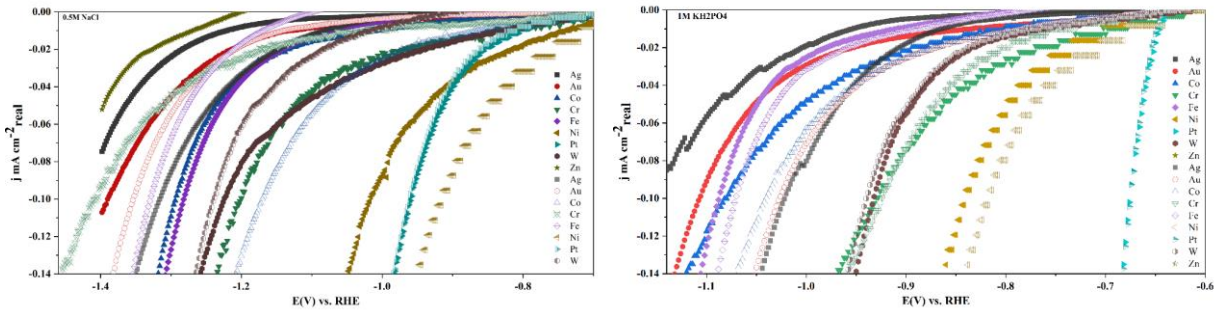

a) b)

Figure 5.2 HER polarization curves, for both freshly polished and oxidatively treated electrodes, in a) 0.1 mol dm^{-3} NaCl solution and b) 0.1 mol dm^{-3} KH_2O_4 solution. Solid symbols indicate freshly polished electrodes, while empty/half-empty symbols represent oxidatively treated electrodes.

Figure 5.3 represents the polarization curves of the analyzed metals in KOH solutions having different concentrations, specifically 0.1 mol dm^{-3} KOH and 1 mol dm^{-3} KOH. The HER activities of the freshly polished electrodes in 0.1 mol dm^{-3} KOH (Figure 5.3a) follow the order Pt > Ni > W > Co > Fe > Cr > Ag > Au > Zn. After undergoing oxidative treatment, the HER performance of Pt, Ni, Co, Ag, and Au increased while that of W, Fe, and Cr decreased. Conversely, the HER activities of the freshly polished electrodes in 1 mol dm^{-3} KOH (Figure 5.3b) follow the order Pt > Ni > Co > W > Au > Fe > Ag > Cr > Zn. After undergoing oxidative treatment, the HER activity of Cr, the sole metal analyzed in this case, decreased. The decrease in the activity of Cr, in both 0.1 and 1 mol dm^{-3} KOH, after oxidative treatment is ascribed to the formation of stable oxide films on the electrode surface, which hinders HER. After a careful comparison of both the data presented in Table 5.1 and Figure 5.3 for the two KOH solutions, it is clear that the majority of the freshly polished electrodes (such as Pt, W, Co, Ag, Au, and Zn) exhibit better HER performance in 1 mol dm^{-3} KOH as compared to 0.1 mol dm^{-3} KOH. Thus, an increase in the concentration of KOH has a positive impact on the HER activity of the metals. According to a study by Faid *et al*. [156], a change in pH and KOH concentration (0.01 to 2 M KOH) affected the HER activity of Ni-based catalysts by influencing the ECSA and Tafel slope. However, the authors observed that at a concentration of 2.0 M KOH, the HER properties of the catalysts were impeded due to the reduced transport kinetics of OH_{ad}. These results imply that there is a possibility of enhancing the HER performance by increasing the concentration of KOH up to a certain threshold.

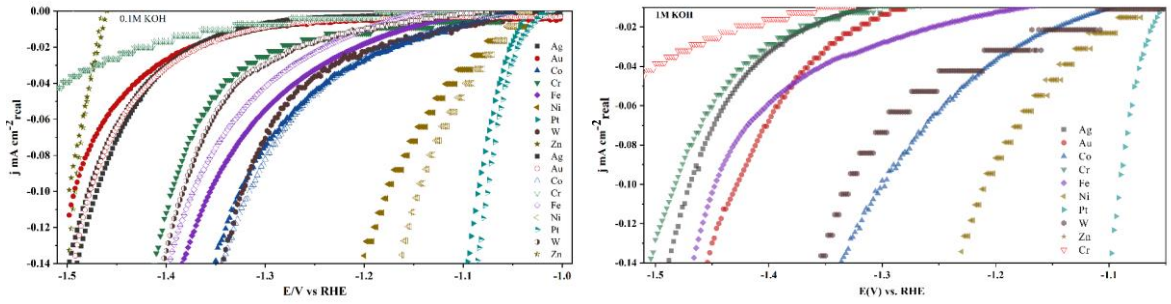

a) b)

Figure 5.3 HER polarization curves for both freshly polished and oxidatively treated electrodes in a) 0.1 mol dm^{-3} KOH solution and b) 1 mol dm^{-3} KOH solution. Solid symbols indicate freshly polished electrodes, while empty or half-empty symbols represent oxidatively treated electrodes.

Figure 5.4 represents the polarization curves of the analyzed metals in 0.1 mol dm^{-3} LiOH. The HER activity for the freshly polished electrodes in LiOH follows the order Pt > Ni > W > Co > Fe > Au > Cr > Ag > Zn. The HER activities of Ni, Co, Cr, Ag, and Au are improved post-oxidation treatment, whereas those of W and Pt were lowered. Comparing the HER activities across the three alkaline solutions (Table 5.1 and 5.2), the HER catalytic performance of the freshly polished metals in 0.1 mol dm^{-3} LiOH is slightly higher than that of 1 mol dm^{-3} KOH, which, in turn, is marginally better than that of 0.1 mol dm^{-3} KOH, which agrees with prior research [157]–[159]. The HER activity of Au in 1 mol dm^{-3} KOH and 0.1 mol dm^{-3} LiOH is much higher than in 0.1 mol dm^{-3} KOH. It seems that Au is sensitive to the electrolyte concentration and nature of the alkali metal ions. A study by Goyal and Koper [160] revealed that the kinetics of the HER on Au electrodes are influenced by electrolyte pH and alkali metal cation concentration. Increasing cation concentration at a mildly alkaline pH (pH = 11) enhances the HER activity of Au electrodes. Additionally, after undergoing oxidative treatments, the HER activities of the metals are higher in LiOH compared to 0.1 mol dm^{-3} KOH. The improved HER performance of the metals in LiOH solution is attributed to the effect of Li ions. Li^+-ion-induced destabilization of the HO-H bond is believed to accelerate sluggish water dissociation [159], [160]. The HER activity of the metals in the investigated electrolyte solutions, as determined by the $\eta_{0.1}$ (Table 5.1 and 5.2), follows the following order: 0.1 M $HClO_4$ > 0.1 M LiOH > 1 M KH_2PO_4 > 0.1 M HCl > 1 M KOH > 0.1M KOH > 0.5 M NaCl. It is widely accepted that the accelerated formation of H_{ads} intermediates from H_3O^+ plays a significant role in enhancing the HER activity of metals in acidic solutions. Conversely, the decreased activity of metals in the HCl solution can be attributed to the negative effects of Cl^- ion poisoning. The higher HER activity of 1 M KOH compared to 0.1 M KOH is primarily due to the concentration effect of K^+ ions [160]. The metals exhibited lowered HER activity in 0.5 M NaCl, once again due to the detrimental impact of Cl^- ion poisoning. The improved HER performance of the metals in LiOH solution is attributed to the effect of Li ions. By positively interacting with the dissociating water molecule (H_{ads}–$OH^{\delta-}$–cat^+), structure-making cations like Li^+ are known to play a crucial part in stabilizing the transition state of the RDS (Volmer step) in alkaline solutions [159], [160] Huang *et al*. [157], have reported that the HER activity of Pt (111), in the pH range of 1 to 14, is boosted with increasing structure-making propensity of cations in the order of $Cs^+ < Rb^+ < K^+ < Na^+ < Li^+$. A similar order of activity $Li^+ > Na^+ > K^+ > Cs^+$ was reported by Taji *et al*. [159] with 0.1 M LiOH having the highest activity at low overpotentials. The Volmer-Heyrovsky and Volmer-Tafel processes' relative contributions to the overall reaction were shown to vary depending on the type of the alkali metal cation, with the Volmer-Heyrovsky being more significant for LiOH electrolytes [159]. Monteiro *et al*. [158] demonstrated that strongly hydrated cations (Li^+) improve HER at higher overpotentials (more alkaline pH), but weakly hydrated cations (K^+) only do so at low overpotentials. The HER activity on Au electrodes at a moderately alkaline pH (pH = 11) was considerably boosted upon raising the cation concentration to a certain level, according to [160]. However, when the pH and hence the near-surface cation concentrations are high, the buildup of these species at the outer Helmholtz plane inhibits HER [158], [160].

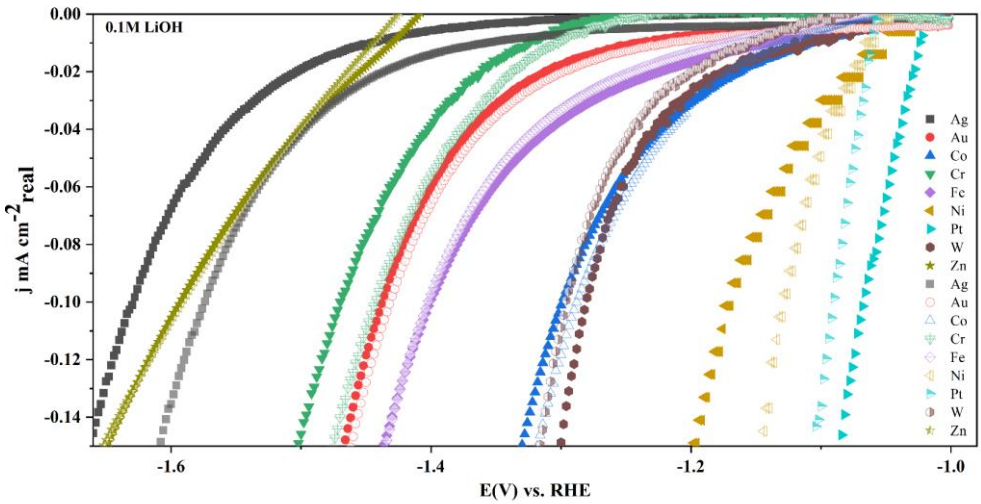

Figure 5.4 HER polarization curves for both freshly polished and oxidatively treated electrodes in 0.1 mol dm^{-3} LiOH solution. Solid symbols indicate freshly polished electrodes, while empty or half-empty symbols represent oxidatively treated electrodes.

Table 5.1 The overpotential (vs. RHE) values are needed for a current density of 0.1 mA cm^{-2}_{real} (vs. RHE) of the freshly polished metals in each solution.

	Overpotential of the metals in the respective solutions (Before Oxidation)						
Metals	**0.1M KOH**	**1M KOH**	**0.1M LiOH**	**0.5M NaCl**	**1M KH_2PO_4**	**0.1M HCl**	**0.1M $HClO_4$**
Ag	-0.4598	-0.4338	-0.6086	-0.7314	-0.4932	-0.3504	-0.3927
Au	-0.4727	-0.3922	-0.4189	-0.7175	-0.4447	-0.3123	-0.4688
Co	-0.304	-0.2649	-0.2785	-0.624	-0.4204	-0.325	-0.1987
Cr	-0.3754	-0.4465	-0.4501	-0.5304	-0.268	-0.6205	-0.3656
Fe	-0.121	-0.1043	-0.0944	-0.3677	-0.2154	-0.3223	-0.2457
Ni	-0.157	-0.1752	-0.1485	-0.3467	-0.1813	-0.182	-0.157
Pt	-0.064	-0.0559	-0.0472	-0.2878	-0.0149	-0.0327	-0.0199
W	-0.2997	-0.2946	-0.2603	-0.5546	-0.2714	-0.2393	-0.2036
Zn	-0.4792	-0.4628	-0.5722	-0.7349	-0.5452	-0.6745	-0.4

Table 5.2 The overpotential (vs. RHE) values needed for a current density of 0.1 mA cm^{-2}_{real} (vs. RHE) of the metals in each solution after oxidative treatment.

	Overpotential of the metals in the respective solutions (After Oxidation)						
Metals	**0.1M KOH**	**1M KOH**	**0.1M LiOH**	**0.5M NaCl**	**1M KH_2PO_4**	**0.1M HCl**	**0.1M $HClO_4$**
Ag	-0.4507		-0.5543	-0.6456	-0.3599		
Au	-0.4567		-0.4113	-0.6837	-0.3668		
Co	-0.295		-0.2683	-0.5	-0.3807		
Cr	-0.5772	-0.5631	-0.4217	-0.7357	-0.2628	-0.6128	-0.4803
Fe	-0.1622		-0.1257	-0.4827	-0.2013		
Ni	-0.1252		-0.1097	-0.2435	-0.1554		
Pt	-0.0564		-0.0708	-0.292	-0.0168	-0.0106	-0.0138
W	-0.3637		-0.2761	-0.5693	-0.2802	-0.2749	-0.22
Zn	-0.4709		-0.5699		-0.5434		

5.2. The hydrogen binding energies of the monometallic polycrystalline electrocatalysts

The HBE data set was compiled by averaging available literature data on periodic DFT calculations from references [15], [138], [141], [161]. However, for metals where reliable literature data was not found (Cr and Zn), we have conducted their own calculations, as described in section 4.2. The compiled HBE values are given in Table A1 (Appendix A).

5.3. The Volcano plots (η-HBE) in acidic solutions

To construct the volcano plots, we have used the *I-E* curves obtained on freshly polished electrodes and after cycling the electrodes to high anodic potentials (approximately +1.4 V vs. RHE in a given electrolyte). The experimentally determined HER overpotential values, needed for the current density of 0.1 mA cm^{-2}_{real}, were then correlated with the DFT calculated HBE to construct volcano curves for all seven solutions. Figure 5.5 shows the HER volcano plots in the acidic solutions (0.1 mol dm^{-3} $HClO_4$ and 0.1 mol dm^{-3} HCl). The shape of the volcano curve is well preserved in the investigated acidic solutions in good agreement with Trasatti' and Nørskov's volcano plots [13], [141]. For both the freshly polished and oxidatively treated electrodes, Pt is situated at the peak of the volcano plot, very close to the optimum point (HBE = 0). This metal has a minimum overpotential close to zero for both cases because all the HER reaction steps involved in this metal are thermo-neutral [37]. The metals, including Ni, Co, Fe, W, and Cr, are located in the strong binding region, while Ag, Au, and Zn are located in the weakly binding region. One can easily observe the impact of the electrolyte on the shape of the volcano curve, as evidenced by the broader overpotential range (form ~ 0 to > -0.6 V) required for HER in HCl compared to $HClO_4$. The reason for this difference in catalytic activities can be attributed to Cl^- ion poisoning in 0.1 mol dm^{-3} HCl and to the non-adsorbing property of ClO_4^- anion in 0.1 mol dm^{-3} $HClO_4$. The effect of SO_4^{2-} and ClO_4^- anions on the HER activity of Pt(110) in 0.1 M KOH was examined by Sheng *et al*. [162]. ClO_4^- was shown to have no effect on the HBE, while the addition of SO_4^{2-} slightly altered the HBE of Pt (110). Conversely, there are studies that assert the insignificance of the effect of electrolyte anions on the HER. A comparable HER/HOR performance of Pt across three electrolytes ($HClO_4$, HNO_3, and H_2SO_4) is reported by [163]. Moreover, a study by [164] revealed that in contrast to the HOR, the HER current densities, which have been examined in low overpotential and underpotential sites, were found to be independent of the nature of the supporting electrolyte ($HClO_4$, H_2SO_4, and HCl).

When it comes to the effect of the exposure of the electrodes to oxidizing conditions, due to the ease with which Pt oxides can be reduced in all solutions, the effects of electrodes' exposure to anodic potentials on the HER activity are negligible. On the other hand, the HER activity of Cr in $HClO_4$ is significantly decreased, while the activity of W also slightly decreased in both HCl and $HClO_4$. Although the impact of oxidation on W is not as apparent for the low current densities utilized to assess the HER activities in this study, these decrease in activities can be explained by the formation of stable oxides, under HER conditions, on Cr and W surfaces which interfere with HER activities of the metals. Consequently, the strong-binding branch is depicted with a degree of uncertainty, and stable oxides on valve metals have the potential to disturb the volcano shape if precautions are not taken to prevent or minimize the presence of oxides, which may not be entirely feasible in certain circumstances.

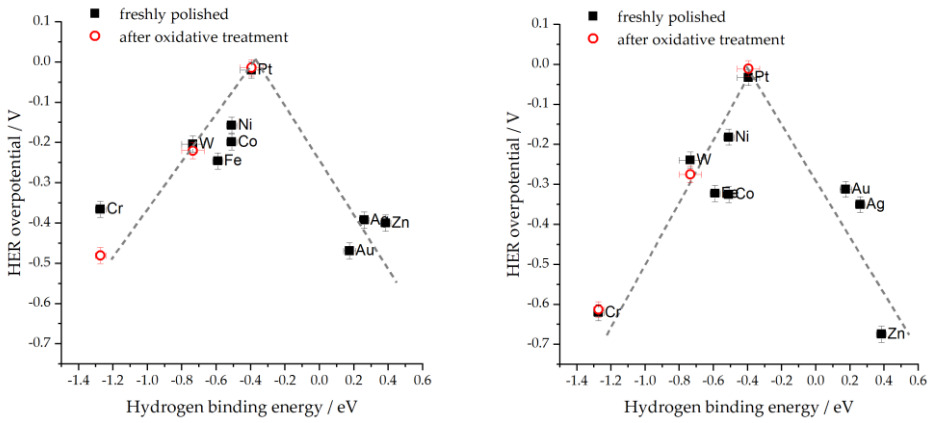

a) b)

Figure 5.5 The HER volcanoes in acidic solutions: (a) 0.1 mol dm^{-3} $HClO_4$; (b) 0.1 mol dm^{-3} HCl. Freshly polished electrodes are represented by squares, and circles are used to represent electrodes after undergoing oxidative treatment.

5.4. The Volcano plots (η-HBE) in neutral solutions

Figure 5.6 shows the HER volcano plots in the alkaline solutions: 0.5 mol dm^{-3} NaCl and 1 mol dm^{-3} KH_2PO_4. Similar to what has been observed in the acidic solutions, Pt exhibits the highest activity level among all the freshly polished electrodes. Overall, the shape of the volcano curve is preserved in the investigated neutral solutions in agreement with those reported in acidic [13], [49] and alkaline solutions [15]. Nevertheless, it is clear that the electrolytes have a substantial impact on the "absolute" activities of the metals being tested. This is exemplified by the higher HER overpotentials observed for the metals in the NaCl solution (Figure 5.6a) compared to those in the KH_2PO_4 solution (Figure 5.6b). In the NaCl solution, the volcano peak experiences a shift of approximately -0.3 V compared to the KH_2PO_4 solution, where Pt demonstrates a minimal overvoltage for HER. In neutral solutions, unique characteristics are observed in the HER activities. Notably, the strong binding branches of the HER volcanoes show a flattened trend for W and Cr. At the same time, Co exhibits unexpectedly low activities in both the pH-neutral solutions investigated. These findings align with the concepts proposed in reference [17], which discuss the activity of metals with highly exothermic hydrogen adsorption.

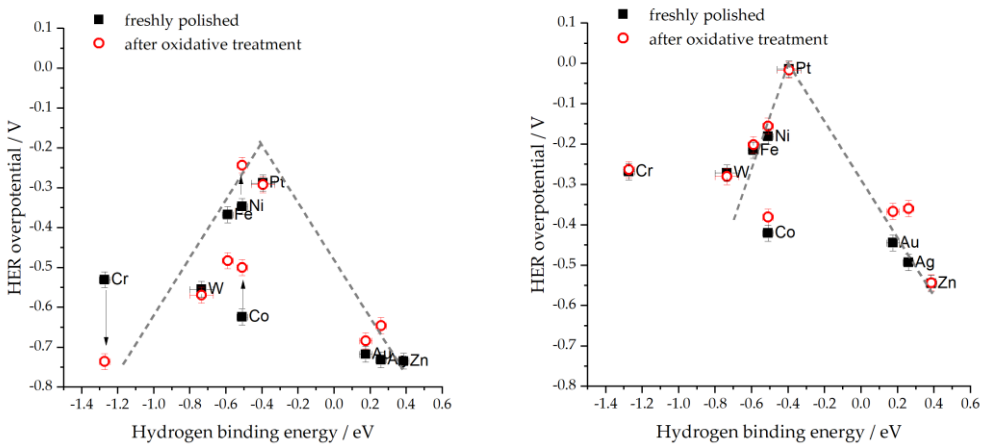

a) b)

Figure 5.6 The HER volcanoes in neutral solutions: (a) 0.5 mol dm^{-3} NaCl (simulated sea water); (b) 1 mol dm^{-3} KH_2PO_4 (pH was adjusted to 7.0 in both electrolytes.). Freshly polished electrodes are represented by squares, and circles are used to represent electrodes after undergoing oxidative treatment. Regarding the NaCl solution, significant changes in activity are indicated by arrows.

To account for the effects of surface oxidation, they can be divided into trivial and non-trivial. As investigations were carried out under hydrodynamic voltammetry conditions, trivial effects of surface oxidation pertain to situations where the metal is actively dissolved during the anodic cycle in conjunction with electrode rotation. In the case of Ag in NaCl solution, for instance, AgCl is generated and reduced over the process, increasing the specific surface area, thus the RF, and subsequently, the activity increases. As W-oxides easily dissolved in alkaline solutions, a similar pattern was anticipated for W in alkaline solutions [21]. However, W activity has shown a modest decline in almost all the investigated electrolytes. On the other hand, developing a stable oxide layer presents two possibilities and is linked to the non-trivial case of activity change. The first possibility is that the oxide layer is stable and obstructs the HER because of its intrinsic inactivity towards the HER and/or insulating characteristics. This situation is likely to apply in the case of Cr in most of the solutions examined and in the case of W in acidic solutions (as discussed in section 5.1). A profound effect of the oxide layer on HER is evident in the case of Cr in $HClO_4$ (Figure 5.5a) and NaCl (Figure 5.6a), as illustrated in Figure 5.7. Yet, the absence of a highly noticeable effect in HCl solution at low current densities raises the question of why this occurs. Still, there is no straightforward answer to this inquiry. While the HER activity of the metals in the HCl solution is significantly lower than in $HClO_4$, the effects of oxidation are not as pronounced, particularly at lower HER current densities (Figure 5.7b). At present, we can only make conjectures regarding potential dissimilarities in the states of chromium oxide films formed in $HClO_4$ and NaCl solutions compared to those formed in HCl solution. Ultimately, it is evident that the chromium oxide films formed in $HClO_4$ and NaCl solutions are not identical, as indicated by the differences observed in their cyclic voltammograms of formation (Figure 5.7, insets).

Another possibility is that the oxide layer boosts HER activity. This occurrence is observed for both Ni and Co in pH-neutral and alkaline solutions, while for Fe, the effect is either minor or negative. The impact of increasing HER is particularly pronounced in 0.5 mol dm^{-3} NaCl (simulated seawater) solution. This results in the activity of Ni surpassing that of Pt after the oxidative treatment, causing the peak of the volcano plot to shift towards Ni (Figure 5.6a). The lower activity of Pt in the simulated seawater can be attributed to the unusual behavior of Pt electrodes in chloride-containing-electrolyte solutions. The formation of a platinum-chloride complex of an unknown stoichiometry is predicted at anodic potentials

[165]. The enhanced HER activity of Ni in NaCl solution, after oxidative treatment, can be explained by the enhanced rate of water dissociation at the metal|oxide interface [18], [19]. Marković group investigated the HER in alkaline solutions using Ag, Cu, and Ni electrodes modified by $Ni(OH)_2$. Their findings showed that the activities of these modified surfaces were comparable to those of unmodified electrodes in acid solutions. Additionally, the presence of $Ni(OH)_2$ enhanced the activity of Ni surfaces by four times compared to Ni surfaces without $Ni(OH)_2$, indicating the significance of the oxide species on the surface. The same authors conducted a systematic study involving Pt(111) and different 3d metal hydroxides, revealing that each catalyst had similar H_{ads} adsorption abilities but varying abilities to adsorb hydroxyl groups. The HER activity demonstrated a consistent rise as the interaction between OH−M decreased. Remarkably, the catalyst with the weakest OH interaction, Pt(111)-$Ni(OH)_2$, exhibited the highest HER activity, approximately seven times greater than the unmodified Pt(111) electrode in 0.1M KOH [18], [79].

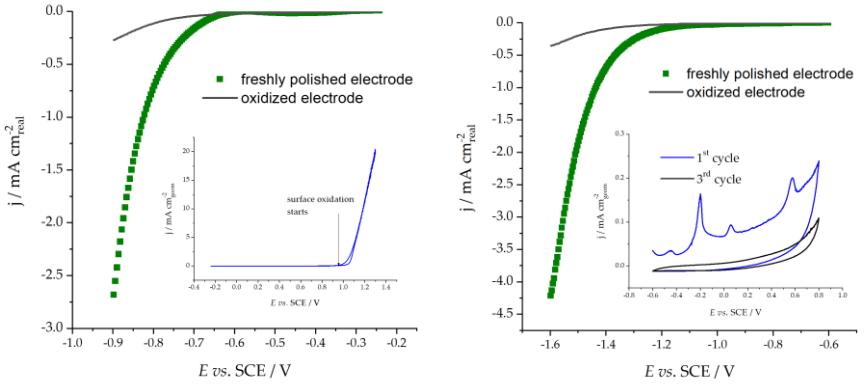

a) b)

Figure 5.7 The polarization curve of the Cr electrode for the HER both before and after undergoing oxidative treatment in (a) 0.1 mol dm^{-3} $HClO_4$ and (b) 0.5 mol dm^{-3} NaCl; the insets display cyclic voltammograms of the Cr electrode, illustrating the occurrence of irreversible oxide layer formation during the cycling process. In the $HClO_4$ solution, a roughly ten times higher current at the anodic vertex potential is observed compared to the NaCl solution.

5.5. The Volcano plots (η-HBE) in alkaline solutions

The HER volcano plots in alkaline solutions, specifically 0.1 mol dm^{-3} LiOH, 0.1 mol dm^{-3} KOH, and 1 mol dm^{-3} KOH, are displayed in Figures 5.8 (a-c). In both cases, i.e., for freshly polished and oxidatively treated electrodes, Pt exhibits the highest activity level among all the metals considered. In acidic solutions, Pt has an insignificant HER overvoltage due to faster HER kinetics. However, in alkaline solutions, the overvoltage is higher (by about -0.1 V), in line with previous research [166], due to the sluggish water dissociation step interfering with the HER process. The HER volcano plots are well preserved in all three alkaline solutions. They are in good agreement with each other and also with those reported by Sheng *et al*. [15] in alkaline solutions and by Trasatti and Nørskov [13], [141] in acidic solutions. For 0.1 mol dm^{-3} KOH, it is possible to identify two branches of the HER volcano plot with strong binding, depending on whether or not there is an oxide layer on the surface. This indicates that the volcano plots are preserved even after the metals are exposed to oxidizing conditions. The impact of the oxidative treatment of the metals on the HER in the alkaline solutions is more noticeable in 0.1 mol dm^{-3} KOH. In this situation, the activities of Cr, Fe, and W are reduced, while that of Ni is improved. The non-trivial effects of surface oxidation, where the formation of a stable oxide layer hampers the HER, are once again operative in the case of Cr in alkaline solutions. On the other hand, the formation of an oxide

layer, which actually enhances the HER activity, is operative for Ni in alkaline solutions, as elaborated in detail in section 5.4.

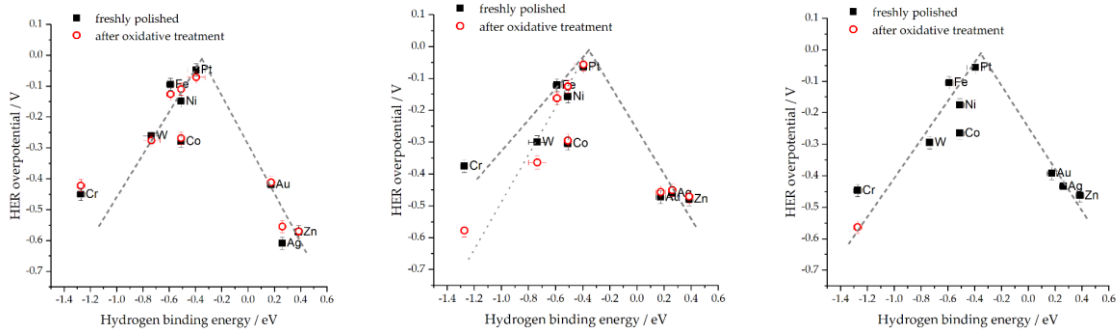

a) b) c)

Figure 5.8 The HER volcanoes in alkaline solutions: (a) 0.1 mol dm^{-3} LiOH; (b) 0.1 mol dm^{-3} KOH; (**c**) 1 mol dm^{-3} KOH. Freshly polished electrodes are represented by squares, and circles are used to represent electrodes after undergoing oxidative treatment. As for 0.1 mol dm^{-3} KOH, it is possible to observe two strongly binding branches of the HER volcano based on the presence of oxide on the surface.

The results indicate that volcano-like relationships for the HER hold true across the broad pH range. Under the specified experimental conditions, considering freshly polished surfaces and making efforts to minimize the presence of oxides as much as possible, Platinum is situated at the apex of the volcano curves. Nevertheless, the presence of strongly adsorbing ions, such as chloride, and the structure-making/breaking cations contribute to the relatively subtle effect of the electrolytes on the HER activity of the metals [90], [111], [159], [167]. Our main objective was to convey a significant discovery that HBE serves as a reliable descriptor for HER activities across the entire pH spectrum. However, it is crucial to consider the influence of surface oxidation and its influence as an additional factor. Without proper precautions, the shape of the volcano curve can be distorted, making it better or worse, depending on the characteristics of the electrolyte used.

Additionally, the formation of oxides and their impact on HER activity is influenced by the electrolyte, emphasizing the need to consider these factors when attempting to enhance HER through metal|oxide interface engineering. There are several potentially significant additional effects to consider. Primarily, impurities have the potential to influence the measured HER activities. From a fundamental standpoint, this can result in a shift in the position of a particular metal on the volcano plot. In this study, since the measurements were conducted in identical reaction conditions, the effect should be uniform for all the metals examined within a specific solution. From a practical perspective, particularly in industrial applications, this could have significant implications if there are metal impurities present that become deposited on the electrode in the HER process. Such impurities can alter the composition of the electrode's surface, thereby influencing its activity. Undoubtedly, this issue warrants further investigation since it remains unclear whether the presence of impurities can have a detrimental or beneficial impact on the HER activity.

Nevertheless, it is essential to highlight that the effect of chloride ions was addressed in both acidic and pH-neutral environments, with the effects being particularly noticeable in pH-neutral solutions. Therefore, it can be inferred that the impacts of impurities are likely to be dependent on the pH of the solution as well. This observation could be attributed to the pH-dependent nature of HBEs [101], where it has been observed that HBE decreases monotonously as the pH of the electrolyte increases. This effect is regarded as accountable for the pH-dependent electrochemistry of HER. However, based on the key

findings of this study, it is not considered to be of primary significance. Specifically, our study demonstrates that new catalysts can be evaluated using HBEs calculated at the metal|vacuum interface, regardless of the pH of the electrolyte in which the HER takes place.

Therefore, the crucial factor is to discover a catalyst that exhibits a comparable strength of H_{ads} adsorption to Pt. Depending on the pH of the solution, the HBEs will systematically shift, while the activity should remain close to that of Pt. The same principle applies to the presence of oxides. Although efforts can be made to minimize their presence, achieving complete elimination may not be feasible. Nonetheless, it is worth noting that the adsorption energies of simple adsorbates exhibit scaling relationships [141]. Consequently, a catalyst that binds H_{ads} in a manner similar to Pt should also exhibit similar behavior to Pt in terms of surface oxidation. Therefore, the quest for new catalysts that exhibit H_{ads} binding similar to Pt entails searching for catalysts that possess a comparable oxophilicity.

5.6. Kinetic parameters

Tafel analysis is a commonly used method for comparing the electrocatalytic activity of different materials. It leads to determining two significant kinetic parameters, specifically, Tafel slope and $j_{0,}$ which are essential factors in understanding reaction mechanisms and catalyst effectiveness. Section 3.1.2 explains the procedures employed for calculating the Tafel slope and j_0. At the same time, it is important to recall that a lower Tafel slope and a higher j_0 typically characterize a better electrocatalyst.

Comparison of Tafel slopes and HER j_0 values in 0.1 mol dm^{-3} $HClO_4$ and 0.1 mol dm^{-3} HCl with the literature data are shown in Table 5.3. Moreover, the HER Tafel plots for both freshly polished and oxidatively treated electrodes in 0.1 mol dm^{-3} $HClO_4$ and 0.1 mol dm^{-3} HCl are presented in Figure 5.9. The HER j_0 values in 0.1 mol dm^{-3} $HClO_4$ and 0.1 mol dm^{-3} HCl agree with [31] and are higher than those reported by [70] and lower than those reported by [80], [103], [168]. Similar to the observation based on the $\eta_{0.1}$, most metals exhibited improved HER performance in $HClO_4$ compared to HCl solution, as indicated by their j_0 values. Within the acidic electrolytes under investigation, polycrystalline Au and Ag electrodes display higher j_0 values, whereas Pt and W exhibit lower values; however, the j_0 values of Ni and Co are comparable to the literature collected j_0 values reported by Nørskov *et al*. [141]. The j_0 values confirm that Pt continues to be the most effective catalyst for the HER in acidic solutions, with Ni and Co ranking next in terms of performance.

Table 5.5 presents Tafel slopes and HER j_0 values in 0.5 mol dm^{-3} NaCl and 1 mol dm^{-3} KH_2PO_4 for freshly polished electrodes and after the electrodes are exposed to oxidative treatments. Moreover, the HER Tafel plots for both freshly polished and oxidatively treated electrodes in 0.5 mol dm^{-3} NaCl and 1 mol dm^{-3} KH_2PO_4 are presented in Figure 5.10. The j_0 values for all the metals (except Cr) are higher in KH_2PO_4 than NaCl, in agreement with the observations based on $\eta_{0.1}$.

Table 5.4 compares Tafel slopes and HER j_0 values in 0.1 mol dm^{-3} KOH and 1 mol dm^{-3} KOH with the literature data. Furthermore, Table 5.5 presents Tafel slopes and HER j_0 values in 0.1 mol dm^{-3} LiOH and 0.1 mol dm^{-3} KOH for freshly polished electrodes after the electrodes are exposed to oxidative treatments. Additionally, Figure 5.11 shows the HER Tafel plots for both freshly polished and oxidatively treated electrodes in 0.1 mol dm^{-3} LiOH, 1 mol dm^{-3} KOH, and 0.1 mol dm^{-3} KOH. The HER j_0 values in the alkaline solutions, namely 0.1 mol dm^{-3} KOH and 1 mol dm^{-3} KOH, are comparable to [15], [85], higher than [169] and lower than those reported by [23], [112], [142], [170]–[177]. The j_0 values for Ag, Co, Ni, and W in 0.1 M KOH in this study are notably comparable, while the values for Pt, Fe, and Au are slightly lower than those reported by Sheng *et al*. [15]. Pt continues to demonstrate its superiority as a catalyst for the HER in alkaline solutions, with Ni and Co following closely behind, as evidenced by their highest j_0 values. Based on the j_0 values in alkaline solutions, the HER activity of the freshly polished electrodes follows the order: 0.1 mol dm^{-3} LiOH > 1 mol dm^{-3} KOH > 0.1 mol dm^{-3} KOH.

While the HER following the oxidative treatment in 1 mol dm^{-3}, KOH was solely carried out for Cr, the j_0 values of all metals (except Ni) are higher in 0.1 mol dm^{-3} LiOH compared to 0.1 mol dm^{-3} KOH after undergoing oxidative treatments. This trend is again consistent with the observations based on $\eta_{0.1}$.

For the examined polycrystalline monometallic surfaces in the investigated electrolytes, the HER j_0 values differ by more than three orders of magnitude. A comparison of the HER j_0 values of the studied metals in the acidic, pH-neural, and alkaline solutions revealed that the HER activity of the freshly polished electrodes follows the order: 0.1 mol dm^{-3} $HClO_4$ > 0.1 mol dm^{-3} HCl ~ 0.1 mol dm^{-3} LiOH > 1 mol dm^{-3} KOH ~ 1 mol dm^{-3} KH_2PO_4 > 0.1 mol dm^{-3} KOH > 0.5 mol dm^{-3} NaCl. Similarly, for the solutions in which the HER was performed for all metals after oxidative treatments, the HER activity of the metals follows the order 0.1 mol dm^{-3} LiOH > 1 mol dm^{-3} KH_2PO_4 > 0.1 mol dm^{-3} KOH > 0.5 mol dm^{-3} NaCl. This order of HER activity of the electrolyte solutions differs slightly from the one observed based on $\eta_{0.1}$. This difference can be attributed to the fact that j_0 calculations, which are determined based on Tafel slopes, are susceptible to some errors.

The HER Tafel slopes for the examined metals in the investigated solutions fall in the range from - 53 mV dec^{-1} to - 292 mV dec^{-1}. Among the studied acidic solutions, Pt exhibits the lowest Tafel slope (Figure 5.9a and b), followed by W, Fe, and Ni. Notably, the Tafel slope for Co is unexpectedly high and does not align with the expected activity pattern. In the pH-neutral solutions: 0.5 M NaCl and 1 mol dm^{-3} KH_2SO_4, Pt have the lowest Tafel slope (Figure 5.10a and b) followed by Fe and Co (Fe ~ Co) in NaCl and by W in KH_2SO_4. Similarly, in the alkaline solutions: 0.1 mol dm^{-3} KOH, 1 mol dm^{-3} KOH, and 0.1 mol dm^{-3} LiOH, Pt has the lowest Tafel slope (Figure 5.11a and b) followed by W. Tafel slopes for Au, Ni, Co, and Pt are lower while that of Ag, Cr, and W are higher in 0.1 mol dm^{-3} KOH in this study compared to those reported by Sheng *et al*. [15]. While there is no distinct pattern in the Tafel slopes of the metals in the solutions being analyzed, significant variations in the Tafel slopes are observed. The HER Tafel slopes are influenced by various factors, including the pH of the electrolyte, the potential range used to determine the Tafel slope, and the H_{ads} surface coverage of the electrodes. It has been documented that the Tafel slope of bulk Pt disk electrodes displays a potential-dependent behavior in a 0.5 mol dm^{-3} H_2SO_4 electrolyte solution. Specifically, the Tafel slope ranges from 36 to 68 mV dec^{-1} initially and then increases to 125 mV dec^{-1} as the overpotential rises [41]. The Tafel slope of single crystal Au facets: Au(111), Au(100), and Au(110) was also found to vary gradually from about −60 mV dec^{-1} at high overpotentials and was consistent across the three Au facets [37].

Table 5.3 Comparison of Tafel slopes and HER exchange current density values in 0.1 mol dm^{-3} $HClO_4$ and 0.1 mol dm^{-3} HCl with the literature data

Electrode	***Log* (j_o (mA/cm^2))**	**Tafel slope (mV dec^{-1})**	**Electrolyte**	**Temperature**	**Surface are used**	**Literature**
Ag	- 4.11±0.01	- 127	0.1 M $HClO_4$	rt	real	this work
Au	- 2.79±0.02	- 263	*	*	real	this work
Au (100)	- 4.3					
Au (110)	-4.52					
Au (111)	- 3.6					
Au (pc)	- 3.85					
Au	- 2.6	- 118	0.1 M $HClO_4$	278 K	geo	[177]
Au	- 2.55	- 128.1	*	283 K	geo	[177]
Au	- 2.12	- 133.3	*	293 K	geo	[177]
Au	- 2	- 137.6	*	303 K	geo	[177]
Au	- 1.72	- 146.7	*	313 K	geo	[177]
Au	- 1.66	- 136	*	323 K	geo	[177]
Co	- 1.88±0.01	- 227	*	rt	real	This work
Cr	- 4.6±0.08	- 102	*	rt	real	This work

Fe	- 4.03±0.02	- 144	*	rt	real	This work
Ni	- 1.63±0.02	- 248	*	rt	real	This work
Pt	- 1.4±0.04	- 53	*	rt	real	This work
Pt (111)	- 0.68	- 74	*	nm		[80]
Pt (111)	0.17	---	*	nm		[103]
W	- 3.91±0.02	- 85	*	rt	real	This work
Ag	- 3.24±0.03	- 156	0.1 M HCl	rt	real	this work
Au	- 2.95±0.02	- 160	*	rt	real	this work
Co	- 2.47±0.03	- 219	*	rt	real	this work
Cr	- 3.58±0.03	- 240	*	rt	real	this work
Fe	- 4.57±0.01	- 139	*	rt	real	this work
Ni	- 2.29±0.04	- 140	*	rt	real	this work
Pt	- 1.46±0.05	- 77	*	rt	real	this work
Pt	0.2	---	*	nm	geo	[168]
Pt	0.079	---	7.72 M HCl	nm	geo	[168]
W	- 4.01±0.03	- 84	0.1 M HCl	rt	real	this work

* represents the same electrolyte as in its previous cell, rt represents room temperature, nm represents not mentioned, and geo indicates geometrical

Table 5.4 Comparison of Tafel slopes and HER exchange current density values in 0.1 mol dm^{-3} KOH and 1 mol dm^{-3} KOH with the literature data.

Electrode	***log* (j_o (mA/cm^2))**	**Tafel slope (mV dec^{-1})**	**Electrolyte**	**Temperature**	**Surface area used**	**Literature**
Ag	- 4.24±0.03	- 134	1 M KOH	rt	real	this work
Ag	- 4.3±0.15	- 139	0.1 M KOH	rt	real	this work
Ag	- 4.3±0.3	- 134±9	*	nm	geo	[15]
Au	- 3.25±0.06	- 175	1 M KOH	rt	real	this work
Au	- 4.53±0.01	- 134	0.1 M KOH	rt	real	this work
Au	- 3.2±0.6	- 168±9	*	nm		[15]
Au	- 2.85	- 167.7	*	278 K	geo	[177]
Au	- 2.82	- 159.8	*	283 K	geo	[177]
Au	- 2.72	- 155.4	*	293 K	geo	[177]
Au	- 2.55	- 157.4	*	303 K	geo	[177]
Au	- 2.26	- 167.5	*	313 K	geo	[177]
Au	- 1.74	- 139.7	*	323 K	geo	[177]
Au	- 1.54	- 141.4	*	333 K	geo	[177]
Co	-2.07 ±0.02	- 248	1 M KOH	rt	real	this work
Co	- 2.49±0.03	- 204	0.1 M KOH	rt	real	this work
Co	-2.5±0.4	126±6	*	nm		[15]
Cr	-4.0 ±0.04	- 149	1 M KOH	rt	real	this work
Cr	- 4.22	- 117	0.1 M KOH	rt	real	this work
Fe	- 3.4 ±0.08	- 172	1 M KOH	rt	real	this work
Fe	- 2.62±0.02	- 206	0.1 M KOH	rt	real	this work
Fe	- 1.9±0.4	- 131±12	*	nm		[15]
Ni	- 1.99±0.05	- 174	1 M KOH	rt	real	this work
Ni	- 1.95±0.05	- 132	0.1 M KOH	rt	real	this work
Ni	- 2.1±0.5	- 135±32	*	nm	geo	[15]
Ni foam	- 1.17	- 144	1 M KOH	nm	geo	[23]
Ni	- 2.60	121	*	nm	geo	[169]
Ni metal with possible surface state of NiOx	- 0.99	146±19	*		geo	[142]
Raney Ni (250)	0.95	84	25 % KOH	nm	geo	[171]

Ni metal with possible surface state of NiHx	- 1.77	105 - 125	1.3 M KOH	nm	geo	[172]
Ni metal with possible surface state of NiHx	- 1.45	115	30 (W%) KOH	nm		[173]
Pt	- 2.07±0.09	- 52	1 M KOH	rt	real	this work
Pt	- 1.93±0.08	- 72	0.1 M KOH	rt	real	this work
Pt	- 0.2±0.01	- 113±1	*	nm	geo	[15]
Pt	- 0.24±0.07	---	*	nm	geo	[112]
Pt (poly)	- 0.16	---	*	nm	geo	[174]
Pt	- 1 – 0.96	---	*	298 K	geo	[175]
Pt (111)	- 2	---	*	275 K	geo	[85]
Pt (111)	- 1.46	---	*	293 K	geo	[85]
Pt (111)	- 1	---	*	313 K	geo	[85]
Pt (111)	- 0.52	---	*	333 K	geo	[85]
Pt (110)	- 0.9	---	*	275 K	geo	[85]
Pt (110)	- 0.52	---	*	293 K	geo	[85]
Pt (110)	- 0.25	---	*	313 K	geo	[85]
Pt (110)	- 0.17	---	*	333 K	geo	[85]
Pt (100)	- 1.3	---	*	275 K	geo	[85]
Pt	0.02	---	1 M KOH (rt)	rt	geo	[176]
Pt (100)	- 0.83	460	8 M KOH	nm	geo	[170]
W	- 3.81±0.03	- 114	1 M KOH	rt	real	this work
W	- 3.97±0.03	- 107	0.1 M KOH	rt	real	this work
W	- 4.2±0.4	- 90±7	*	nm		[15]

* represents the same electrolyte as in its previous cell, rt represents room temperature, nm represents not mentioned, and geo indicates geometrical

Table 5.5 Tafel slopes and HER exchange current density values in 0.1 M LiOH, 0.1 M KOH, 0.5 M NaCl, and 1 M KH_2PO_4 for freshly polished electrodes and after the electrodes are exposed to oxidative treatments

Freshly polished electrodes			**After electrodes are exposed to oxidation potential**		
Electrode	***log (j₀)* mA/cm^2**	**Tafel slope (mV dec^{-1})**	**Electrolyte**	***log (j₀)* mA/cm^2**	**Tafel slope (mV dec^{-1})**
Ag	- 4.39±0.01	- 180	0.1 M LiOH	- 3.89±0.02	- 192±0.84
Au	- 3.48±0.01	- 169	*	- 3.38±0.01	- 173±0.36
Co	- 2.48±0.01	- 189	*	- 2.5±0.01	- 179±0.27
Cr	- 3.56±0.02	- 177	*	- 3.44±0.02	- 174±0.8
Fe	- 2.71±0.01	- 222	*	- 2.94±0.01	- 197±0.67
Ni	- 1.92±0.05	- 162	*	- 2.14±0.04	- 95±1.2
Pt	- 1.58±0.1	- 81	*	- 1.78±0.07	- 88±2.4
W	- 3.16±0.03	- 120	*	- 3.36±0.02	- 177±0.45
Ag	- 4.3±0.15	- 139±0.39)	0.1 M KOH	- 4.29±0.09	- 137±2.3
Au	- 4.53±0.01	- 134±2.3	*	- 4.3±0.04	- 138±1.1
Co	- 2.49±0.03	- 204±1.7	*	- 2.58±0.03	- 177±1.3
Cr	- 4.22±0.03	- 117±0.67	*	- 3.55±0.1	- 233±4.7
Fe	- 2.62±0.02	- 206±0.86	*	- 2.91±0.02	- 184±0.9
Ni	- 1.95±0.05	- 132±2.2	*	- 1.89±0.05	- 174±3
Pt	- 1.93±0.08	- 72±2	*	- 1.93±0.1	- 61±2
W	-(3.97±0.03)	- 107±0.74	*	- 4.0±0.03	-123±0.73
Ag	- 4.85±0.02	- 196±0.63	0.5 M NaCl	- 3.71±0.01	- 239±0.31
Au	- 3.74±0.02	- 263±1	*	- 4.34±0.01	- 205±0.35
Co	- 4.43±0.03	- 182±1	*	- 2.9±0.01	- 263±0.55

Cr	- 3.16±0.03	- 246±1.5	*	- 3.4±0.02	- 308±1.7
Fe	- 4.42±0.01	- 179±0.23	*	- 4.82±0.01	- 173±0.29
Ni	- 2.44±0.03	- 239±2.3	*	- 2.05±0.03	- 234±2.2
Pt	- 2.77±0.03	- 164±1.3	*	- 2.90±0.04	- 154±1.5
W	- 2.87±0.07	- 292±5.6	*	- 4.13±0.02	- 182±0.87
Ag	- 3.31±0.06	- 214±3.2	1 M KH_2PO_4	- 2.95±0.06)	- 184±2.8
Au	- 3.51±0.02	- 178±0.73	*	- 3.0±0.03)	- 183±1.1
Co	- 2.48±0.03	- 257±2.3	*	- 2.86±0.02)	- 204±1.3
Cr	- 2.84±0.03	- 168±1.3	*	- 4.59±0.11)	- 93±1.9
Fe	- 4.42±0.01	- 125±0.14	*	- 4.24±0.02)	- 127±0.39
Ni	- 2.22±0.05	- 148±2.3	*	- 2.04±0.03)	- 152±1.7
Pt	- 1.3±0.07	- 53±1.6	*	- 1.35±0.08)	- 47±1.5
W	- 4.1±0.05	- 93±0.88	*	- 3.96±0.05)	- 99±1

* represents the same electrolyte as in its previous cell

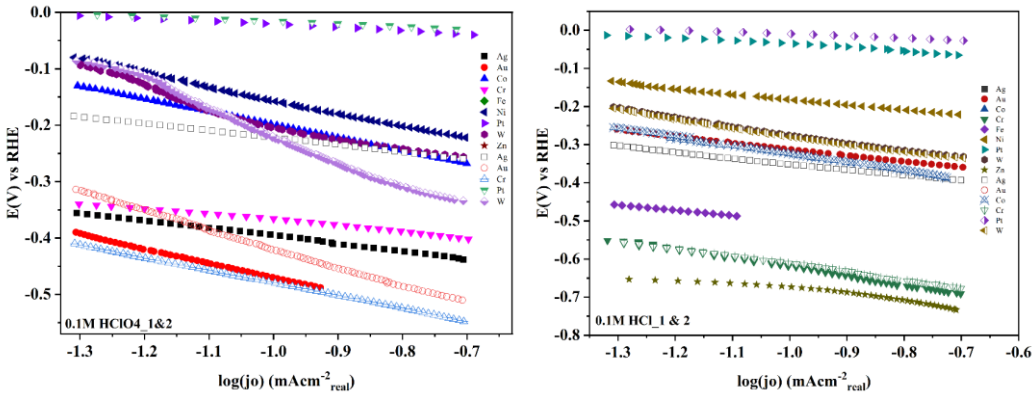

a) b)

Figure 5.9 The HER Tafel plots for the freshly polished and oxidatively treated electrodes a) in 0.1 mol dm^{-3} $HClO_4$ b) in 0.1 mol dm^{-3} HCl. Solid symbols indicate freshly polished electrodes, while empty or half-empty symbols represent oxidatively treated electrodes.

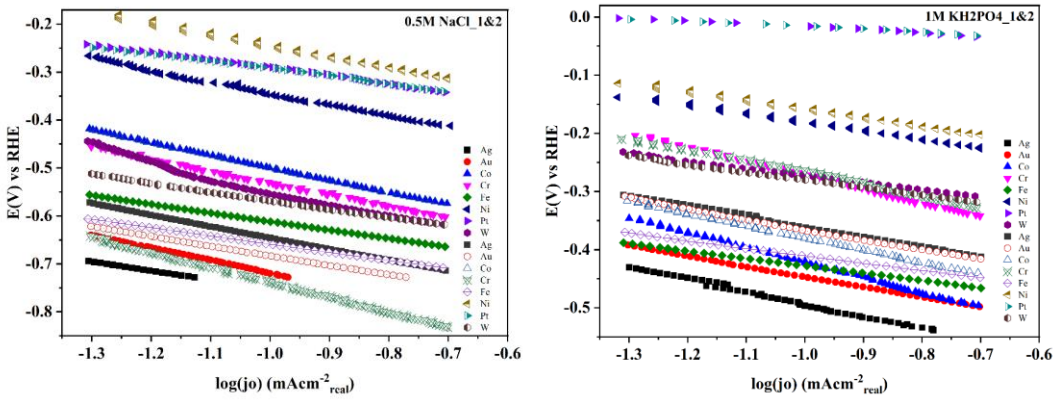

a) b)

Figure 5.10 The HER Tafel plots for the freshly polished and oxidatively treated electrodes a) in 0.5 mol dm^{-3} NaCl and b) in 1 mol dm^{-3} KH_2PO_4. Solid symbols indicate freshly polished electrodes, while empty or half-empty symbols represent oxidatively treated electrodes.

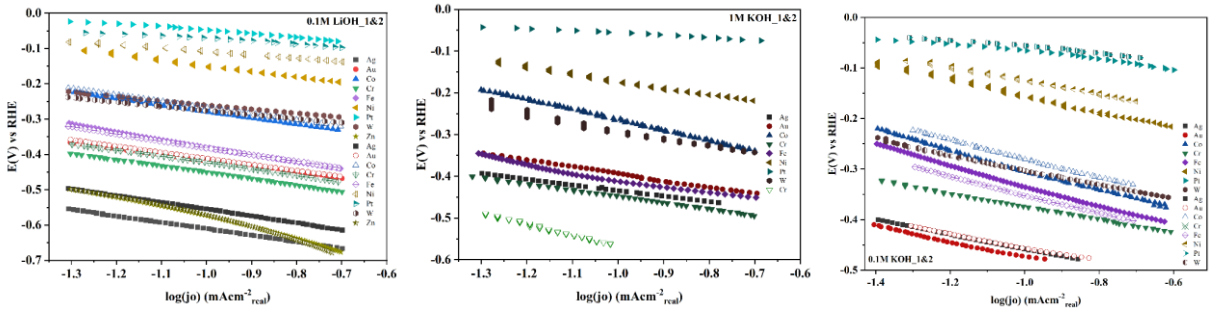

a) b) c)

Figure 5.11 The HER Tafel plots for the freshly polished and oxidatively treated electrodes a) in 0.1 mol dm^{-3} LiOH, b) in 1 mol dm^{-3} KOH, and c) in 0.1 mol dm^{-3} KOH. Solid symbols indicate freshly polished electrodes, while empty or half-empty symbols represent oxidatively treated electrodes.

5.7. KMC simulations—model

Now let's consider the process of the HER in alkaline media, where the initial step involves the dissociation of water (Volmer reaction) to generate adsorbed hydrogen (H_{ads}) on the surface of the catalyst:

$$H_2O + e^- + (*C) \rightarrow H_{ads} + OH^- \quad (5.1)$$

where *C represents the free adsorption site at the catalyst surface. In the subsequent stages, the H_{ads} on the catalyst surface is desorbed through either the Tafel reaction (as described in Equation. 6.2) or the Heyrovsky reaction (Equation 6.3).

$$H_{ads} + H_{ads} \rightarrow H_2 + 2(*C) \quad (5.2)$$

$$H_2O + e^- + H_{ads} + (*C) \rightarrow H_2 + (*C) + OH^- \quad (5.3)$$

HER follows the mechanism above when it occurs on a catalyst that is either unsupported or supported on a surface that cannot accept H_{ads}. In other words, this mechanism operates when hydrogen spillover is not active. Thus, the reaction will proceed via the Volmer-Tafel or the Volmer-Heyrovsky combination [178]. In the context of our analysis, we can refer to this particular scenario as a "surface path." Conversely, suppose the catalyst is placed on a support material capable of accepting Hads. In that case, there will be a balance between the amount of H_{ads} on the catalyst's surface and the portion of H_{ads} that has spilled onto the support material [178].

$$H_{ads}(*C) + (*S) \rightarrow (*C) + H_{ads}(*S) \quad (5.4)$$

Here, *S represents an adsorption site located on the surface of the support material. At this point, H_2 can be generated through the recombination of the H_{ads} present on the support material:

$$H_{ads}(*S) + H_{ads}(*S) \rightarrow H_2 + 2(*S) \quad (5.5)$$

We will refer to this path as the "interface path." It is essential to highlight that surface diffusion occurs since the H_{ads} species on the catalyst and the support material are dynamic. For the spillover process to occur, surface mobility is a prerequisite. Consequently, the diffusion processes of H_{ads} on both the C and S surfaces are crucial components of the interface path for HER. Therefore, the dynamics of our model systems can be explained by the processes above, which can be categorized into direct and reversed ones. The geometry of the system contains 130×130 unit cells. Considering the typical lattice constants of transition metals, this size would approximately correspond to a fraction of the surface measuring around 50x50 nm. First-principles calculations are not suitable for considering domains of this size, but they are sufficiently large to capture cooperative interactions between the catalyst and the support through KMC calculations. The unit cells represent individual adsorption sites, each categorized as either a catalyst or a support site. In defining the system configurations, we maintained the circular shape of catalyst islands on the support material. However, drawing inspiration from the discoveries made by [23], who showed enhanced HER by applying r(GO) onto Ni foam, we investigated a distinct scenario in which the support is alternatively deposited on the catalyst surface, which can be identified as a decorated catalyst surface. However, to keep things simple, we continued to refer to the decorator and support using the same notation (S). This notation is feasible because the crucial factor in our KMC model is the length of the interface, and the subtle geometric effects, such as the transfer of H_{ads} over a convex or concave interface, are not significant.

In our research, we adopted a similar approach to our previous work [26] and conducted conceptual modeling of the Hydrogen Evolution Reaction (HER) on supported (decorated) catalysts. To scale the reaction rates, we used a factor of 10^n, where n is an integer number. This choice was based on the observation that the activation barriers for the various elementary processes considered in our model

were comparable. The kinetic barriers for these processes, such as surface diffusion, H2 dissociation, and spillover from Pd atoms to Au(111) and Cu(111), were found to range from 0.12 to 0.18 eV [27].

Additional evidence provided by Nilekar *et al*. [28] indicated that surface diffusion barriers on transition metals are approximately 12% of the adsorbate's binding energy. For hydrogen, this translates to a range of 0.20-0.30 eV. Activation energies for the HER on transition metal surfaces generally fall within the same range as those for surface diffusion, although they can vary depending on the surface orientation [25]. Considering that the Arrhenius equation is used to describe the rate constants of elementary processes, a change in the reaction rate from 10^{-2} to 10^{2} corresponds to an alteration in the activation energy within the range of ±0.12 eV. Therefore, for values of n ranging from -2 to 2, the relative rates correspond to minor fluctuations in the activation energies of the various elementary processes included in our model. The reported rates of H_2 production are dimensionless, but they can be considered equivalent to experimentally measured currents.

5.8. KMC simulations—insights

In the initial set of computations, we examined the case where Eq. 5.1 exhibits a slower rate than all the remaining procedures in the model (formal rate 0.01, all other rates 1 or higher). This condition corresponds to the sluggish water dissociation and, thus, the slow rate of H_{ads} formation, which is typically regarded as challenging for the HER in alkaline environments [179], [180]. Nevertheless, the scenario changes when dealing with elevated HER overpotentials. In such cases, the formation of H_{ads} is quicker, while the H_{ads} desorption step becomes the RDS. For example, it has been determined that for polycrystalline Ni, the Heyrovsky reaction serves as the RDS at higher HER overpotentials, specifically when the surface coverage by H_{ads} is high. On the other hand, metallic surfaces that exhibit weak binding affinity towards H_{ads}, such as Au and Ag, will continue to have low water dissociation rates and H_{ads} coverage. Under these circumstances, the rate of spillover and the rate of H_{ads} desorption from S do not impact the overall production of H_2, while the formation of H_2 through reaction (5.5) is negligible. In this case, the coverage of the metal surface by H_{ads} is minimal, less than 0.01 monolayer (ML). As a result, the likelihood of H_{ads} spilling over onto the support is low, regardless of the spillover rate. In such a case, we can deduce that the process of spillover does not significantly impact the production of H_2. Additionally, the dispersion of the catalyst does not affect the rate of H_2 production in this specific case. The following scenario relates to the HER occurring at high overpotentials on metals, demonstrating a robust affinity or strong bonding with H_{ads}. Considering the findings presented in [179], [180], we established the Heyrovsky reaction as the RDS with a rate of 0.01. We omitted the Tafel reaction from the mechanism while assigning rates of 1 to all other steps, except for the spillover process (Eq. 5.4). In this particular scenario, the spillover rate was varied from 0.01 to 100. Each combination of rates for the elementary processes was evaluated across three different dispersions. These were 1, 4, and 16 evenly distributed catalyst islands of various sizes. Nevertheless, the coverage of the support by the metal remained consistent at 0.125 ML in all instances. An additional scenario involved placing the support on top of the metal in identical arrangements, leading to a metal coverage of 0.875 ML. Following the equilibration of each system, several parameters were evaluated, including the rate of H_2 production from the support, the overall H_2 production, the coverage of the metal surface by H_{ads}, and the coverage of the support by H_{ads} were determined (Figure 5.12). The results indicate that as the spillover rate increases, the rate of H_2 production accelerates. Moreover, in the catalyst@support (C@S) configuration, it is evident, from Figure 5.12 a and b, that the support plays a dominant role in the overall process.

The H_{ads} coverage of the catalyst surface reduces with dispersion, whereas the H_{ads} coverage of the support rises. Given the identical set of reaction rates, the H_2 production originating from the support in the support@catalyst (S@C) system is essentially the same as the production seen in the (C@S) system. Nevertheless, the total H_2 production is significantly higher in this case due to the involvement of a larger

number of catalyst sites that contribute to H_2 production, extending beyond the C|S interface. Although there are seven times more catalyst sites in the S@C than in the C@S system, when the total rates of H_2 generation are compared for the quickest spillover situation, the rate of H_2 generation in the S@C system is only two times greater. The overall H_2 generation is thus greatly influenced by the interface path. Also, spillover helps clean catalyst sites and prevents poisoning by H_{ads}.

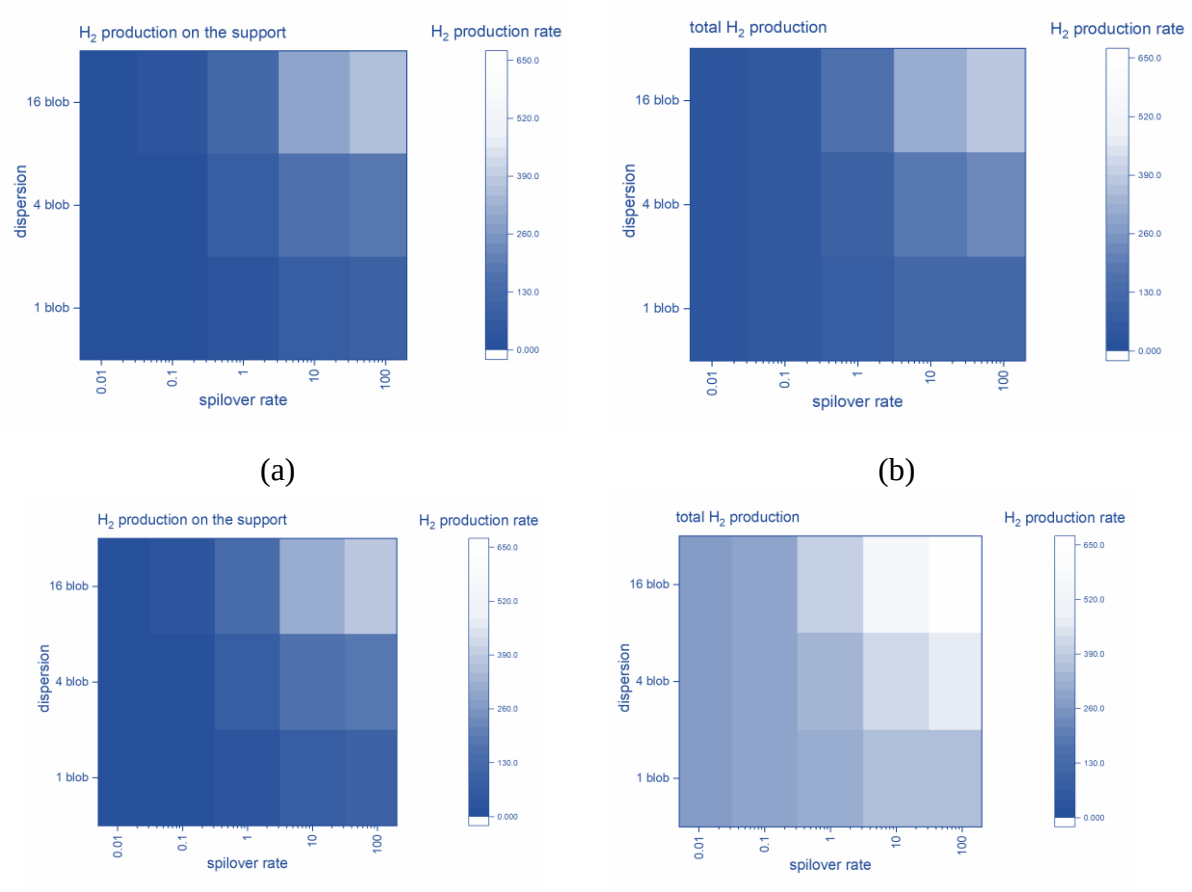

Figure 5.12 Heat maps illustrating the H_2 generation at a slow rate of Heyrovsky reaction, as a function of catalyst dispersion and spillover rate. Panels (a) and (b) represent H_2 production from the support and overall production, respectively, for the C@S configuration. Panels (c) and (d) depict H_2 production from the support and overall production, respectively, for the S@C configuration.

The impact of metal coverage is considered in the next set of simulations. Various quantities of catalyst/support islands are uniformly placed on the support/catalyst, as depicted in Figure 5.13 (a). At the same time, the rates of H_{ads} diffusion on the support (Eq. 5.4) and the rate of H_2 desorption from the support (Eq. 5.5) were adjusted within the range of 1 to 100. Nevertheless, for a specific simulation, we set the diffusion (Eq. 5.4) and desorption rates (Eq. 5.5) equal, resulting in rates of 1-1, 10-10, and 100-100. Explicitly, the diffusion barrier is proportional to the binding energy of H_{ads} [28], while the recombination of H_{ads} will occur at a faster rate for weaker binding. For each combination of the rates under consideration, spillover rates of 0.01, 1, and 100 were tested. The results for the pair of rates 100-100 for reactions (5.4) and (5.5) are presented in Figure 5.13 (b-e). As the spillover rate rises, there is a corresponding rise in H_2 generation from the S phase, while the coverage of H_{ads} on the metal phase decreases. In the C@S system, the overall H_2 generation rises with the catalyst fraction and peaks when the metal coverage reaches 0.5 ML.

Conversely, in the S@C configuration, the overall H_2 production decreases as the catalyst fraction increases, reaching its maximum at a catalyst fraction of 0.5 ML. These results imply that the C|S interface determines the observed trends. Most hydrogen is generated at the support material and the C|S interface when the spillover rate is rapid or at least similar to the rates of other processes within the system. In contrast, the system's leading site of hydrogen generation occurs at the C|S interface, specifically on the S side, if H_{ads} diffusion on the support is not quicker than the other processes in the system (including H_{ads} recombination on the support in our simulation). This is evident in the spatial maps depicting H_2 production in the C@S configuration. In these maps, all rates are set to 1, except for the rate of the Heyrovsky reaction, which is set to 0.01 (Figure 5.13, a).

Nonetheless, a cohesive representation can be provided to demonstrate that as the catalyst coverage on the support increases from a low level, H_2 production also rises. However, as the catalyst coverage exceeds 0.5 ML, the H_2 production starts to decrease (Figure 5.14, with the spillover rate set to 1). At this moment, the length of the C|S boundary begins to diminish. Consequently, if the spillover path dominates H_2 generation, this drop will result in a general decline in the rate of H_2 generation. Subsequently, this leads to the formation of a curve resembling a volcano when plotting the rate of H_2 production against the fraction of metal on the support. Naturally, the precise location of the apex on the volcano-shaped curve would be influenced by the rates of all processes in the system and the extent of catalyst coverage on the support, as evidenced by previous studies on Ni deposited on r(GO).

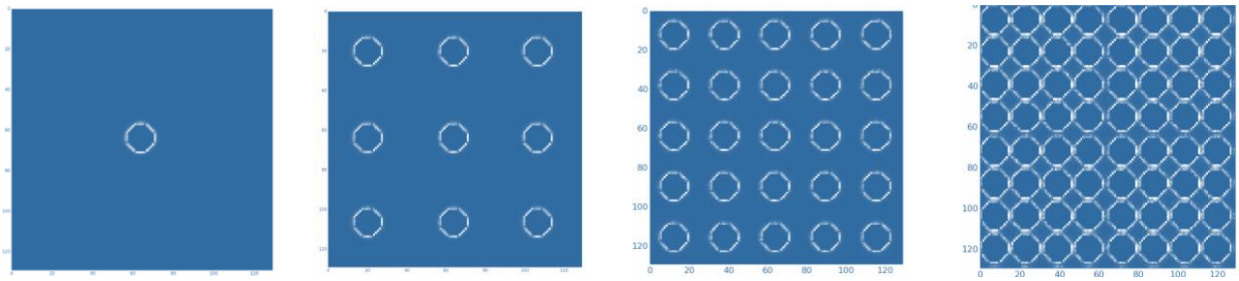

(a)

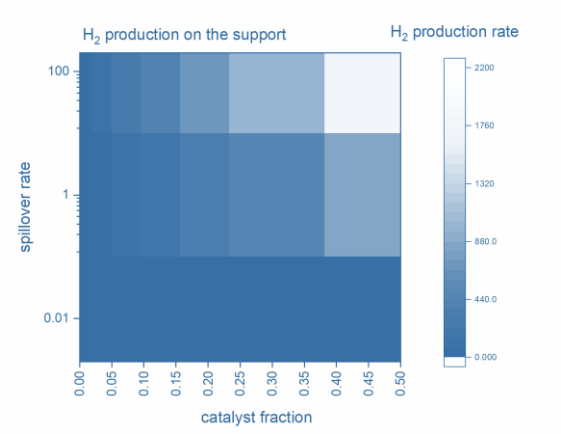

(b)

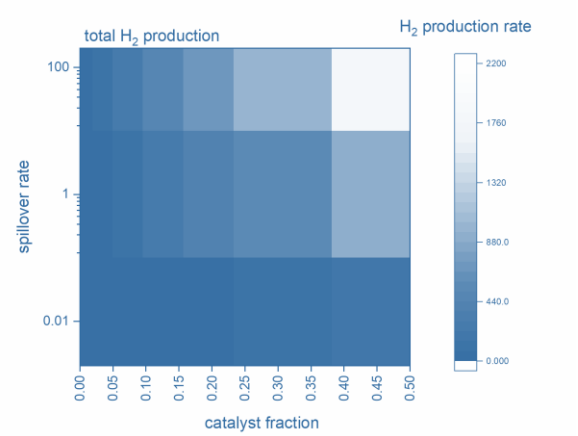

(c)

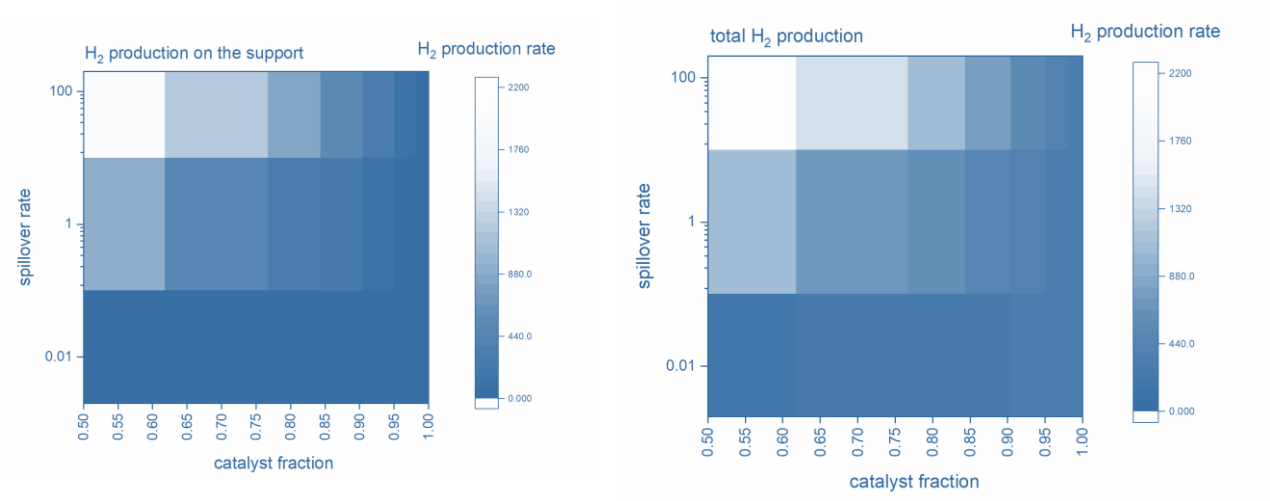

(d) (e)

Figure 5.13 Spatial distribution of H_2 production in the system with slow Heyrovsky reaction with different coverage of the catalyst phase (brighter colors indicate higher intensity of H_2 production); Heat maps illustrating H_2 generation, at a slow rate of Heyrovsky reaction, as a function of catalyst coverage and spillover rate. Panels (b) and (c) represent H_2 production from the support and overall production, respectively, for the C@S configuration. Panels (d) and (e) depict H_2 production from the support and overall production, respectively, for the S@C configuration.

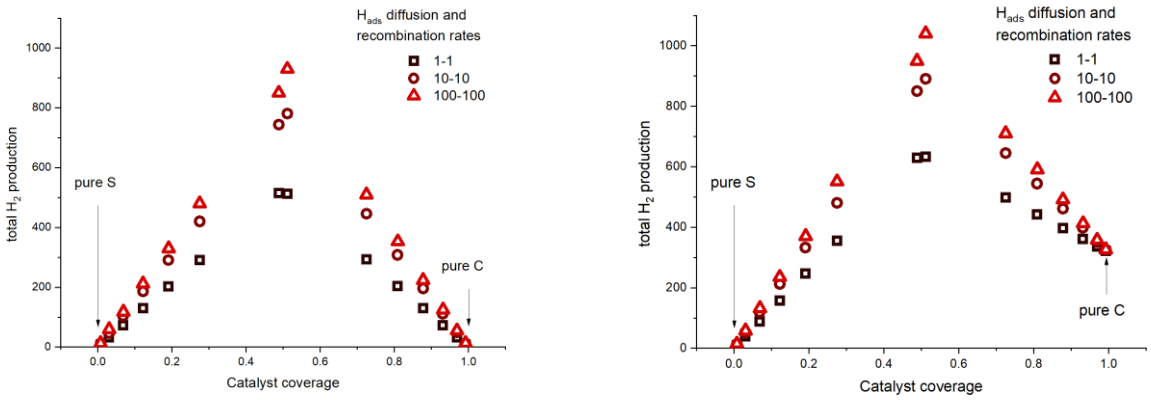

(a) (b)

Figure 5.14 Dependence of the H_2 production rate as a function of the catalyst coverage for three different sets of rates of H_{ads} diffusion and recombination on the support (spillover rate set to 1). Panel (a) illustrates H_2 production from the support, while Panel (b) displays the total H_2 production.

5.9. Selecting the right catalyst-support combination

Based on the obtained results, some specific guidelines can be derived to assist in selecting an appropriate combination of catalyst@support materials that exhibit high HER activity. This pertains to choosing a catalyst with optimal H_{ads} affinity and a support material with lower H_{ads} activity. The aim is to prevent the support from promoting H_{ads} formation while allowing it to accept H_{ads} from the catalyst. If the support satisfies this criterion, H_{ads} diffusion and recombination will also occur quickly, significantly increasing the spillover path's contribution. In the pursuit of identifying suitable catalyst/support pairing, the HER volcano curve in alkaline media [15] served as a valuable reference. Our focus lies on the peak of the volcano curve, aiming for catalyst/support pairs exhibiting high activity regardless of spillover

contributions. Considering that Pt is known as the most active metal for the HER, primarily due to the optimal strength of the Pt-H_{ads} bond, we select catalysts composed of metals with $E_H = E_H(Pt) \pm 0.15$ eV. Feasible catalyst options that fulfill this requirement include Ni, Co, Fe, Rh, Ru, Pd, Ir, and Pt [15], [138]. These metals display substantial HER activities and maintain a high H_{ads} coverage under elevated HER overpotentials.

To facilitate the formation of H_2, support materials with a weak affinity towards H_{ads} are needed. Consequently, we establish a lower threshold of E_H = -2.26 eV for the support. Given that the gas phase H_2 has a bond energy of 4.52 eV, H_{ads} formation on the support will be endothermic. Now we need to decide on the upper limit of the E_H on the support and set it as $E_H(C)$ + 0.65 eV. This implies that the H_{ads} bonding on the support should be less favorable than the catalyst surface by a maximum of 0.65 eV.

Additionally, this criterion sets a maximum thermodynamic barrier of 0.65 eV for transferring H_{ads} from the catalyst to the support (Figure 5.15). This value was chosen to allow for its override at ambient temperature [32]. Therefore, for the set of the preferred catalysts, E_H on the support lies between -2.26 and -1.92 eV, which is fulfilled by rGO. Consequently, drawing from our previous research [21], [181], we examine various metal-r(GO) combinations to assess their HER activities and compare them to their pure metal phases. It is essential to acknowledge that the scheme depicted in Figure 5.15 represents an extreme scenario where H binding on the support does not promote the formation of H_{ads}.

Nevertheless, it is conceivable to have stronger bonding on the support, resulting in the stages of H_2 formation along the reaction pathway being entirely uphill from a thermodynamic perspective. For instance, in reference [26], they used additional criteria based on $\Delta_{ads}G_H$. These considerations included catalysts with $\Delta_{ads}G_H$ values ranging from 0 to -0.45 eV and support with $|\Delta_{ads}G_H| < 0.15$ eV. However, determining the overall rate relies on the kinetic barriers of individual processes, which are currently challenging to estimate.

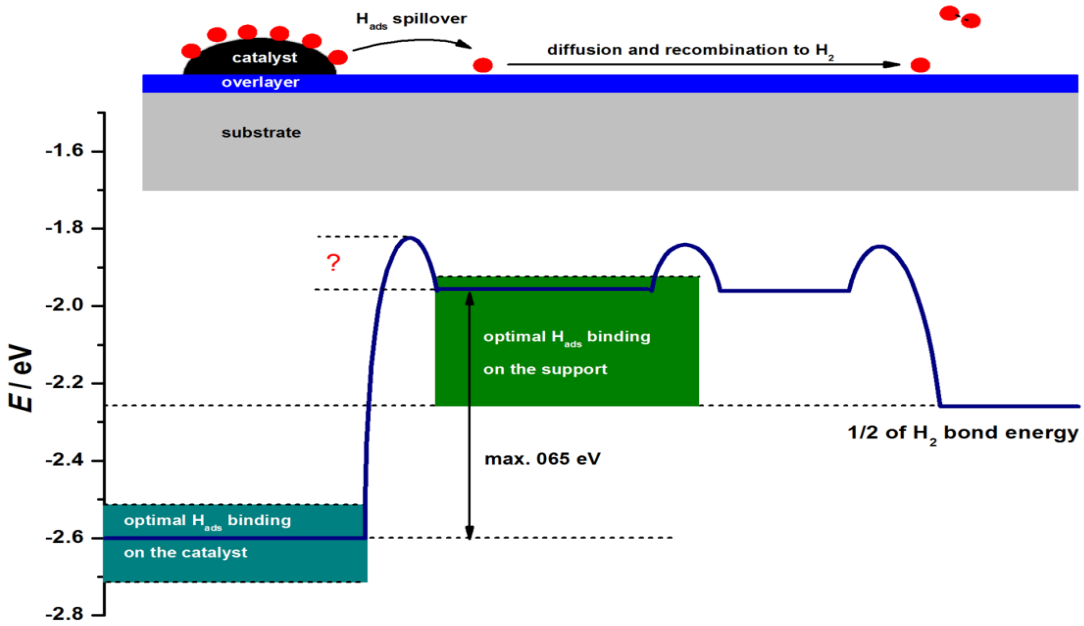

Figure 5.15 A schematic diagram illustrating the spillover process and H_2 production on the rGO-support, along with an energy profile depicting the reaction pathway being considered.

5.10. Trends in HER

According to the information presented in Sections 5.7 and 5.8, there is a strong possibility that the hydrogen spillover can enhance the rate of the HER on metals, particularly when HER occurs at a high level of H_{ads} coverage on the surface. Analysis of the overall catalytic activity trends in HER, as represented by a volcano curve [15], suggests that the spillover process can influence HER for metals located on the strong binding branch of the HER volcano plot. Accordingly, metals such as Fe, Co, Ni, Pd, and Pt (along with Ru, Rh, and Ir, as previously discussed) will likely experience a beneficial impact from hydrogen spillover. Conversely, metals that exhibit weak binding with H_{ads}, such as Ag, Au, and Zn, are expected to be unaffected by the effects of hydrogen spillover. To investigate this, a series of experiments were conducted involving the simultaneous reduction of GO and deposition of metals. This methodology has been previously shown to successfully prepare Ni@rGO composites [21], [181]. The details of the procedures are outlined in Section 4.1.6. We examined rGO-supported electrodeposited Au, Ag, Co, Ni, Fe, Pd, Pt, and Zn electrodes, and their HER activity was assessed at 10 mA cm^{-2} (η_{10}) [155]. The results (shown in Figure 5.16, a and b) strongly align with our assumptions. Specifically, the results indicate that when Au, Ag, and Zn are deposited on rGO, their activity is either similar or lower than when directly deposited on the Cu substrate. It is worth noting that η_{10} of the Cu substrate was found to be -0.65 V, slightly lower than that of electrodeposited Ag (Figure 5.16, a).

The other catalysts, however, all exhibit positive shifts in η_{10} when deposited on rGO. The effect was tested for various electrodeposition times and confirmed for many electrodes. Interestingly, Pd showed unexpectedly low activity, but when deposited on rGO, its electrocatalytic activity experienced an increase. Intriguingly, the impact of the rGO support was particularly notable for Pd and Co, resulting in significant activity improvements. On the other hand, similar activity enhancements were observed by Fe and Ni (Figure 5.16, c). By utilizing the obtained η_{10} values for metals deposited on the Cu substrate and M@rGO catalysts, along with the HBEs (calculated using DFT, Section 4.2), the HER volcano curve was constructed (Figure 5.16, c). The overall shape of the volcano curve is preserved in agreement with previous observations in alkaline media [15]. However, the significant findings lie in the alterations within the strong binding branch. Specifically, the entire branch experiences a shift towards lower HER overvoltages (in absolute values) for the metals under consideration.

The results obtained regarding the trends in HER activity are consistent with the outcomes of KMC simulations and the underlying assumptions about the conditions in which the spillover process enhances HER activity. The HER behavior observed for Ni aligns with our previous research, and Fe and Co exhibit similar characteristics to Ni. This similarity should not be surprising given that all three metals have comparable HER activity in alkaline media. The effect of rGO on Pd activity is noteworthy, possibly due to surface cleaning and reduced H sorption on Pd. However, this explanation remains speculative and needs further investigation for validation. Conversely, the possibility of such a mechanism has been considered significant in the context of Pd deposition on carbon surfaces, particularly for hydrogen storage applications [130], [182]. Notably, the concept of hydrogen spillover was also explored in the case of Pt-doped activated carbon and experimentally verified through inelastic neutron scattering [131].

The results presented provide clear evidence that interfacing metals with a strong H binding affinity and rGO leads to an enhancement in the rate of HER. This behavior of the investigated metals remains consistent across various deposition times, as depicted in Figure 5.17. Furthermore, in certain instances, the observed trends align with the predictions made by KMC simulations. These trends indicate increased activity up to a certain level of support coverage with the catalyst, followed by a subsequent decrease. This particular trend is observed in the case of Ni and is also partially evident for Fe (Figure 5.17). In summary, the process of interfacing contributes to the HER; however, it is important to note that the

overall shape of the volcano curve is preserved and is primarily determined by the energetics of H_{ads} at the surface of the catalyst.

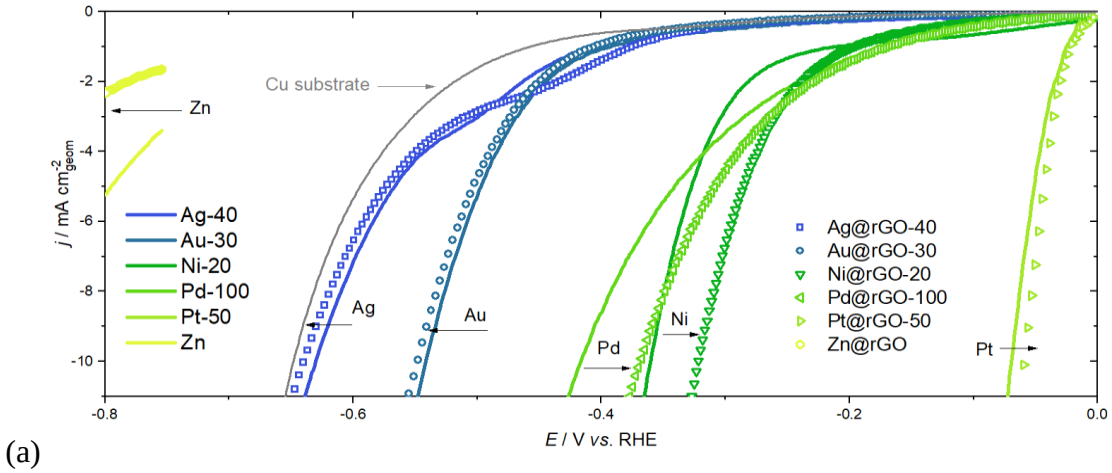

(a)

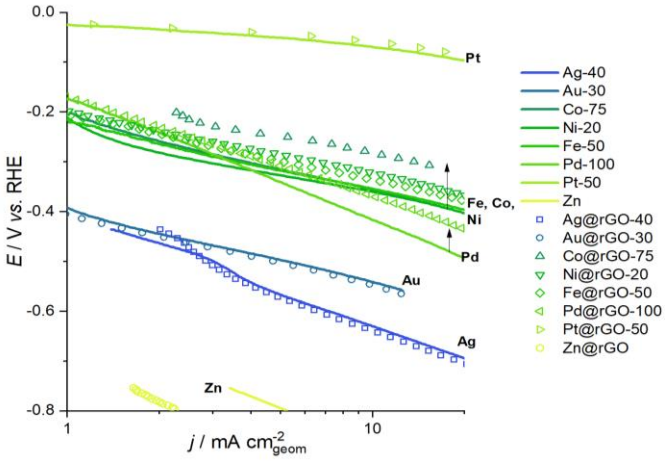

(b)

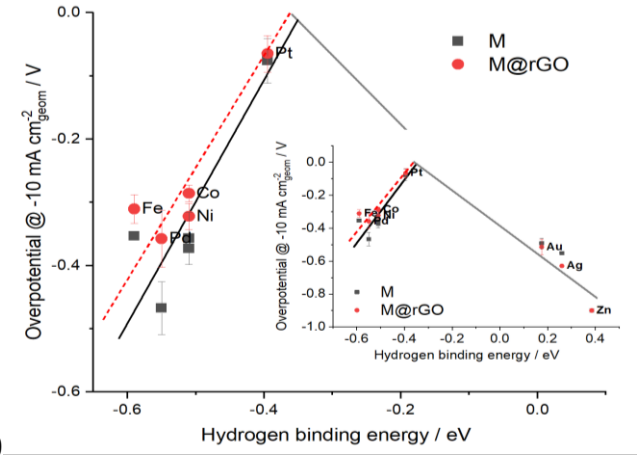

(c)

Figure 5.16 (a) HER polarization curves for selected metals with (M@rGO-X) and without rGO support (M-X), where X represents the deposition time in seconds. (b) Tafel plots for the entire series of catalysts, denoted using the same notation as in (a). (c) Volcano plot constructed using η10 values and calculated hydrogen binding energies, focusing on the strong binding branch. The inset provides the complete HER volcano curve. Error bars depict the range of η10 values for different deposition times.

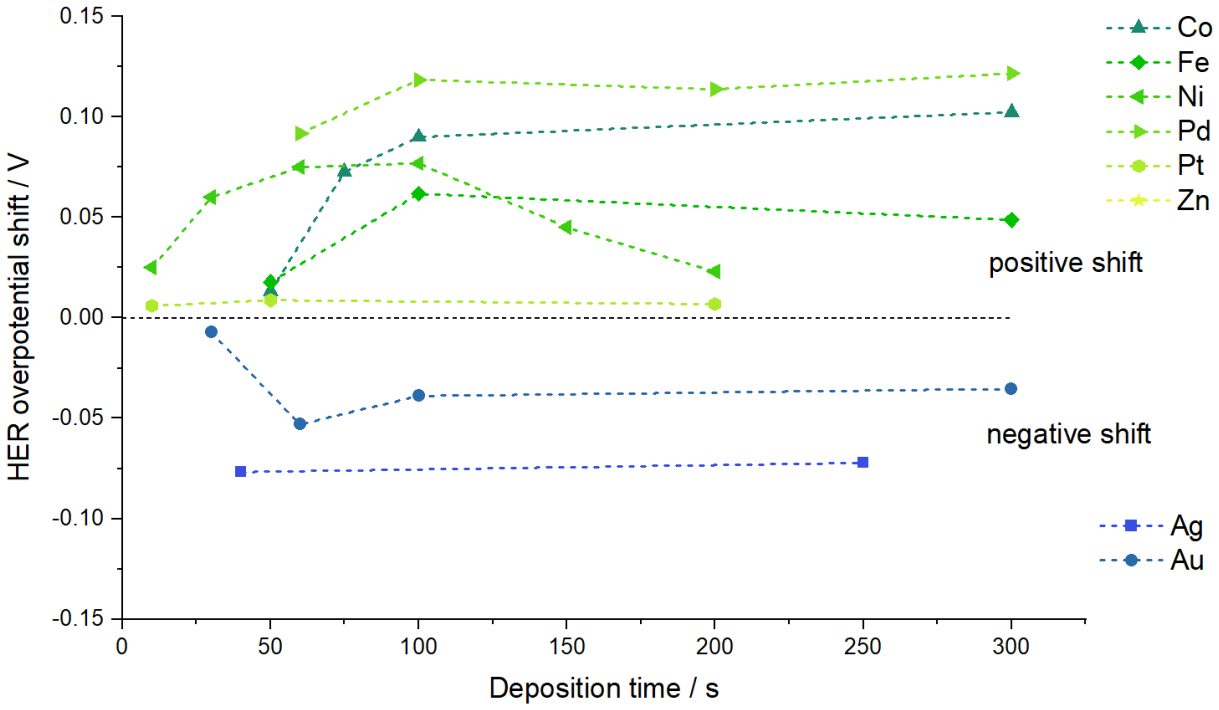

Figure 5.17 The relationship between the electrodeposition time and the HER overpotential of considered M@rGO catalysts

The empirical contribution of the interface path in experimental findings is not as significant as in the KMC simulations. However, it is important to note that the simulations should be regarded as mere guidelines. Furthermore, it is worth mentioning that the contribution of interfacial effects would be highly advantageous in the case of finely dispersed particles (Figure 5.12, the effects of dispersion). However, achieving such finely dispersed particles through electrodeposition is challenging. In certain support-catalyst combinations discussed in this study, there are compelling indications that hydrogen spillover plays a role, as previously mentioned [130], [131], [182]. However, it is important to acknowledge that there are also contrasting views regarding Pd-graphene systems [129], [183]. These theoretical calculations indicated that there might be no hydrogen spillover from small Pd clusters deposited on the graphene surface. However, it is also possible that the graphene surfaces used in these studies were defectless or too perfect. Specifically, pristine graphene exhibits a weak binding affinity for H_{ads}. However, the strength of this bonding significantly increases when defects and functional groups are introduced onto the surface [184]. As a result, perfect or defectless graphene does not meet the requirements for the support provided in Section 6.3. Indeed, our research group has previously presented evidence that positive effects are observed when Ni is deposited on various graphene-based surfaces. Specifically, rGO, which contains many defects and a certain proportion of oxygen functional groups within its basal plane, has shown positive effects [21]. However, the observed effect was absent when Ni was applied to graphene nanoplatelets possessing a well-ordered structure, an intact sp^2 basal plane, and oxygen functional groups concentrated exclusively at the edges. The absence of visualization techniques to observe such phenomena is a common issue in studies focused on spillover, as mentioned in [24]. However, the consistency between the theoretical assumptions and the experimental findings supports the proposed mechanism.

Up until now, the advantages of combining Ni with r(GO) have been demonstrated in the context of rGO-modified Ni foam [23], as well as in the case of Ni deposited on rGO [21], [181]. To enhance the impacts of interfacing Ni and rGO, a Ni@rGO composite is prepared by electrochemically depositing it directly from an electrodeposition bath containing GO. Then its performance is compared to that of Ni deposited under identical conditions but without GO (Figure 5.18, a). The Ni@rGO electrode's activity is far higher than its pure Ni equivalent. The range of the positive shifts in the HER overpotential agrees with those reported in Figure 5.17 for Ni deposited on GO films prepared by drop-casting. Moreover, the morphology is different; for Ni (Figure 5.18, b), the resulting deposits appear dendritic, whereas Ni@rGO exhibits a flake-like morphology (Figure 5.18, c). In other words, the morphology of GO is preserved in the case of Ni@rGO, whereas Ni is deposited onto the surface of GO sheets.

Whenever M@rGO composites are produced, either through electrodeposition of metal on drop-casted GO film or through co-deposition of metal and rGO, it is consistently observed that there is a lower amount of metal deposited in the rGO-containing deposits. Under constant current conditions, a portion of the charge is utilized to reduce GO, leading to a noticeable depolarization of the electrode during the electrodeposition process when GO is present.

Due to these factors, the modest enhancements in HER activity achieved through the formation of the M|rGO interface would become significantly more notable if the currents were normalized with respect to the mass of the active metal. Another aspect to consider is ECSA. Despite the lower amount of deposited metal, it is possible that its dispersion is higher, which could contribute to an increased ECSA. Nevertheless, accurately determining the ECSA for all the metals investigated poses a challenge, mainly when deposited on rGO. When relying solely on capacitance measurements, it becomes impossible to differentiate between the response of the catalyst and that of the support material. Distinct dispersion characteristics of Ni can be observed in Figure 5.18 (b and c), with the presence of small particles becoming noticeable in the case of Ni@rGO.

Nevertheless, cyclic voltammetry (Figure 5.18 (a), inset) reveals a comparable response of the two electrodes in the region of Ni oxidation, although the pure Ni electrode exhibits a slightly higher magnitude. This result provides clear evidence that the ECSAs of these two electrodes are highly similar, suggesting that the lower quantity of Ni in Ni@rGO is compensated by its enhanced dispersion. Furthermore, the HER activities depicted in Figure 6.18 (a) accurately depict the correlation between the intrinsic HER activities of Ni and Ni@rGO. Importantly, it should be emphasized that the mass-specific activity of Ni@rGO significantly surpasses that of the pure Ni electrode.

In conclusion, we propose that the strategy of selecting metal catalyst-support combinations can be universally applied and generalized. In the first place, it should be noted that the conclusions obtained from KMC simulations hold true in both acidic and alkaline environments, provided that there is significant coverage of the catalyst by H_{ads} during HER conditions. In these situations, the spillover process works well to increase HER activity. Therefore, to choose the catalyst-support combination, HBEs can be computationally screened. A significant body of literature has accumulated a wealth of reports that offer datasets encompassing HBEs, such as [26], [138]. These datasets and others can be utilized to expedite the search for novel catalyst-support combinations. Section 5.9 provides guidelines that can be flexibly applied, except the criterion about the disparity in binding energies between the catalyst and support. Overcoming a barrier larger than 0.65 eV is improbable unless high-temperature conditions are used.

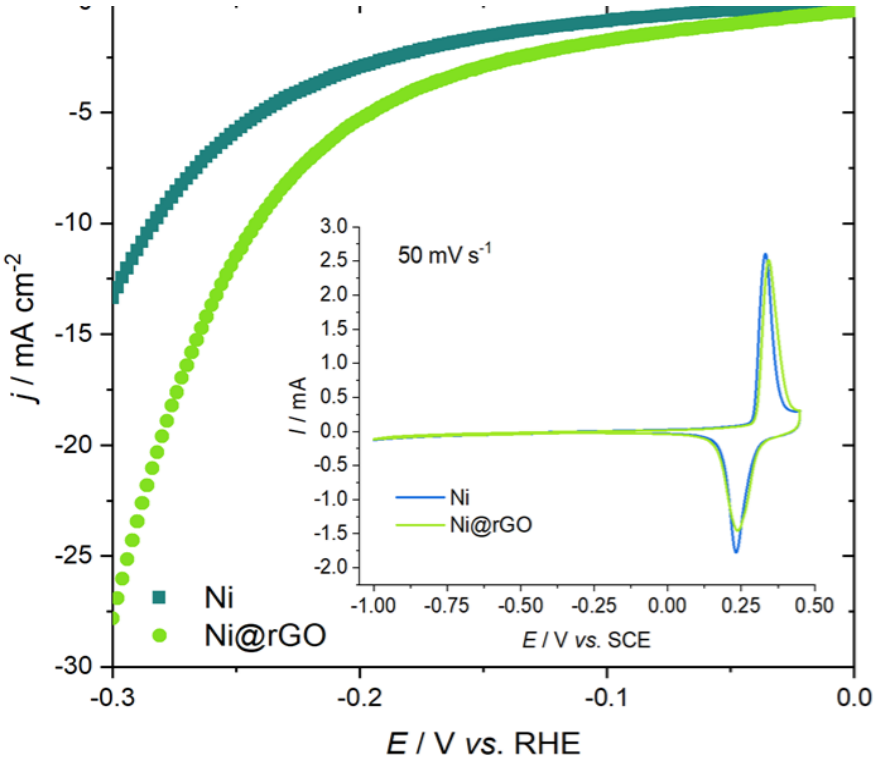

(a)

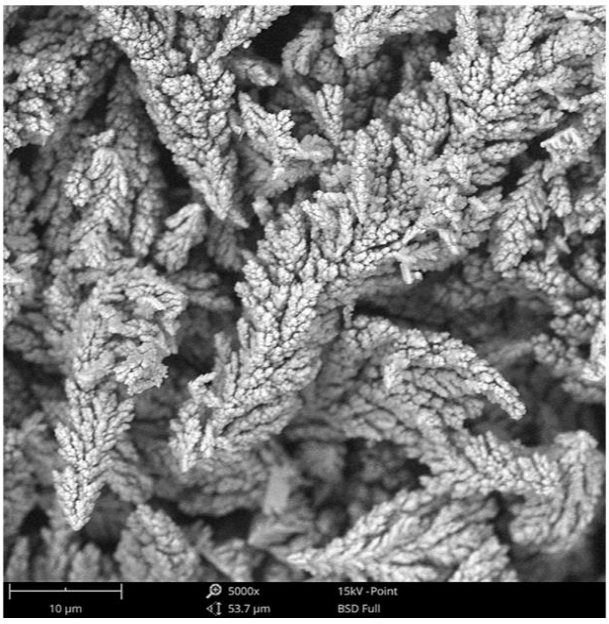

(b)

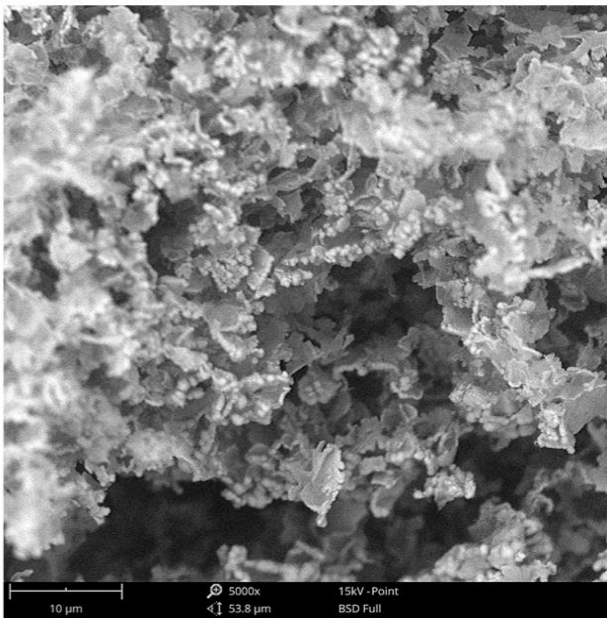

(c)

Figure 5.18 (a) HER polarization curves for simultaneously deposited Ni@rGO (Ni metal decorated with reduced graphene oxide) compared to pure Ni deposit. The inset shows cyclic voltammograms of these two electrodes. (b) Scanning Electron Microscope image of pure Ni deposits. (c) Scanning Electron Microscope image of Ni@rGO deposits (Ni metal decorated with reduced graphene oxide).

Chapter six - Conclusions

In this thesis work, the main aim was to assess the applicability of hydrogen evolution reaction (HER) volcano curves for identifying active catalysts in the entire pH range. Moreover, the study is aimed to investigate whether the effects of interfacial processes, specifically hydrogen spillover, could be observed on the volcano curves to aid in identifying actively supported catalysts. Thus, the first part of the thesis work involves analyzing HER trends on metallic surfaces in different solutions spanning a wide pH range. Correlating HER overpotentials required for a specific current density with calculated hydrogen binding energies (HBEs) reveals the presence of HER volcano curves in the wide pH range. This suggests that HBE can serve as a descriptor for identifying active electrocatalysts across the entire pH range, including pH-neutral solutions, where Cr exhibits superior HER activity compared to W, Fe, and Co. The effect of electrolytes on the HER varies depending on the specific metal. Still, Pt stands out as the most active catalyst on freshly polished surfaces, maintaining its position at the peak of the volcano plot. Surface oxidation also plays a significant role in the HER activities, either enhancing or hindering the HER. Cr and W experience HER hindrance due to surface oxidation. On the other hand, Ni and Co benefit from surface oxidation in alkaline and pH-neutral solutions, which can be attributed to the enhanced dissociation of water at the metal-oxide interface. Notably, in a NaCl solution, the activity of Ni surpasses that of Pt after undergoing oxidation, leading to a shift of the HER volcano peak towards the cheaper Ni metal.

In the second part of the thesis, Kinetic Monte Carlo (KMC) simulations are used to investigate whether HER can be accelerated using hydrogen spillover on the substrate. Based on the insights from KMC, a series of catalysts with reduced graphene oxide (rGO) as a support are synthesized. It is observed that the HER can be enhanced when the support material facilitates hydrogen spillover. The support materials do not have a positive effect in the case of weakly binding metals, Au, Ag, and Zn. In contrast, metals that exhibit stronger H_{ads} binding affinity experience better HER activities when deposited on rGO. The volcano curve, constructed based on the measured HER activities vs. calculated H binding energies, retains its general shape. Notably, the impact of hydrogen spillover becomes evident on the strong binding branch of the volcano plot, resulting in a shift towards lower overpotentials for the HER.

References

[1] A. Raveendran, M. Chandran, and R. Dhanusuraman, "A comprehensive review on the electrochemical parameters and recent material development of electrochemical water splitting electrocatalysts," *RSC Adv*, vol. 13, no. 6, pp. 3843–3876, 2023, doi: 10.1039/d2ra07642j.

[2] A. P. Murthy, J. Madhavan, and K. Murugan, "Recent advances in hydrogen evolution reaction catalysts on carbon/carbon-based supports in acid media," *J Power Sources*, vol. 398, pp. 9–26, Sep. 2018, doi: 10.1016/J.JPOWSOUR.2018.07.040.

[3] S. Wang, A. Lu, and C. J. Zhong, "Hydrogen production from water electrolysis: role of catalysts," *Nano Convergence*, vol. 8, no. 1. Korea Nano Technology Research Society, Dec. 01, 2021. doi: 10.1186/s40580-021-00254-x.

[4] H. Zhou *et al.*, "Water splitting by electrolysis at high current densities under 1.6 volts," *Energy Environ Sci*, vol. 11, no. 10, pp. 2858–2864, Oct. 2018, doi: 10.1039/c8ee00927a.

[5] J. M. Buriak, C. Toro, and K. S. Choi, "Chemistry of Materials for Water Splitting Reactions," *Chemistry of Materials*, vol. 30, no. 21, pp. 7325–7327, Nov. 2018, doi: 10.1021/acs.chemmater.8b04419.

[6] K. Zeng and D. Zhang, "Recent progress in alkaline water electrolysis for hydrogen production and applications," *Progress in Energy and Combustion Science*, vol. 36, no. 3. pp. 307–326, Jun. 2010. doi: 10.1016/j.pecs.2009.11.002.

[7] Z. Yan, J. L. Hitt, J. A. Turner, and T. E. Mallouk, "Renewable electricity storage using electrolysis," *Proc Natl Acad Sci U S A*, vol. 117, no. 23, pp. 12558–12563, Jun. 2020, doi: 10.1073/pnas.1821686116.

[8] X. Li *et al.*, "Water Splitting: From Electrode to Green Energy System," *Nano-Micro Letters*, vol. 12, no. 1. Springer, Jun. 01, 2020. doi: 10.1007/s40820-020-00469-3.

[9] Z. Angeles-Olvera, A. Crespo-Yapur, O. Rodríguez, J. L. Cholula-Díaz, L. M. Martínez, and M. Videa, "Nickel-Based Electrocatalysts for Water Electrolysis," *Energies*, vol. 15, no. 5. MDPI, Mar. 01, 2022. doi: 10.3390/en15051609.

[10] M. A. Khan *et al.*, "Seawater electrolysis for hydrogen production: A solution looking for a problem?," *Energy Environ Sci*, vol. 14, no. 9, pp. 4831–4839, Sep. 2021, doi: 10.1039/d1ee00870f.

[11] X. Zou and Y. Zhang, "Noble metal-free hydrogen evolution catalysts for water splitting," *Chem Soc Rev*, vol. 44, no. 15, pp. 5148–5180, Jul. 2015, doi: 10.1039/C4CS00448E.

[12] E. Cossar, F. Murphy, and E. A. Baranova, "Nickel-based anodes in anion exchange membrane water electrolysis: a review," *Journal of Chemical Technology and Biotechnology*, vol. 97, no. 7. John Wiley and Sons Ltd, pp. 1611–1624, Jul. 01, 2022. doi: 10.1002/jctb.7094.

[13] S. Trasatti, "Work function, electronegativity, and electrochemical behaviour of metals: III. Electrolytic hydrogen evolution in acid solutions," *J Electroanal Chem Interfacial Electrochem*, vol. 39, no. 1, pp. 163–184, Sep. 1972, doi: 10.1016/S0022-0728(72)80485-6.

[14] W. Schmickler and S. Trasatti, "Comment on 'Trends in the Exchange Current for Hydrogen Evolution' [J. Electrochem. Soc., 152, J23 (2005)]," *J Electrochem Soc*, vol. 153, no. 12, p. L31, 2006, doi: 10.1149/1.2358294.

[15] W. Sheng, M. Myint, J. G. Chen, and Y. Yan, "Correlating the hydrogen evolution reaction activity in alkaline electrolytes with the hydrogen binding energy on monometallic surfaces," *Energy Environ Sci*, vol. 6, no. 6, pp. 1509–1512, Jun. 2013, doi: 10.1039/c3ee00045a.

[16] M. A. Khan *et al.*, “Seawater electrolysis for hydrogen production: a solution looking for a problem?,” *Energy Environ Sci*, vol. 14, no. 9, pp. 4831–4839, Sep. 2021, doi: 10.1039/D1EE00870F.

[17] P. Quaino, F. Juarez, E. Santos, and W. Schmickler, “Volcano plots in hydrogen electrocatalysis-uses and abuses,” *Beilstein Journal of Nanotechnology*, vol. 5, no. 1, pp. 846–854, 2014, doi: 10.3762/bjnano.5.96.

[18] N. Danilovic *et al.*, “Enhancing the alkaline hydrogen evolution reaction activity through the bifunctionality of Ni(OH)2/metal catalysts,” *Angewandte Chemie - International Edition*, vol. 51, no. 50, pp. 12495–12498, Dec. 2012, doi: 10.1002/anie.201204842.

[19] R. Subbaraman *et al.*, “Trends in activity for the water electrolyser reactions on 3d M(Ni,Co,Fe,Mn) hydr(oxy)oxide catalysts,” *Nat Mater*, vol. 11, no. 6, pp. 550–557, 2012, doi: 10.1038/nmat3313.

[20] A. Chalgin, C. Song, P. Tao, W. Shang, T. Deng, and J. Wu, “Effect of supporting materials on the electrocatalytic activity, stability and selectivity of noble metal-based catalysts for oxygen reduction and hydrogen evolution reactions,” *Progress in Natural Science: Materials International*, vol. 30, no. 3, pp. 289–297, Jun. 2020, doi: 10.1016/J.PNSC.2020.01.003.

[21] S. J. Gutić, A. S. Dobrota, M. Leetmaa, N. V. Skorodumova, S. V. Mentus, and I. A. Pašti, “Improved catalysts for hydrogen evolution reaction in alkaline solutions through the electrochemical formation of nickel-reduced graphene oxide interface,” *Physical Chemistry Chemical Physics*, vol. 19, no. 20, pp. 13281–13293, May 2017, doi: 10.1039/C7CP01237C.

[22] S. J. Gutić *et al.*, “Simple routes for the improvement of hydrogen evolution activity of Ni-Mo catalysts: From sol-gel derived powder catalysts to graphene supported co-electrodeposits,” *Int J Hydrogen Energy*, vol. 43, no. 35, pp. 16846–16858, Aug. 2018, doi: 10.1016/j.ijhydene.2017.11.131.

[23] D. Chanda, J. Hnát, A. S. Dobrota, I. A. Pašti, M. Paidar, and K. Bouzek, “The effect of surface modification by reduced graphene oxide on the electrocatalytic activity of nickel towards the hydrogen evolution reaction,” *Physical Chemistry Chemical Physics*, vol. 17, no. 40, pp. 26864–26874, Oct. 2015, doi: 10.1039/C5CP04238K.

[24] W. Karim *et al.*, “Catalyst support effects on hydrogen spillover,” *Nature*, vol. 541, no. 7635, pp. 68–71, Jan. 2017, doi: 10.1038/nature20782.

[25] R. Prins, “Hydrogen spillover. Facts and fiction,” *Chemical Reviews*, vol. 112, no. 5. pp. 2714–2738, May 09, 2012. doi: 10.1021/cr200346z.

[26] Y. Tan *et al.*, “Discovery of Hydrogen Spillover-Based Binary Electrocatalysts for Hydrogen Evolution: From Theory to Experiment,” *ACS Catal*, vol. 12, no. 19, pp. 11821–11829, Oct. 2022, doi: 10.1021/ACSCATAL.2C02594/SUPPL_FILE/CS2C02594_SI_001.PDF.

[27] S. J. Gutić *et al.*, “Simple routes for the improvement of hydrogen evolution activity of Ni-Mo catalysts: From sol-gel derived powder catalysts to graphene supported co-electrodeposits,” *Int J Hydrogen Energy*, vol. 43, no. 35, pp. 16846–16858, Aug. 2018, doi: 10.1016/j.ijhydene.2017.11.131.

[28] D. Chanda, J. Hnát, A. S. Dobrota, I. A. Pašti, M. Paidar, and K. Bouzek, “The effect of surface modification by reduced graphene oxide on the electrocatalytic activity of nickel towards the hydrogen evolution reaction,” *Physical Chemistry Chemical Physics*, vol. 17, no. 40, pp. 26864–26874, 2015, doi: 10.1039/c5cp04238k.

[29] N. Mahmood, Y. Yao, J. W. Zhang, L. Pan, X. Zhang, and J. J. Zou, “Electrocatalysts for Hydrogen Evolution in Alkaline Electrolytes: Mechanisms, Challenges, and Prospective Solutions,” *Advanced Science*, vol. 5, no. 2. Wiley-VCH Verlag, Feb. 01, 2018. doi: 10.1002/advs.201700464.

[30] Y. Kojima *et al.*, “Hydrogen generation using sodium borohydride solution and metal catalyst coated on metal oxide,” *Int J Hydrogen Energy*, vol. 27, no. 10, pp. 1029–1034, Oct. 2002, doi: 10.1016/S0360-3199(02)00014-9.

[31] J. Brauns and T. Turek, “Alkaline water electrolysis powered by renewable energy: A review,” *Processes*, vol. 8, no. 2. MDPI AG, Feb. 01, 2020. doi: 10.3390/pr8020248.

[32] T. Ogawa, M. Takeuchi, and Y. Kajikawa, “Analysis of Trends and Emerging Technologies in Water Electrolysis Research Based on a Computational Method: A Comparison with Fuel Cell Research,” *Sustainability 2018, Vol. 10, Page 478*, vol. 10, no. 2, p. 478, Feb. 2018, doi: 10.3390/SU10020478.

[33] Q. Li *et al.*, “Anion Exchange Membrane Water Electrolysis: The Future of Green Hydrogen,” *The Journal of Physical Chemistry C*, Mar. 2023, doi: 10.1021/ACS.JPCC.3C00319.

[34] T.-M. Fakultet and B. N. Grgur, *UNIVERZITET U BEOGRADU*.

[35] S. B. Strbac and R. R. Adzic, “Electrocatalysis, Fundamentals - Electron Transfer Process; Current-Potential Relationship; Volcano Plots,” *Encyclopedia of Applied Electrochemistry*, pp. 417–423, 2014, doi: 10.1007/978-1-4419-6996-5_485.

[36] I. A. Pašti, “Electrochemical Measurements of Catalytic Activity-Focus on energy conversion,” 2020.

[37] S. J. Gutić, A. S. Dobrota, E. Fako, N. V. Skorodumova, N. López, and I. A. Pašti, “Hydrogen evolution reaction-from single crystal to single atom catalysts,” *Catalysts*, vol. 10, no. 3. MDPI, Mar. 01, 2020. doi: 10.3390/catal10030290.

[38] A. Oshchepkov, “Investigation of the hydrogen electrode reactions on Ni electrocatalysts in alkaline medium,” 2017. [Online]. Available: https://tel.archives-ouvertes.fr/tel-02003369

[39] A. P. Murthy, J. Theerthagiri, and J. Madhavan, “Insights on Tafel Constant in the Analysis of Hydrogen Evolution Reaction,” *Journal of Physical Chemistry C*, vol. 122, no. 42, pp. 23943–23949, Oct. 2018, doi: 10.1021/ACS.JPCC.8B07763/SUPPL_FILE/JP8B07763_SI_001.PDF.

[40] S. Štrbac, M. Smiljanić, T. Wakelin, J. Potočnik, and Z. Rakočević, “Hydrogen evolution reaction on bimetallic Ir/Pt(poly) electrodes in alkaline solution,” *Electrochim Acta*, vol. 306, pp. 18–27, May 2019, doi: 10.1016/J.ELECTACTA.2019.03.100.

[41] T. Shinagawa, A. T. Garcia-Esparza, and K. Takanabe, “Insight on Tafel slopes from a microkinetic analysis of aqueous electrocatalysis for energy conversion,” *Scientific Reports 2015 5:1*, vol. 5, no. 1, pp. 1–21, Sep. 2015, doi: 10.1038/srep13801.

[42] S. Watzele, J. Fichtner, B. Garlyyev, J. N. Schwämmlein, and A. S. Bandarenka, “On the Dominating Mechanism of the Hydrogen Evolution Reaction at Polycrystalline Pt Electrodes in Acidic Media,” *ACS Catal*, vol. 8, no. 10, pp. 9456–9462, Oct. 2018, doi: 10.1021/ACSCATAL.8B03365/SUPPL_FILE/CS8B03365_SI_001.PDF.

[43] M. Zeng and Y. Li, “Recent advances in heterogeneous electrocatalysts for the hydrogen evolution reaction,” *Journal of Materials Chemistry A*, vol. 3, no. 29. Royal Society of Chemistry, pp. 14942–14962, Jun. 01, 2015. doi: 10.1039/c5ta02974k.

[44] E. Skúlason *et al.*, “Modeling the electrochemical hydrogen oxidation and evolution reactions on the basis of density functional theory calculations,” *Journal of Physical Chemistry C*, vol. 114, no. 42, pp. 18182–18197, Oct. 2010, doi: 10.1021/jp1048887.

[45] J. Durst, A. Siebel, C. Simon, F. Hasché, J. Herranz, and H. A. Gasteiger, “New insights into the electrochemical hydrogen oxidation and evolution reaction mechanism,” *Energy Environ Sci*, vol. 7, no. 7, pp. 2255–2260, 2014, doi: 10.1039/c4ee00440j.

[46] X. Xie *et al.*, "Electrocatalytic Hydrogen Evolution in Neutral pH Solutions: Dual-Phase Synergy," *ACS Catal*, vol. 9, no. 9, pp. 8712–8718, Sep. 2019, doi: 10.1021/acscatal.9b02609.

[47] J. Verma and S. Goel, "Cost-effective electrocatalysts for Hydrogen Evolution Reactions (HER): Challenges and Prospects," *International Journal of Hydrogen Energy*. Elsevier Ltd, 2022. doi: 10.1016/j.ijhydene.2022.09.075.

[48] R. Parsons, "The rate of electrolytic hydrogen evolution and the heat of adsorption of hydrogen," *Transactions of the Faraday Society*, vol. 54, pp. 1053–1063, 1958, doi: 10.1039/tf9585401053.

[49] J. K. Nørskov *et al.*, "Trends in the Exchange Current for Hydrogen Evolution," *J Electrochem Soc*, vol. 152, no. 3, p. J23, 2005, doi: 10.1149/1.1856988.

[50] A. Eftekhari, "Electrocatalysts for hydrogen evolution reaction," *International Journal of Hydrogen Energy*, vol. 42, no. 16. Elsevier Ltd, pp. 11053–11077, Apr. 20, 2017. doi: 10.1016/j.ijhydene.2017.02.125.

[51] N. Pentland, J. O. Bockris, and E. Sheldon, "Hydrogen Evolution Reaction on Copper, Gold, Molybdenum, Palladium, Rhodium, and Iron Mechanism and Measurement Technique under High Purity Conditions," *J Electrochem Soc*, vol. 104, no. 3, p. 182, 1957, doi: 10.1149/1.2428530.

[52] W. A. Badawy, H. E. Feky, N. H. Helal, and H. H. Mohammed, "Cathodic hydrogen evolution on molybdenum in NaOH solutions," *Int J Hydrogen Energy*, vol. 38, no. 23, pp. 9625–9632, Aug. 2013, doi: 10.1016/J.IJHYDENE.2013.05.098.

[53] A. Lasia, "Mechanism and kinetics of the hydrogen evolution reaction," *Int J Hydrogen Energy*, vol. 44, no. 36, pp. 19484–19518, Jul. 2019, doi: 10.1016/J.IJHYDENE.2019.05.183.

[54] B. E. Conway and L. Bai, "Determination of the adsorption behaviour of 'overpotential-deposited' hydrogen-atom species in the cathodic hydrogen-evolution reaction by analysis of potential-relaxation transients," *Journal of the Chemical Society, Faraday Transactions 1: Physical Chemistry in Condensed Phases*, vol. 81, no. 8, pp. 1841–1862, Jan. 1985, doi: 10.1039/F19858101841.

[55] B. Liu, J. B. He, Y. J. Chen, Y. Wang, and N. Deng, "Phytic acid-coated titanium as electrocatalyst of hydrogen evolution reaction in alkaline electrolyte," *Int J Hydrogen Energy*, vol. 38, no. 8, pp. 3130–3136, Mar. 2013, doi: 10.1016/J.IJHYDENE.2012.12.099.

[56] A. Eftekhari, "Molybdenum diselenide (MoSe2) for energy storage, catalysis, and optoelectronics," *Appl Mater Today*, vol. 8, pp. 1–17, Sep. 2017, doi: 10.1016/J.APMT.2017.01.006.

[57] T. Burchardt, "The hydrogen evolution reaction on NiPx alloys," *Int J Hydrogen Energy*, vol. 25, no. 7, pp. 627–634, Jul. 2000, doi: 10.1016/S0360-3199(99)00089-0.

[58] T. Burchardt, "Hydrogen evolution on NiPx alloys: the influence of sorbed hydrogen," *Int J Hydrogen Energy*, vol. 26, no. 11, pp. 1193–1198, Nov. 2001, doi: 10.1016/S0360-3199(01)00053-2.

[59] Z. Xing, Q. Li, D. Wang, X. Yang, and X. Sun, "Self-supported nickel nitride as an efficient high-performance three-dimensional cathode for the alkaline hydrogen evolution reaction," *Electrochim Acta*, vol. 191, pp. 841–845, Feb. 2016, doi: 10.1016/J.ELECTACTA.2015.12.174.

[60] R. B. Levy and M. Boudart, "Platinum-like behavior of tungsten carbide in surface catalysis," *Science*, vol. 181, no. 4099, pp. 547–549, 1973, doi: 10.1126/SCIENCE.181.4099.547.

[61] J. D. Benck, T. R. Hellstern, J. Kibsgaard, P. Chakthranont, and T. F. Jaramillo, "Catalyzing the hydrogen evolution reaction (HER) with molybdenum sulfide nanomaterials," *ACS Catal*, vol. 4, no. 11, pp. 3957–3971, Oct. 2014, doi: 10.1021/CS500923C/ASSET/IMAGES/MEDIUM/CS-2014-00923C_0014.GIF.

[62] D. D. Vasić, I. A. Pašti, and S. V. Mentus, “DFT study of platinum and palladium overlayers on tungsten carbide: Structure and electrocatalytic activity toward hydrogen oxidation/evolution reaction,” *Int J Hydrogen Energy*, vol. 38, no. 12, pp. 5009–5018, Apr. 2013, doi: 10.1016/J.IJHYDENE.2013.02.020.

[63] M. E. Strayer *et al.*, “Charge Transfer Stabilization of Late Transition Metal Oxide Nanoparticles on a Layered Niobate Support,” *J Am Chem Soc*, vol. 137, no. 51, pp. 16216–16224, Dec. 2015, doi: 10.1021/JACS.5B11230/SUPPL_FILE/JA5B11230_SI_001.PDF.

[64] G. B. Darband, M. Aliofkhazraei, and S. Shanmugam, “Recent advances in methods and technologies for enhancing bubble detachment during electrochemical water splitting,” *Renewable and Sustainable Energy Reviews*, vol. 114, p. 109300, Oct. 2019, doi: 10.1016/J.RSER.2019.109300.

[65] N. Dubouis and A. Grimaud, “The hydrogen evolution reaction: From material to interfacial descriptors,” *Chem Sci*, vol. 10, no. 40, pp. 9165–9181, 2019, doi: 10.1039/c9sc03831k.

[66] M. Auinger *et al.*, “Near-surface ion distribution and buffer effects during electrochemical reactions,” *Physical Chemistry Chemical Physics*, vol. 13, no. 36, pp. 16384–16394, Sep. 2011, doi: 10.1039/c1cp21717h.

[67] N. M. Marković, B. N. Grgur, and P. N. Ross, “Temperature-Dependent Hydrogen Electrochemistry on Platinum Low-Index Single-Crystal Surfaces in Acid Solutions,” *Journal of Physical Chemistry B*, vol. 101, no. 27, pp. 5405–5413, Jul. 1997, doi: 10.1021/JP970930D.

[68] J. Janata, “Physical Electrochemistry. Fundamentals, Techniques and Applications. By Eliezer Gileadi.,” *Angewandte Chemie International Edition*, vol. 50, no. 41, pp. 9538–9538, Oct. 2011, doi: 10.1002/ANIE.201104618.

[69] E. Skúlason *et al.*, “Modeling the electrochemical hydrogen oxidation and evolution reactions on the basis of density functional theory calculations,” *Journal of Physical Chemistry C*, vol. 114, no. 42, pp. 18182–18197, Oct. 2010, doi: 10.1021/JP1048887/ASSET/IMAGES/MEDIUM/JP-2010-048887_0006.GIF.

[70] J. Ferez, E. R. Gonzalez, and H. M. Villuiias, “Hydrogen Evolution Reaction on Gold Single-Crystal Electrodes in Acid Solutions,” *Journal of Physical Chemistry B*, vol. 102, no. 52, pp. 10931–10935, 1998, doi: 10.1021/JP9831987.

[71] D. Eberhardt, E. Santos, and W. Schmickler, “Hydrogen evolution on silver single crystal electrodes—first results,” *Journal of Electroanalytical Chemistry*, vol. 461, no. 1–2, pp. 76–79, Jan. 1999, doi: 10.1016/S0022-0728(98)00093-X.

[72] G. Brisard, N. Bertrand, P. N. Ross, and N. M. Marković, “Oxygen reduction and hydrogen evolution–oxidation reactions on Cu(hkl) surfaces,” *Journal of Electroanalytical Chemistry*, vol. 480, no. 1–2, pp. 219–224, Jan. 2000, doi: 10.1016/S0022-0728(99)00463-5.

[73] N. M. Markoví and P. N. Ross, “Surface science studies of model fuel cell electrocatalysts,” *Surf Sci Rep*, vol. 45, no. 4–6, pp. 117–229, Apr. 2002, doi: 10.1016/S0167-5729(01)00022-X.

[74] J. Durst *et al.*, “(Invited) Hydrogen Oxidation and Evolution Reaction (HOR/HER) on Pt Electrodes in Acid vs. Alkaline Electrolytes: Mechanism, Activity and Particle Size Effects,” *ECS Trans*, vol. 64, no. 3, pp. 1069–1080, Aug. 2014, doi: 10.1149/06403.1069ECST/XML.

[75] S. Zhang, X. Zhang, Y. Rui, R. Wang, and X. Li, “Recent advances in non-precious metal electrocatalysts for pH-universal hydrogen evolution reaction,” *Green Energy & Environment*, vol. 6, no. 4, pp. 458–478, Aug. 2021, doi: 10.1016/J.GEE.2020.10.013.

[76] J. Durst, A. Siebel, C. Simon, F. Hasché, J. Herranz, and H. A. Gasteiger, "New insights into the electrochemical hydrogen oxidation and evolution reaction mechanism," *Energy Environ Sci*, vol. 7, no. 7, pp. 2255–2260, 2014, doi: 10.1039/c4ee00440j.

[77] J. Herranz *et al.*, "Interfacial effects on the catalysis of the hydrogen evolution, oxygen evolution and CO2-reduction reactions for (co-)electrolyzer development," *Nano Energy*, vol. 29, pp. 4–28, Nov. 2016, doi: 10.1016/J.NANOEN.2016.01.027.

[78] W. Sheng, Z. Zhuang, M. Gao, J. Zheng, J. G. Chen, and Y. Yan, "Correlating hydrogen oxidation and evolution activity on platinum at different pH with measured hydrogen binding energy," *Nat Commun*, vol. 6, Jan. 2015, doi: 10.1038/ncomms6848.

[79] D. Strmcnik *et al.*, "Improving the hydrogen oxidation reaction rate by promotion of hydroxyl adsorption," *Nat Chem*, vol. 5, no. 4, pp. 300–306, Apr. 2013, doi: 10.1038/nchem.1574.

[80] Y. Zheng, Y. Jiao, A. Vasileff, and S. Z. Qiao, "The Hydrogen Evolution Reaction in Alkaline Solution: From Theory, Single Crystal Models, to Practical Electrocatalysts," *Angew Chem Int Ed Engl*, vol. 57, no. 26, pp. 7568–7579, Jun. 2018, doi: 10.1002/ANIE.201710556.

[81] D. Strmcnik, P. P. Lopes, B. Genorio, V. R. Stamenkovic, and N. M. Markovic, "Design principles for hydrogen evolution reaction catalyst materials," 2016. [Online]. Available: http://www.elsevier.com/open-access/userlicense/1.0/

[82] T. Shinagawa and K. Takanabe, "Electrocatalytic Hydrogen Evolution under Densely Buffered Neutral pH Conditions," *Journal of Physical Chemistry C*, vol. 119, no. 35, pp. 20453–20458, Aug. 2015, doi: 10.1021/ACS.JPCC.5B05295/SUPPL_FILE/JP5B05295_SI_001.PDF.

[83] N. M. Marković, S. T. Sarraf, H. A. Gasteiger, and P. N. Ross, "Hydrogen electrochemistry on platinum low-index single-crystal surfaces in alkaline solution," *Journal of the Chemical Society, Faraday Transactions*, vol. 92, no. 20, pp. 3719–3725, Jan. 1996, doi: 10.1039/FT9969203719.

[84] N. Danilovic, R. Subbaraman, D. Strmcnik, V. R. Stamenkovic, and N. M. Markovic, "Electrocatalysis of the HER in acid and alkaline media," *Journal of The Serbian Chemical Society*, vol. 78, no. 12, pp. 2007–2015, 2013, doi: 10.2298/JSC131118136D.

[85] T. J. Schmidt, P. N. Ross, and N. M. Markovic, "Temperature dependent surface electrochemistry on Pt single crystals in alkaline electrolytes: Part 2. The hydrogen evolution/oxidation reaction," *Journal of Electroanalytical Chemistry*, vol. 524–525, pp. 252–260, May 2002, doi: 10.1016/S0022-0728(02)00683-6.

[86] J. Zheng, W. Sheng, Z. Zhuang, B. Xu, and Y. Yan, "Universal dependence of hydrogen oxidation and evolution reaction activity of platinum-group metals on pH and hydrogen binding energy," *Sci Adv*, vol. 2, no. 3, Mar. 2016, doi: 10.1126/sciadv.1501602.

[87] Y. Wang *et al.*, "Pt–Ru catalyzed hydrogen oxidation in alkaline media: oxophilic effect or electronic effect?," *Energy Environ Sci*, vol. 8, no. 1, pp. 177–181, Dec. 2014, doi: 10.1039/C4EE02564D.

[88] M. J. T. C. Van Der Niet, N. Garcia-Araez, J. Hernández, J. M. Feliu, and M. T. M. Koper, "Water dissociation on well-defined platinum surfaces: The electrochemical perspective," *Catal Today*, vol. 202, no. 1, pp. 105–113, Mar. 2013, doi: 10.1016/J.CATTOD.2012.04.059.

[89] N. M. Marković, T. J. Schmidt, B. N. Grgur, H. A. Gasteiger, R. J. Behm, and P. N. Ross, "Effect of Temperature on Surface Processes at the Pt(111)−Liquid Interface: Hydrogen Adsorption, Oxide Formation, and CO Oxidation," *Journal of Physical Chemistry B*, vol. 103, no. 40, pp. 8568–8577, Oct. 1999, doi: 10.1021/JP991826U.

[90] I. Ledezma-Yanez, W. D. Z. Wallace, P. Sebastián-Pascual, V. Climent, J. M. Feliu, and M. T. M. Koper, "Interfacial water reorganization as a pH-dependent descriptor of the hydrogen evolution rate on platinum electrodes," *Nat Energy*, vol. 2, no. 4, Mar. 2017, doi: 10.1038/nenergy.2017.31.

[91] J. Rossmeisl, K. Chan, E. Skúlason, M. E. Björketun, and V. Tripkovic, "On the pH dependence of electrochemical proton transfer barriers," *Catal Today*, vol. 262, pp. 36–40, Mar. 2016, doi: 10.1016/J.CATTOD.2015.08.016.

[92] J. Rossmeisl, K. Chan, R. Ahmed, V. Tripković, and M. E. Björketun, "PH in atomic scale simulations of electrochemical interfaces," *Physical Chemistry Chemical Physics*, vol. 15, no. 25, pp. 10321–10325, Jul. 2013, doi: 10.1039/c3cp51083b.

[93] Z. Zhou, Z. Pei, L. Wei, S. Zhao, X. Jian, and Y. Chen, "Electrocatalytic hydrogen evolution under neutral pH conditions: current understandings, recent advances, and future prospects," *Energy Environ Sci*, vol. 13, no. 10, pp. 3185–3206, Oct. 2020, doi: 10.1039/D0EE01856B.

[94] A. P. Murthy, D. Govindarajan, J. Theerthagiri, J. Madhavan, and K. Parasuraman, "Metal-doped molybdenum nitride films for enhanced hydrogen evolution in near-neutral strongly buffered aerobic media," *Electrochim Acta*, vol. 283, pp. 1525–1533, Sep. 2018, doi: 10.1016/J.ELECTACTA.2018.07.094.

[95] T. Shinagawa and K. Takanabe, "Identification of intrinsic catalytic activity for electrochemical reduction of water molecules to generate hydrogen," *Physical Chemistry Chemical Physics*, vol. 17, no. 23, pp. 15111–15114, Jun. 2015, doi: 10.1039/C5CP02330K.

[96] T. Shinagawa, A. T. Garcia-Esparza, and K. Takanabe, "Mechanistic Switching by Hydronium Ion Activity for Hydrogen Evolution and Oxidation over Polycrystalline Platinum Disk and Platinum/Carbon Electrodes," *ChemElectroChem*, vol. 1, no. 9, pp. 1497–1507, Sep. 2014, doi: 10.1002/CELC.201402085.

[97] B. E. Conway and B. V. Tilak, "Interfacial processes involving electrocatalytic evolution and oxidation of H2, and the role of chemisorbed H," *Electrochim Acta*, vol. 47, no. 22–23, pp. 3571–3594, Aug. 2002, doi: 10.1016/S0013-4686(02)00329-8.

[98] I. Katsounaros *et al.*, "The effective surface pH during reactions at the solid–liquid interface," *Electrochem commun*, vol. 13, no. 6, pp. 634–637, Jun. 2011, doi: 10.1016/J.ELECOM.2011.03.032.

[99] T. Shinagawa and K. Takanabe, "Towards Versatile and Sustainable Hydrogen Production through Electrocatalytic Water Splitting: Electrolyte Engineering," *ChemSusChem*, vol. 10, no. 7, pp. 1318–1336, Apr. 2017, doi: 10.1002/CSSC.201601583.

[100] B. E. Conway and G. Jerkiewicz, "Relation of energies and coverages of underpotential and overpotential deposited H at Pt and other metals to the 'volcano curve' for cathodic H2 evolution kinetics," *Electrochim Acta*, vol. 45, no. 25–26, pp. 4075–4083, Aug. 2000, doi: 10.1016/S0013-4686(00)00523-5.

[101] S. Zhu, X. Qin, Y. Yao, and M. Shao, "PH-Dependent Hydrogen and Water Binding Energies on Platinum Surfaces as Directly Probed through Surface-Enhanced Infrared Absorption Spectroscopy," *J Am Chem Soc*, vol. 142, no. 19, pp. 8748–8754, May 2020, doi: 10.1021/JACS.0C01104/SUPPL_FILE/JA0C01104_SI_001.PDF.

[102] Y. Sun *et al.*, "Electrodeposited cobalt-sulfide catalyst for electrochemical and photoelectrochemical hydrogen generation from water," *J Am Chem Soc*, vol. 135, no. 47, pp. 17699–17702, Nov. 2013, doi: 10.1021/JA4094764/SUPPL_FILE/JA4094764_SI_001.PDF.

[103] W. Sheng, H. A. Gasteiger, and Y. Shao-Horn, "Hydrogen Oxidation and Evolution Reaction Kinetics on Platinum: Acid vs Alkaline Electrolytes," *J Electrochem Soc*, vol. 157, no. 11, p. B1529, 2010, doi: 10.1149/1.3483106.

[104] B. E. Conway and L. Bai, "State of adsorption and coverage by overpotential-deposited H in the H2 evolution reaction at Au and Pt," *Electrochim Acta*, vol. 31, no. 8, pp. 1013–1024, Aug. 1986, doi: 10.1016/0013-4686(86)80017-2.

[105] J. O. Bockris and E. C. Potter, "The Mechanism of the Cathodic Hydrogen Evolution Reaction," *J Electrochem Soc*, vol. 99, no. 4, p. 169, Apr. 1952, doi: 10.1149/1.2779692/XML.

[106] A. B. Laursen *et al.*, "Electrochemical hydrogen evolution: Sabatiers principle and the volcano plot," *J Chem Educ*, vol. 89, no. 12, pp. 1595–1599, Nov. 2012, doi: 10.1021/ed200818t.

[107] N. Danilovic *et al.*, "Enhancing the alkaline hydrogen evolution reaction activity through the bifunctionality of Ni(OH)2/metal catalysts," *Angew Chem Int Ed Engl*, vol. 51, no. 50, pp. 12495–12498, Dec. 2012, doi: 10.1002/ANIE.201204842.

[108] J. Greeley, T. F. Jaramillo, J. Bonde, I. Chorkendorff, and J. K. Nørskov, "Computational high-throughput screening of electrocatalytic materials for hydrogen evolution," *Nat Mater*, vol. 5, no. 11, pp. 909–913, Nov. 2006, doi: 10.1038/nmat1752.

[109] S. Lu and Z. Zhuang, "Investigating the Influences of the Adsorbed Species on Catalytic Activity for Hydrogen Oxidation Reaction in Alkaline Electrolyte," *J Am Chem Soc*, vol. 139, no. 14, pp. 5156–5163, Apr. 2017, doi: 10.1021/JACS.7B00765/SUPPL_FILE/JA7B00765_SI_001.PDF.

[110] J. Tymoczko, F. Calle-Vallejo, W. Schuhmann, and A. S. Bandarenka, "Making the hydrogen evolution reaction in polymer electrolyte membrane electrolysers even faster," *Nature Communications 2016 7:1*, vol. 7, no. 1, pp. 1–6, Mar. 2016, doi: 10.1038/ncomms10990.

[111] R. Subbaraman *et al.*, "Enhancing hydrogen evolution activity in water splitting by tailoring Li^+-$Ni(OH)_2$-Pt interfaces," *Science*, vol. 334, no. 6060, pp. 1256–1260, Dec. 2011, doi: 10.1126/SCIENCE.1211934.

[112] D. J. Weber, M. Janssen, and M. Oezaslan, "Effect of Monovalent Cations on the HOR/HER Activity for Pt in Alkaline Environment," *J Electrochem Soc*, vol. 166, no. 2, pp. F66–F73, 2019, doi: 10.1149/2.0301902JES.

[113] I. T. McCrum and M. J. Janik, "pH and Alkali Cation Effects on the Pt Cyclic Voltammogram Explained Using Density Functional Theory," *Journal of Physical Chemistry C*, vol. 120, no. 1, pp. 457–471, Jan. 2016, doi: 10.1021/ACS.JPCC.5B10979/SUPPL_FILE/JP5B10979_SI_001.PDF.

[114] S. Khoobiar, "Particle to Particle Migration of Hydrogen Atoms on Pt-Alumina Catalysts from Particle to Neighboring Particles," 1964.

[115] W. Curtis Conner and J. L. Falconer, "Spillover in Heterogeneous Catalysis," 1995.

[116] G. M. Psofogiannakis and G. E. Froudakis, "Fundamental studies and perceptions on the spillover mechanism for hydrogen storage," *Chemical Communications*, vol. 47, no. 28, pp. 7933–7943, Jul. 2011, doi: 10.1039/C1CC11389E.

[117] X. Zheng *et al.*, "Understanding the effect of interfacial interaction on metal/metal oxide electrocatalysts for hydrogen evolution and hydrogen oxidation reactions on the basis of first-principles calculations," *Catal Sci Technol*, vol. 10, no. 14, pp. 4743–4751, Jul. 2020, doi: 10.1039/D0CY00960A.

[118] Z. Zhang, J. Liu, J. Gu, L. Su, and L. Cheng, “An overview of metal oxide materials as electrocatalysts and supports for polymer electrolyte fuel cells,” *Energy Environ Sci*, vol. 7, no. 8, pp. 2535–2558, Jul. 2014, doi: 10.1039/C3EE43886D.

[119] S. Sharma and B. G. Pollet, “Support materials for PEMFC and DMFC electrocatalysts—A review,” *J Power Sources*, vol. 208, pp. 96–119, Jun. 2012, doi: 10.1016/J.JPOWSOUR.2012.02.011.

[120] D. Wang, Z. P. Liu, and W. M. Yang, “Proton-Promoted Electron Transfer in Photocatalysis: Key Step for Photocatalytic Hydrogen Evolution on Metal/Titania Composites,” *ACS Catal*, vol. 7, no. 4, pp. 2744–2752, Apr. 2017, doi: 10.1021/ACSCATAL.7B00225/SUPPL_FILE/CS7B00225_SI_001.PDF.

[121] E. R. Hamo and B. A. Rosen, “Transition metal carbides as cathode supports for PEM fuel cells,” *Nano Research 2022 15:12*, vol. 15, no. 12, pp. 10218–10233, Sep. 2022, doi: 10.1007/S12274-022-4831-3.

[122] C. Tang, D. Wang, Z. Wu, and B. Duan, “Tungsten carbide hollow microspheres as electrocatalyst and platinum support for hydrogen evolution reaction,” *Int J Hydrogen Energy*, vol. 40, no. 8, pp. 3229–3237, Mar. 2015, doi: 10.1016/J.IJHYDENE.2014.12.105.

[123] S. Shahgaldi and J. Hamelin, “Improved carbon nanostructures as a novel catalyst support in the cathode side of PEMFC: a critical review,” *Carbon N Y*, vol. 94, pp. 705–728, Nov. 2015, doi: 10.1016/J.CARBON.2015.07.055.

[124] H. J. Qiu *et al.*, “Nanoporous Graphene with Single-Atom Nickel Dopants: An Efficient and Stable Catalyst for Electrochemical Hydrogen Production,” *Angewandte Chemie International Edition*, vol. 54, no. 47, pp. 14031–14035, Nov. 2015, doi: 10.1002/ANIE.201507381.

[125] J. Deng, P. Ren, D. Deng, and X. Bao, “Enhanced Electron Penetration through an Ultrathin Graphene Layer for Highly Efficient Catalysis of the Hydrogen Evolution Reaction,” *Angewandte Chemie International Edition*, vol. 54, no. 7, pp. 2100–2104, Feb. 2015, doi: 10.1002/ANIE.201409524.

[126] H. Zhang, W. Ren, C. Guan, and C. Cheng, “Pt decorated 3D vertical graphene nanosheet arrays for efficient methanol oxidation and hydrogen evolution reactions,” *J Mater Chem A Mater*, vol. 5, no. 41, pp. 22004–22011, Oct. 2017, doi: 10.1039/C7TA07340B.

[127] R. M, V. M. A, and B. J. E, “Adlineation, portholes and spillover.,” *Z Phys Chem Neue Folge*, vol. 64, no. 1, pp. 171–177, 1969, Accessed: Mar. 31, 2023. [Online]. Available: https://jglobal.jst.go.jp/en/detail?JGLOBAL_ID=201602012762916040

[128] H. Shen, H. Li, Z. Yang, and C. Li, “Magic of hydrogen spillover: Understanding and application,” *Green Energy & Environment*, vol. 7, no. 6, pp. 1161–1198, Dec. 2022, doi: 10.1016/J.GEE.2022.01.013.

[129] M. Blanco-Rey, J. I. Juaristi, M. Alducin, M. J. López, and J. A. Alonso, “Is Spillover Relevant for Hydrogen Adsorption and Storage in Porous Carbons Doped with Palladium Nanoparticles?,” *Journal of Physical Chemistry C*, vol. 120, no. 31, pp. 17357–17364, Aug. 2016, doi: 10.1021/acs.jpcc.6b04006.

[130] S. K. Konda and A. Chen, “Palladium based nanomaterials for enhanced hydrogen spillover and storage,” *Materials Today*, vol. 19, no. 2. Elsevier, pp. 100–108, Mar. 01, 2016. doi: 10.1016/j.mattod.2015.08.002.

[131] C. S. Tsao *et al.*, “Hydrogen spillover effect of pt-doped activated carbon studied by inelastic neutron scattering,” *Journal of Physical Chemistry Letters*, vol. 2, no. 18, pp. 2322–2325, Sep. 2011, doi: 10.1021/jz2010368.

[132] M. M. Bettahar, “Role of H and OH surface species in the reduction of the CO double bond,” *Molecular Catalysis*, vol. 502, p. 111338, Feb. 2021, doi: 10.1016/J.MCAT.2020.111338.

[133] E. Yoo *et al.*, "Atomic Hydrogen Storage in Carbon Nanotubes Promoted by Metal Catalysts," *Journal of Physical Chemistry B*, vol. 108, no. 49, pp. 18903–18907, Dec. 2004, doi: 10.1021/JP047056Q.

[134] Y.-N. Zhou *et al.*, "Boosting hydrogen evolution through hydrogen spillover promoted by Co-based support effect," *J Mater Chem A Mater*, vol. 11, no. 13, pp. 6945–6951, Mar. 2023, doi: 10.1039/D2TA09784B.

[135] J. Li *et al.*, "A fundamental viewpoint on the hydrogen spillover phenomenon of electrocatalytic hydrogen evolution," *Nature Communications 2021 12:1*, vol. 12, no. 1, pp. 1–12, Jun. 2021, doi: 10.1038/s41467-021-23750-4.

[136] H. Q. Fu *et al.*, "Hydrogen Spillover-Bridged Volmer/Tafel Processes Enabling Ampere-Level Current Density Alkaline Hydrogen Evolution Reaction under Low Overpotential," *J Am Chem Soc*, vol. 144, no. 13, pp. 6028–6039, Apr. 2022, doi: 10.1021/JACS.2C01094/SUPPL_FILE/JA2C01094_SI_001.PDF.

[137] A. R. Zeradjanin, J. P. Grote, G. Polymeros, and K. J. J. Mayrhofer, "A Critical Review on Hydrogen Evolution Electrocatalysis: Re-exploring the Volcano-relationship," *Electroanalysis*, vol. 28, no. 10, pp. 2256–2269, Oct. 2016, doi: 10.1002/ELAN.201600270.

[138] J. Greeley and J. K. Nørskov, "Large-scale, density functional theory-based screening of alloys for hydrogen evolution," *Surf Sci*, vol. 601, no. 6, pp. 1590–1598, Mar. 2007, doi: 10.1016/j.susc.2007.01.037.

[139] J. Greeley, J. K. Nørskov, L. A. Kibler, A. M. El-Aziz, and D. M. Kolb, "Hydrogen evolution over bimetallic systems: Understanding the trends," *ChemPhysChem*, vol. 7, no. 5, pp. 1032–1035, May 2006, doi: 10.1002/cphc.200500663.

[140] N. Danilovic, R. Subbaraman, D. Strmcnik, V. R. Stamenkovic, and N. M. Markovic, "Electrocatalysis of the HER in acid and alkaline media," *Journal of the Serbian Chemical Society*, vol. 78, no. 12, pp. 2007–2015, Jan. 2013, doi: 10.2298/JSC131118136D.

[141] J. K. Nørskov *et al.*, "Trends in the Exchange Current for Hydrogen Evolution," *J Electrochem Soc*, vol. 152, no. 3, p. J23, Jan. 2005, doi: 10.1149/1.1856988/XML.

[142] O. A. Petrii and G. A. Tsirlina, "Electrocatalytic activity prediction for hydrogen electrode reaction: intuition, art, science," *Electrochim Acta*, vol. 39, no. 11–12, pp. 1739–1747, Aug. 1994, doi: 10.1016/0013-4686(94)85159-X.

[143] W. Schmickler and E. Santos, "Interfacial Electrochemistry, Second Edition," 2010.

[144] E. Santos, P. Hindelang, P. Quaino, E. N. Schulz, G. Soldano, and W. Schmickler, "Hydrogen electrocatalysis on single crystals and on nanostructured electrodes," *Chemphyschem*, vol. 12, no. 12, pp. 2274–2279, Aug. 2011, doi: 10.1002/CPHC.201100309.

[145] H. Ooka, J. Huang, and K. S. Exner, "The Sabatier Principle in Electrocatalysis: Basics, Limitations, and Extensions," *Front Energy Res*, vol. 9, p. 155, May 2021, doi: 10.3389/FENRG.2021.654460/BIBTEX.

[146] M. Łukaszewski, M. Soszko, and A. Czerwiński, "Electrochemical Methods of Real Surface Area Determination of Noble Metal Electrodes-an Overview," *Int. J. Electrochem. Sci*, vol. 11, pp. 4442–4469, 2016, doi: 10.20964/2016.06.71.

[147] S. Trasatti and O. A. Petrii, "Real surface area measurements in electrochemistry," *Pure and Applied Chemistry*, vol. 63, no. 5, pp. 711–734, Jan. 1991, doi: 10.1351/pac199163050711.

[148] S. Watzele *et al.*, "Determination of Electroactive Surface Area of Ni-, Co-, Fe-, and Ir-Based Oxide Electrocatalysts," *ACS Catal*, vol. 9, no. 10, pp. 9222–9230, Oct. 2019, doi: 10.1021/acscatal.9b02006.

[149] G. Kresse and J. Hafner, “Ab initio molecular dynamics for liquid metals,” *Phys Rev B*, vol. 47, no. 1, pp. 558–561, 1993, doi: 10.1103/PhysRevB.47.558.

[150] G. Kresse and J. Furthmüller, “Efficiency of ab-initio total energy calculations for metals and semiconductors using a plane-wave basis set,” *Comput Mater Sci*, vol. 6, no. 1, pp. 15–50, Jul. 1996, doi: 10.1016/0927-0256(96)00008-0.

[151] G. Kresse and J. Furthmüller, “Efficient iterative schemes for ab initio total-energy calculations using a plane-wave basis set,” *Phys Rev B*, vol. 54, no. 16, pp. 11169–11186, Oct. 1996, doi: 10.1103/PhysRevB.54.11169.

[152] J. P. Perdew, K. Burke, and M. Ernzerhof, “Generalized Gradient Approximation Made Simple,” *Phys Rev Lett*, vol. 77, no. 18, pp. 3865–3868, Oct. 1996, doi: 10.1103/PhysRevLett.77.3865.

[153] P. E. Blöchl, “Projector augmented-wave method,” *Phys Rev B*, vol. 50, no. 24, pp. 17953–17979, Dec. 1994, doi: 10.1103/PhysRevB.50.17953.

[154] M. Leetmaa and N. V. Skorodumova, “KMCLib 1.1: Extended random number support and technical updates to the KMCLib general framework for kinetic Monte-Carlo simulations,” *Comput Phys Commun*, vol. 196, pp. 611–613, Nov. 2015, doi: 10.1016/J.CPC.2015.06.016.

[155] C. C. L. McCrory, S. Jung, I. M. Ferrer, S. M. Chatman, J. C. Peters, and T. F. Jaramillo, “Benchmarking Hydrogen Evolving Reaction and Oxygen Evolving Reaction Electrocatalysts for Solar Water Splitting Devices,” *J Am Chem Soc*, vol. 137, no. 13, pp. 4347–4357, Apr. 2015, doi: 10.1021/ja510442p.

[156] A. Y. Faid, F. Foroughi, S. Sunde, and B. Pollet, “Unveiling hydrogen evolution dependence on KOH concentration for polycrystalline and nanostructured nickel-based catalysts,” *J Appl Electrochem*, vol. 52, no. 12, pp. 1819–1826, Dec. 2022, doi: 10.1007/s10800-022-01749-z.

[157] B. Huang *et al.*, “Cation- and pH-Dependent Hydrogen Evolution and Oxidation Reaction Kinetics,” *J Am Chem Soc*, vol. 1, no. 10, pp. 1674–1687, Oct. 2021, doi: 10.1021/jacsau.1c00281.

[158] M. C. O. Monteiro, A. Goyal, P. Moerland, and M. T. M. Koper, “Understanding Cation Trends for Hydrogen Evolution on Platinum and Gold Electrodes in Alkaline Media,” *ACS Catal*, vol. 11, no. 23, pp. 14328–14335, Dec. 2021, doi: 10.1021/acscatal.1c04268.

[159] Y. Taji *et al.*, “Alkali metal cations change the hydrogen evolution reaction mechanisms at Pt electrodes in alkaline media,” *Nano Materials Science*, Oct. 2022, doi: 10.1016/j.nanoms.2022.09.003.

[160] A. Goyal and M. T. M. Koper, “The Interrelated Effect of Cations and Electrolyte pH on the Hydrogen Evolution Reaction on Gold Electrodes in Alkaline Media,” *Angewandte Chemie - International Edition*, vol. 60, no. 24, pp. 13452–13462, Jun. 2021, doi: 10.1002/anie.202102803.

[161] J. Greeley and M. Mavrikakis, “Surface and Subsurface Hydrogen: Adsorption Properties on Transition Metals and Near-Surface Alloys,” *Journal of Physical Chemistry B*, vol. 109, no. 8, pp. 3460–3471, Mar. 2005, doi: 10.1021/JP046540Q.

[162] W. Sheng, Z. Zhuang, M. Gao, J. Zheng, J. G. Chen, and Y. Yan, “Correlating hydrogen oxidation and evolution activity on platinum at different pH with measured hydrogen binding energy,” *Nat Commun*, vol. 6, Jan. 2015, doi: 10.1038/ncomms6848.

[163] G. A. Kamat *et al.*, “Acid anion electrolyte effects on platinum for oxygen and hydrogen electrocatalysis,” *Commun Chem*, vol. 5, no. 1, Dec. 2022, doi: 10.1038/s42004-022-00635-1.

[164] E. Lamy-Pitara, S. El Mouahid, and J. Barbier, “Effect of anions on catalytic and electrocatalytic hydrogenations and on the electrocatalytic oxidation and evolution of hydrogen on platinum,” 2000. [Online]. Available: www.elsevier.nl/locate/electacta

[165] N. Priyantha and S. Malavipathirana, “Effect of chloride ions on the electrochemical behaviour of platinum surfaces,” *Journal of the National Science Council of Sri Lanka*, vol. 24, no. 3, pp. 237–246, 1996, doi: 10.4038/jnsfsr.v24i3.5556.

[166] C. C. L. McCrory, S. Jung, I. M. Ferrer, S. M. Chatman, J. C. Peters, and T. F. Jaramillo, “Benchmarking Hydrogen Evolving Reaction and Oxygen Evolving Reaction Electrocatalysts for Solar Water Splitting Devices,” *J Am Chem Soc*, vol. 137, no. 13, pp. 4347–4357, Apr. 2015, doi: 10.1021/ja510442p.

[167] X. Ding, B. Garlyyev, S. A. Watzele, T. Kobina Sarpey, and A. S. Bandarenka, “Spotlight on the Effect of Electrolyte Composition on the Potential of Maximum Entropy: Supporting Electrolytes Are Not Always Inert,” *Chemistry - A European Journal*, vol. 27, no. 39, pp. 10016–10020, Jul. 2021, doi: 10.1002/chem.202101537.

[168] D. M. Hall, J. R. Beck, and S. N. Lvov, “Electrochemical kinetics of the hydrogen reaction on platinum in concentrated HCl(aq),” *Electrochem commun*, vol. 57, no. 1, pp. 74–77, Aug. 2015, doi: 10.1016/J.ELECOM.2015.05.012.

[169] F. Bao *et al.*, “Understanding the Hydrogen Evolution Reaction Kinetics of Electrodeposited Nickel-Molybdenum in Acidic, Near-Neutral, and Alkaline Conditions,” *ChemElectroChem*, vol. 8, no. 1, pp. 195–208, Jan. 2021, doi: 10.1002/CELC.202001436.

[170] D. M. F. Santos, C. A. C. Sequeira, D. Macciò, A. Saccone, and J. L. Figueiredo, “Platinum–rare earth electrodes for hydrogen evolution in alkaline water electrolysis,” *Int J Hydrogen Energy*, vol. 38, no. 8, pp. 3137–3145, Mar. 2013, doi: 10.1016/J.IJHYDENE.2012.12.102.

[171] D. Miousse, A. Lasia, and V. Borck, “Hydrogen evolution reaction on Ni-Al-Mo and Ni-Al electrodes prepared by low pressure plasma spraying,” *J Appl Electrochem*, vol. 25, no. 6, pp. 592–602, Jun. 1995, doi: 10.1007/BF00573217/METRICS.

[172] J. Divisek, “Determination of the kinetics of hydrogen evolution by analysis of the potential-current and potential-coverage curves,” *J Electroanal Chem Interfacial Electrochem*, vol. 214, no. 1–2, pp. 615–632, Dec. 1986, doi: 10.1016/0022-0728(86)80128-0.

[173] J. -Y. Huot, “Hydrogen Evolution and Interface Phenomena on a Nickel Cathode in 30 w/o KOH : I . Kinetics Parameters and Electrode Impedance Between 303 and 363 K,” *J Electrochem Soc*, vol. 136, no. 7, pp. 1933–1939, Jul. 1989, doi: 10.1149/1.2097088/XML.

[174] W. Sheng, H. A. Gasteiger, and Y. Shao-Horn, “Hydrogen Oxidation and Evolution Reaction Kinetics on Platinum: Acid vs Alkaline Electrolytes,” *J Electrochem Soc*, vol. 157, no. 11, p. B1529, 2010, doi: 10.1149/1.3483106.

[175] D. Tang, J. Lu, L. Zhuang, and P. Liu, “Calculations of the exchange current density for hydrogen electrode reactions: A short review and a new equation,” *Journal of Electroanalytical Chemistry*, vol. 644, no. 2, pp. 144–149, Jun. 2010, doi: 10.1016/J.JELECHEM.2009.11.031.

[176] S. Ernst and C. H. Hamann, “The pH-dependence of the hydrogen exchange current density at smooth platinum in alkaline solution (KOH),” *J Electroanal Chem Interfacial Electrochem*, vol. 60, no. 1, pp. 97–100, Mar. 1975, doi: 10.1016/S0022-0728(75)80206-3.

[177] Z. Q. Tang, L. W. Liao, Y. L. Zheng, J. Kang, and Y. X. Chen, “Temperature Effect on Hydrogen Evolution Reaction at Au Electrode,” *Chinese Journal of Chemical Physics*, vol. 25, no. 4, p. 469, Aug. 2012, doi: 10.1088/1674-0068/25/04/469-474.

[178] H. Wolfschmidt, O. Paschos, and U. Stimming, “Hydrogen Reactions on Nanostructured Surfaces,” *Fuel Cell Science: Theory, Fundamentals, and Biocatalysis*, pp. 1–70, Oct. 2010, doi: 10.1002/9780470630693.CH1.

[179] N. Krstajić, M. Popović, B. Grgur, M. Vojnović, and D. Šepa, "On the kinetics of the hydrogen evolution reaction on nickel in alkaline solution - Part I. The mechanism," *Journal of Electroanalytical Chemistry*, vol. 512, no. 1–2, pp. 16–26, Oct. 2001, doi: 10.1016/S0022-0728(01)00590-3.

[180] J. M. Jakšić, M. V. Vojnović, and N. V. Krstajić, "Kinetic analysis of hydrogen evolution at Ni–Mo alloy electrodes," *Electrochim Acta*, vol. 45, no. 25–26, pp. 4151–4158, Aug. 2000, doi: 10.1016/S0013-4686(00)00549-1.

[181] S. J. Gutic, M. Šabanovic, D. Metarapi, I. A. Pašti, F. Korac, and S. V. Mentus, "Electrochemically synthesized Ni@reduced graphene oxide composite catalysts for hydrogen evolution in alkaline media - The effects of graphene oxide support," *Int J Electrochem Sci*, vol. 14, no. 9, pp. 8532–8543, Sep. 2019, doi: 10.20964/2019.09.23.

[182] V. B. Parambhath, R. Nagar, K. Sethupathi, and S. Ramaprabhu, "Investigation of spillover mechanism in palladium decorated hydrogen exfoliated functionalized graphene," *Journal of Physical Chemistry C*, vol. 115, no. 31, pp. 15679–15685, Aug. 2011, doi: 10.1021/jp202797q.

[183] A. Granja-DelRío, M. Alducin, J. I. Juaristi, M. J. López, and J. A. Alonso, "Absence of spillover of hydrogen adsorbed on small palladium clusters anchored to graphene vacancies," *Appl Surf Sci*, vol. 559, p. 149835, Sep. 2021, doi: 10.1016/J.APSUSC.2021.149835.

[184] A. S. Dobrota, I. A. Pašti, S. V. Mentus, and N. V. Skorodumova, "A general view on the reactivity of the oxygen-functionalized graphene basal plane," *Physical Chemistry Chemical Physics*, vol. 18, no. 9, pp. 6580–6586, Feb. 2016, doi: 10.1039/C5CP07612A.

Appendices

Appendix

Table A1. Roughness factors and hydrogen binding energies (HBE) for the investigated metals.

Metals	Ag	Au	Co	Cr	Fe	Ni	Pt	W	Zn
RF	17.7± 0.9	9 ± 2	9.9 ± 1.5	2.4 ± 0.2	3.4 ± 0.2	2.7 ± 0.2	6 ± 1	2.1 ± 0.2	24 ± 4
HBE/eV[1]	0.26± 0.03	0.175± 0.035	−0.51± 0.03	−1.273± 0.03	−0.59± 0.03	−0.51± 0.03	−0.395± 0.065	−0.735± 0.065	0.39± 0.03

[1] We adopted a 30 meV uncertainty for the calculated HBE of Cr and Zn. This value aligns with the typical accuracy of the computational approach employed and is consistent with the scattering of data observed for other metals.

Table A2. Experimental conditions for electrodeposition of M and M@rGO electrodes. All the used chemicals were of practical grade and were used without any further purification.

Metal	**Electrodeposition bath**	**Deposition conditions**	**Deposition time / s**
Ag	5×10^{-3} M AgI + 2 M KI in water (AgI is dissolved in excess KI), pH ≈ 7	−0.5 A dm^{-2} 30 °C	40, 250
Au	0.05 M $HAuCl_4$ + 0.42 M Na_2SO_3 + 0.42 M $Na_2S_2O_3$ + 0.3 M Na_2HPO_4, pH ≈ 6	−0.5 A dm^{-2} 60 °C	30, 60, 100, 300
Co	59.4 g dm^{-3} $CoSO_4\times7H_2O$ + 12 g dm^{-3} Na_2SO_4 + 12 g dm^{-3} H_3BO_3	−1.2 V vs. Ag/AgCl/KCl, room temperature	50, 75, 100, 300
Fe	300 g dm^{-3} $FeSO_4\times7H_2O$ + 6 g dm^{-3} $FeCl_2\times H_2O$ + 2.8 g dm^{-3} H_3BO_3; pH adjusted to 2.5 with H_2SO_4;	−5 A dm^{-2}, room temperature	50, 100, 300
Ni	76 g dm^{-3} $NiSO_4\times6H_2O$ + 12 g dm^{-3} H_3BO_3	−1.2 V vs. Ag/AgCl/KCl, room temperature	10, 30, 60, 100, 150, 200
Pd	100 g dm^{-3} $PdCl_2\times4H_2O$ + NH_3 in excess + NH_4Cl to pH ≈ 9	−0.3 A dm^{-2} room temperature	60, 100, 200, 300
Pt	20 g dm^{-3} $H_2[Pt(OH)_6]$ + 15 g dm^{-3} KOH	−0.75 A dm^{-2} 75 °C	10, 50, 100
Zn	300 g dm^{-3} $ZnSO_4$ + 100 g dm^{-3} Na_2SO_4 + 8 g dm^{-3} H_2SO_4	−15 A dm^{-2} room temperature	30

Biography of the author

Goitom K. Gebremariam was born on May 05, 1986. He completed his elementary school in “Aila Elementary School, Adiquala” in 1998, and his junior school in “Tsinatna Junior School, Adiquala” in 2001 and his high school in “Adiquala Secondary School, Adiquala” in 2005. He enrolled in Applied Chemistry at Eritrea Institute of Technology in 2005 and graduated in 2010, with an average grade of 3.42 (8.55).

He worked as a graduate assistant at Eritrea Institute of Technology from 2010 to 2012. Then he enrolled for his master’s degree in Organic Chemistry, at Eritrea Institute of Technology in 2012 and graduated in 2014 with an average grade of 3.72 (9.3). His master’s thesis was titled “The assessment of the degree of heavy metal contamination of the waste water irrigated vegetables”. He worked as an assistant lecturer from 2014 to 2015 and as a lecturer from 2016 to 2020. While working as a lecturer he has actively participated in handling senior chemistry courses, different laboratory works, and he was actively engaged in researches related to environmental pollution. Moreover, he has worked as a member of the executive committee of Eritrean Chemical Society (ECS) and he has also contributed in the peer review of some manuscripts from the science domain internationals and from springer nature.

He enrolled in doctoral academic studies at the Faculty of Physical Chemistry of the University of Belgrade in 2020 as a scholarship holder under the “World in Serbia” project funded by the Ministry of Education, Science and Technological Development of the Republic of Serbia. Goitom is the author of seven papers published in international scientific journals (up to the time of writing this biography).

Bibliography

- Sanjin J Gutić, Dino Metarapi, Aleksandar Z Jovanović, Goitom K Gebremariam, Ana S Dobrota, Bojana Nedić Vasiljević, Igor A Pašti, Redrawing HER Volcano with Interfacial Processes—The Role of Hydrogen Spillover in Boosting H_2 Evolution in Alkaline Media *Catalysts 2023, 13(1), 89; https://doi.org/10.3390/catal13010089*
- Goitom K Gebremariam, Aleksandar Z Jovanović, Ana S Dobrota, Natalia V Skorodumova, Igor A Pašti, Hydrogen Evolution Volcano(es)—From Acidic to Neutral and Alkaline Solutions *Catalysts 2022, 12(12), 1541; https://doi.org/10.3390/catal12121541*
- Goitom Kfle, Ghebray Asgedom, Tedros Goje, Felema Abbebe, Lula Habtom, Hagos Hanes, The Level of Heavy Metal Contamination in Selected Vegetables and Animal Feed Grasses Grown in Wastewater Irrigated Area, around Asmara, Eritrea *Journal of Chemistry Volume 2020 | Article ID 1359710 | https://doi.org/10.1155/2020/1359710*
- Ezra Russom, Goitom Kfle, Ghebray Asgedom, Tedros Goje, Heavy Metals Content of Spices Available on the Market of Asmara, Eritrea *European Journal of Nutrition & Food Safety 11(3): 156-163, 2019 doi: 10.9734/EJNFS/2019/v11i330158*
- Goitom Kfle, Mussie Sium, Arumugam Manohar, Semere Debretsion, Aron Tesfamariam, Nahom Tesfalem, Abel Okbaselasie, Kibrom Tesfay, Investigation of the Physico-Chemical Standards of the Ground Waters around Mai-Bella Area in Asmara *Journal of Geoscience and Environment Protection, 7, 148-161, 2019 doi: 10.4236/gep.2019.79011*
- Goitom Kfle, Tesfamichael Haile, Mussie Sium, Semere Debretsion, Henok Abrham, Martha Ghirmay, Helen Tsegay, Filimon Nega, Analysis of the Mineral Content of Wood Ashes of Selected Plants Used for Soil Amendments in Eritrea *International Journal of Plant and Soil Science 25(6): 1-12, 2018 DOI: 10.9734/IJPSS/2018/45727*
- Goitom Kfle, Ghebray Asgedom, Determining Heavy Metals Contamination Levels of Soils and Vegetables Irrigated with Wastewater around Asmara City, Eritrea *Eritrean Journal of Science and Engineering, 4, 1-28, 2018*

Statement of authorship

Name and surname of the author Goitom Gebremariam

Index number 2020/0322

I declare

that the doctoral dissertation is entitled

"Investigation of the influence of electrolytes and the role of reduced graphene oxide as a support for metal catalysts on the catalytic activity toward the hydrogen evolution reaction"

- the result of our own research work;
- that the dissertation, in whole or in parts, was not proposed for obtaining a second degree according to the study programs of other higher education institutions;
- that the results are correctly stated and
- that I have not violated copyrights and used the intellectual property of other persons.

Signature of the author

Belgrade 01/08/2023

_____

Statement on the identity of the printed and electronic versions of the doctoral thesis

Name and surname of the author Goitom Gebremariam

Index number 2020/0322

Study program Physical Chemistry

The title of the work "Investigation of the influence of electrolytes and the role of reduced graphene oxide as a support for metal catalysts on the catalytic activity toward the hydrogen evolution reaction"

Mentor Prof. Igor Pašti

I declare that the printed version of my doctoral thesis is identical to the electronic version that I submitted, which is stored in the **Digital Repository of the University of Belgrade**.

I allow the publication of my personal data related to obtaining the academic title of Doctor of Science, such as name and surname, year and place of birth and date of thesis defense.

These personal data can be published on the web pages of the digital library, in the electronic catalog and in the publications of the University of Belgrade.

Signature of the author

Belgrade 01/08/2023

_____

Statement of use

I authorize the "Svetozar Marković" University Library to enter my doctoral dissertation in the Digital Repository of the University of Belgrade under the title:

"Investigation of the influence of electrolytes and the role of reduced graphene oxide as a support for metal catalysts on the catalytic activity toward the hydrogen evolution reaction"

which is my author's work.

I submitted the dissertation with all attachments in an electronic format suitable for permanent archiving.

My doctoral dissertation stored in the Digital Repository of the University of Belgrade and available in open access can be used by anyone who respects the provisions contained in the selected type of Creative Commons license that I chose.

1. Authorship (CC BY)
2. Authorship - Non-Commercial (CC BY-NC)
3. Authorship - non-commercial - no adaptation (CC BY-NC-ND)
4. Authorship - non-commercial - share under the same conditions (CC BY-NC-SA)
5. Authorship - no modification (CC BY-ND)
6. Authorship - share under the same conditions (CC BY-SA)

(Please circle only one of the six licenses offered.
A brief description of the licenses is an integral part of this statement).

Signature of the author

Belgrade 01/08/2023

_____

1. **Authorship**. You permit the reproduction, distribution and public communication of the work, and adaptations, if the author's name is indicated in the manner specified by the author or the licensor, even for commercial purposes. This is the most free of all licenses.

2. **Authorship - non-commercial**. You permit the reproduction, distribution and public communication of the work, and adaptations, if the name of the author is indicated in the manner specified by the author or licensor. This license does not permit commercial use of the work.

3. **Authorship - non-commercial - no processing**. You permit the reproduction, distribution, and public communication of the work, without modification, transformation, or use of the work in your own work, provided that the author's name is indicated in the manner specified by the author or licensor. This license does not permit commercial use of the work. In relation to all other licenses, this license limits the maximum scope of the right to use the work.

4. **Authorship - non-commercial** - share under the same conditions. You allow the reproduction, distribution and public communication of the work, and adaptations, if the name of the author is indicated in the manner determined by the author or licensor and if the adaptation is distributed under the same or similar license. This license does not permit commercial use of works and adaptations.

5. **Authorship - no adaptation**. You permit the reproduction, distribution, and public communication of the work, without modification, transformation, or use of the work in your own work, provided that the author's name is indicated in the manner specified by the author or licensor. This license permits commercial use of the works.

6. **Authorship - share under the same conditions**. You permit the reproduction, distribution, and public communication of the work, and adaptations, provided that the author's name is credited in a manner specified by the author or licensor and the adaptation is distributed under the same or similar license. This license permits the commercial use of works and adaptations. It is similar to software licenses, i.e. open source licenses.

Изјава о ауторству

Име и презиме аутора Гоитом Гебремариам

Број индекса 2020/0322

Изјављујем

да је докторска дисертација под насловом

„ Истраживање утицаја електролита и улоге редукованог графен-оксида као носача металних катализатора на каталитичку активност за реакцију издвајања водоника “

- резултат сопственог истраживачког рада;
- да дисертација у целини ни у деловима није била предложена за стицање друге дипломе према студијским програмима других високошколских установа;
- да су резултати коректно наведени и
- да нисам кршио/ла ауторска права и користио/ла интелектуалну својину других лица

Потпис аутора

У Београду, 01.08.2023

_____

Изјава о истоветности штампане и електронске верзије докторског рад

Име и презиме аутора Гоитом Гебремариам

Број индекса 2020/0322

Студијски програм Физичка хемија

Наслов рада „Истраживање утицаја електролита и улоге редукованог графен-оксида као носача металних катализатора на каталитичку активност за реакцију издвајања водоника“

Ментор Проф. Игор Пашти

Изјављујем да је штампана верзија мог докторског рада истоветна електронској верзији коју сам предао/ла ради похрањена у **Дигиталном репозиторијуму Универзитета у Београду**.

Дозвољавам да се објаве моји лични подаци везани за добијање академског назива доктора наука, као што су име и презиме, година и место рођења и датум одбране рада.

Ови лични подаци могу се објавити на мрежним страницама дигиталне библиотеке, у електронском каталогу и у публикацијама Универзитета у Београду.

Потпис аутора

У Београду, 01.08.2023

_____

Изјава о коришћењу

Овлашћујем Универзитетску библиотеку „Светозар Марковић“ да у Дигитални репозиторијум Универзитета у Београду унесе моју докторску дисертацију под насловом:

„Истраживање утицаја електролита и улоге редукованог графен-оксида као носача металних катализатора на каталитичку активност за реакцију издвајања водоника“

која је моје ауторско дело.

Дисертацију са свим прилозима предао/ла сам у електронском формату погодном за трајно архивирање.

Моју докторску дисертацију похрањену у Дигиталном репозиторијуму Универзитета у Београду и доступну у отвореном приступу могу да користе сви који поштују одредбе садржане у одабраном типу лиценце Креативне заједнице (Creative Commons) за коју сам се одлучио/ла.

1. Ауторство (CC BY)
2. Ауторство – некомерцијално (CC BY-NC)
3. Ауторство – некомерцијално – без прерада (CC BY-NC-ND)
4. Ауторство – некомерцијално – делити под истим условима (CC BY-NC-SA)
5. Ауторство – без прерада (CC BY-ND)
6. Ауторство – делити под истим условима (CC BY-SA)

(Молимо да заокружите само једну од шест понуђених лиценци.

Кратак опис лиценци је саставни део ове изјаве).

Потпис аутора

У Београду, 01.08.2023

_____

1. **Ауторство**. Дозвољавате умножавање, дистрибуцију и јавно саопштавање дела, и прераде, ако се наведе име аутора на начин одређен од стране аутора или даваоца лиценце, чак и у комерцијалне сврхе. Ово је најслободнија од свих лиценци.

2. **Ауторство – некомерцијално**. Дозвољавате умножавање, дистрибуцију и јавно саопштавање дела, и прераде, ако се наведе име аутора на начин одређен од стране аутора или даваоца лиценце. Ова лиценца не дозвољава комерцијалну употребу дела.

3. **Ауторство – некомерцијално – без прерада**. Дозвољавате умножавање, дистрибуцију и јавно саопштавање дела, без промена, преобликовања или употребе дела у свом делу, ако се наведе име аутора на начин одређен од стране аутора или даваоца лиценце. Ова лиценца не дозвољава комерцијалну употребу дела. У односу на све остале лиценце, овом лиценцом се ограничава највећи обим права коришћења дела.

4. **Ауторство – некомерцијално – делити под истим условима**. Дозвољавате умножавање, дистрибуцију и јавно саопштавање дела, и прераде, ако се наведе име аутора на начин одређен од стране аутора или даваоца лиценце и ако се прерада дистрибуира под истом или сличном лиценцом. Ова лиценца не дозвољава комерцијалну употребу дела и прерада.

5. **Ауторство – без прерада**. Дозвољавате умножавање, дистрибуцију и јавно саопштавање дела, без промена, преобликовања или употребе дела у свом делу, ако се наведе име аутора на начин одређен од стране аутора или даваоца лиценце. Ова лиценца дозвољава комерцијалну употребу дела.

6. **Ауторство – делити под истим условима**. Дозвољавате умножавање, дистрибуцију и јавно саопштавање дела, и прераде, ако се наведе име аутора на начин одређен од стране аутора или даваоца лиценце и ако се прерада дистрибуира под истом или сличном лиценцом. Ова лиценца дозвољава комерцијалну употребу дела и прерада. Слична је софтверским лиценцама, односно лиценцама отвореног кода.